

Direction and intensity of Earth's magnetic
field at the Permo-Triassic boundary: A
geomagnetic reversal recorded by the
Siberian Trap Basalts, Russia

*Inaugural-Dissertation
zur Erlangung des Doktorgrades
der Fakultät für Geowissenschaften der
Ludwig-Maximilians-Universität München*

vorgelegt von
Christoph Heunemann

4. August 2003

1. Berichterstatter: Prof. Dr. H. C. Soffel
2. Berichterstatter: Prof. Dr. V. Bachtadse

Tag der mündlichen Prüfung: 12.11.2003

Contents

List of Figures	3
List of Tables	5
Glossary	6
Preamble	8
Zusammenfassung	9
Abstract	13
1 Introduction	17
1.1 The Earth's magnetic field	17
1.2 Polarity transitions	19
1.2.1 Palaeomagnetic records of reversals	19
1.2.2 Models of geomagnetic reversals	20
1.3 The Mesozoic dipole low	22
1.4 Scientific aims	24
2 The Siberian Trap Basalts	25
2.1 Geological Setting	25
2.2 Age and duration of the Siberian Trap volcanism	27
2.3 Origin of the Siberian Trap Basalts	28
3 Palaeomagnetic Results	30
3.1 Sampling	30
3.2 NRM demagnetisation	32
3.3 Palaeomagnetic Record	41
3.4 Fold and reversal test	47
3.5 Palaeosecular Variation	50
3.6 Magnetostratigraphic correlation	52

4	Rockmagnetic Studies	56
4.1	Microscopy: Evidence for high-temperature oxidation	56
4.2	Rockmagnetic parameters	58
4.3	Continuous thermal demagnetisation of the NRM	61
4.4	Summary	63
5	Palaeointensity determinations	67
5.1	Sample selection	67
5.2	Methods	67
5.3	Reliability criteria	70
5.4	Interpretation of the Arai-plots	73
5.5	Results	74
6	Discussion: Features of the record	83
6.1	Transitional VGP path	83
6.2	Phase 1: Stability of the transitional cluster	87
6.3	Phase 2: Independent or reversal-related?	88
6.4	Phase 3: Stable normal polarity	89
6.5	Asymmetry of the intensity across the reversal	91
6.6	Angular secular variation and intensity	91
6.7	Duration of the record	92
7	Conclusions	95
	Bibliography	98
	Acknowledgments	112
	Appendix	114
A	Compilation of the VDM between 56 and 280 Ma	114
	Curriculum Vitae	116

List of Figures

1.1	The variation of the VDM during the Mesozoic	23
2.1	Geological outline of north-western and central Siberia	26
2.2	Compilation of published ages of the Siberian Traps	29
3.1	Simplified geological map of the Noril'sk area	32
3.2	Stratigraphy of the sampled sections	33
3.3	Outcrop of the Ivakinsky suite	34
3.4	Well preserved surface of a flow	34
3.5	Geological map of the Abagalakh/Icon river valley	35
3.6	Zijderveld plots of representative samples of reversed polarity	36
3.7	Zijderveld plots of representative samples carrying transitional directions	36
3.8	Decay of the NRM during thermal demagnetisation	37
3.9	Zijderveld plots of normal directions	37
3.10	Inclination and declination record of the Listvjanka and Abagalakh section	43
3.11	Plot of all directions in stereographic projection	44
3.12	Compilation of palaeomagnetic poles obtained from the Siberian Traps	46
3.13	Movement of the VGPs during the emplacement of the flows	48
3.14	Result of the internal fold test	50
3.15	Magnetostratigraphic correlation of borehole and in situ data	53
3.16	Correlation between the STB and the global P/T magnetostratigraphic scale	54
4.1	Light-microscopical and SEM observations	64
4.2	Representative $M_S(T)$ -curves	65
4.3	Continuous thermal demagnetisation	65
4.4	Self-reversal identified by continuous thermal demagnetisation	66
5.1	Representative NRM-TRM plots for quality class A and B results	69
5.2	Rejected palaeointensity results	71
5.3	NRM-TRM plots for different stratigraphic levels	72
5.4	Palaeointensities and VDMs across the studied sections	75

6.1	Movement of the VGPs across the studied sections	85
6.2	VGPs corrected for plate motion	86
6.3	Comparison of VDM distribution for different time intervals	90

List of Tables

3.1	Volcanic suites sampled in the Noril'sk area	31
3.2	Mean characteristic directions of the Listvjanka and Abagalakh section . .	38
3.3	Mean characteristic directions of the Talnakh section	41
3.4	Mean directions and poles of the observed directional groups	42
3.5	Selected poles for the STB and the Siberian platform around the P/T boundary	47
3.6	Results of the palaeosecular variation estimates	51
4.1	Results of the rockmagnetic investigations	59
5.1	Results of the palaeointensity experiments	76
A.1	Compilation of the VDM between 56 and 280 Ma	114

Glossary

Abbreviations

APWP	apparent polar wander path
BSE	backscattered electron
ChRM	characteristic remanent magnetisation
CMB	core-mantle boundary
EDX analyses	energy dispersive X-ray analyses
LIP	large igneous province
MD	multidomain
MDL	Mesozoic dipole low
NRM	natural remanent magnetisation
PSV	palaeosecular variation
P/T	Permo-Triassic
pTRM	partial thermoremanent magnetisation
PSD	pseudo single domain
SEM	scanning electron microscope
SBG	submarine basaltic glass
SD	single domain
SP	superparamagnetic
STB	Siberian Trap Basalts
TRM	thermoremanent magnetisation
TCRM	thermochemical remanent magnetisation
VFTB	Variable Field Translation Balance
VDM	virtual dipole moment
VGP	virtual geomagnetic pole

Symbols and constants

α_{95}/A_{95} [°]	radius of the 95% confidence circle of a palaeomagnetic direction/pole
d_m/d_p [°/°]	95% confidence limits of the latitude/longitude of a VGP
k	precision parameter for the dispersion of palaeomagnetic directions

T_C [°C]	Curie-temperature
T_b [°C]	blocking temperature
T_{ub} [°C]	unblocking temperature
T_0	room temperature
H_c [T]	coercive force
H_{cr} [T]	remanence coercivity
M_s [$\frac{Am^2}{kg}$]	specific saturation magnetisation
M_{rs} [$\frac{Am^2}{kg}$]	specific saturation remanence

Preamble

Parts of this thesis are based on, or directly taken from papers to be published in scientific journals. Below, these papers are listed in order of their appearance in the text:

Heunemann, C., Krása, D., Gurevitch, E.L., Soffel, H.C. and Bachtadse, V. Directions and intensities of the Earth's magnetic field during a reversal: results from the Permo-Triassic Siberian Trap Basalts, Russia, *Earth Planet. Sci. Lett.* (in press)

Gurevitch, E.L., Heunemann, C., Rad'ko, V., Westphal, M., Bachtadse, V., Pozzi, J. P. and Feinberg, H., Palaeomagnetism and magnetostratigraphy of the Permian-Triassic Siberian trap basalts, *Tectonophysics* (in press)

Krásá, D., Heunemann, C., Leonhardt, R. and Petersen, N. (2003); Experimental procedure to detect multidomain remanence during Thellier-Thellier experiments, *Phys. Chem. Earth*, 28, 681–687

Zusammenfassung

Das Magnetfeld der Erde wird durch Konvektionsströmungen im flüssigen, eisenreichen äußeren Erdkern erzeugt. Eine der deutlichsten Ausprägungen der dynamischen Prozesse im äußeren Kern sind Polaritätswechsel des Magnetfeldes. Allerdings sind die dafür verantwortlichen Mechanismen bisher kaum verstanden. Die mathematische Formulierung der Vorgänge im äußeren Kern ist von derartiger Komplexität, dass vollständige numerische Modelle noch nicht vorliegen. Der letzte Polaritätswechsel fand vor ungefähr 780000 Jahren statt, so dass direkte Beobachtungen einer Feldumkehr bisher nicht möglich waren. Daher muß man auf die Aufzeichnungen solcher Ereignisse in sedimentären oder magmatischen Gesteinen zurückgreifen. Die Beschreibung charakteristischer Merkmale des Richtungs- und Intensitätsverhaltens des Erdmagnetfeldes während einer Umkehr kann demnach einen wesentlichen Beitrag zum Verständnis des Geodynamos leisten. Obwohl auf diesem Gebiet Fortschritte gemacht wurden, so liefern doch unterschiedliche Aufzeichnungen von Feldumkehrungen widersprüchliche Resultate und lassen Freiraum für eine Vielzahl von Interpretationsmöglichkeiten. Einige Schlüsselfragen, wie z. B. die ob alle Feldumkehrungen in der gleichen Weise vonstatten gehen, sind daher noch ungeklärt.

Detaillierte Untersuchungen der Richtungs- und Intensitätsänderungen während Feldumkehrungen beschränken sich bisher auf das Känozoikum. Um die Modelle, die basierend auf diesem bis jetzt verfügbaren Datensatz entwickelt wurden, zu überprüfen, sind Aufzeichnungen von Polaritätswechseln aus der älteren geologischen Vergangenheit erforderlich. In Rahmen dieser Arbeit wurden Lavasequenzen der Permo-Triassischen (250 Ma) sibirischen Trap-Basalte untersucht. Sie zeigen Details einer geomagnetischen Feldumkehr von inverser zu normaler Polarität und liefern damit neue Einblicke in intermediäre Feldzustände aus diesem Zeitbereich.

Drei Sektionen (Talnakh, Listvjanka und Abagalakh) mit insgesamt 86 aufeinanderfolgenden Lavaflüssen wurden in der Region von Noril'sk beprobt. Zusammengefaßt überdecken sie die gesamte Mächtigkeit der hier aufgeschlossenen Lavasequenz. Die Proben wurden zur Analyse ihrer paläomagnetischen Richtungsinformation schrittweise abmagnetisiert. Paläointensitäten wurden mit einer abgewandelten und weiter entwickel-

ten Variante der Thellier-Methode bestimmt. Anhand umfassender gesteinsmagnetischer und mikroskopischer Untersuchungen konnten die Remanenzträger identifiziert und die von ihnen getragene paläomagnetische Information auf ihre Zuverlässigkeit überprüft werden.

Träger der charakteristischen remanenten Magnetisierung sind stets Magnetit und titanarmer Titanomagnetit. Die Erzkörner weisen in den meisten Fällen Entmischungslamellen auf, ein deutliches Anzeichen einer syngenetischen, primären Oxidation bei hohen Temperaturen. Diese Hochtemperatur-Oxidation tritt beim Abkühlen des Lavaflusses oberhalb von 500°C bis 600°C auf. Es kann daher gefolgert werden, dass die magnetischen Informationen über die Richtung und Intensität des Paläofeldes kurz nach der Extrusion der einzelnen Lavaflüsse erworben wurden.

Die natürliche remanente Magnetisierung zeigt meist nur eine Richtungskomponente. Thermische Entmagnetisierung und Entmagnetisierung im Wechselfeld liefern identische Ergebnisse. Gelegentlich beobachtete Überprägungen haben maximale Entblockungstemperaturen von etwa 350°C oder Remanenzkoerzitivkräfte von bis zu 20 mT. Paläointensitätsexperimente ergaben für rund 50% der Proben auswertbare Ergebnisse. Diese relativ hohe Erfolgsrate ist mit der durch die Hochtemperatur-Oxidation erhöhten magnetischen und thermischen Stabilität der Remanenzträger zu erklären.

Die Lavaflüsse im unteren Teil der Sequenz zeigen inverse charakteristische remanente Magnetisierungen. Die Paläointensität liegt in diesem Bereich bei 10 μ T. Die darüberliegenden Lavaflüsse liefern eine detaillierte Aufzeichnung der Feldkonfiguration während des Polaritätswechsels. Eine Anhäufung (Cluster) solcher intermediären Richtungen bzw. der damit verbundenen virtuellen geomagnetischen Pole (VGPs) ist in mittleren nördlichen Breiten zu beobachten. Sie umfasst die Ergebnisse von 15 Lavaflüssen. Dieses Richtungsverhalten konnte anhand von zwei parallelen Sektionen (Talnakh und Listvjanka) nachgewiesen werden. Innerhalb dieses Clusters zeigt der Verlauf der Paläointensität einen deutlichen und wohldefinierten Anstieg von ungefähr 6 μ T auf 13 μ T. Eine derartige Verdopplung der lokalen Magnetfeldstärke ist nur durch großräumige Änderungen der Prozesse im äußeren Erdkern zu erklären. Zeitskalen für Veränderungen der Konvektionsmuster im äußeren Kern liegen in der Größenordnung von 10^3 Jahren. Diese Beobachtungen sprechen für Phasen erhöhter Stabilität der Feldkonfiguration von einigen Hundert bis wenigen Tausend Jahren im Verlauf des Polaritätswechsels. Zumindest in dem hier vorliegenden Fall ist es unwahrscheinlich, dass dieser intermediäre Cluster ein Artefakt erhöhter Extrusionraten durch eine lokalisierte Intensivierung der vulkanischen Aktivität darstellt. Die VGPs der darüberliegenden Lavaflüsse bewegen sich in Richtung der Position wie sie für stabile normale Polarität

zu erwarten wäre. Nach Rotation der zeitlichen Abfolge der intermediären VGPs in das spät-paläozoische/früh-mesozoische geographische Referenzsystem wird deutlich, dass die große Mehrzahl der intermediären Richtungen auf einem schmalen Band entlang eines Längengrades liegt. Dieses verläuft rechtwinklig zu so genannten "far-" oder "near-sided" Pfaden. Solche "far-" oder "near-sided" Pfade wären ein Hinweis für die Dominanz von zonalen und daher achsensymmetrischen Komponenten der Multipole des Erdmagnetfeldes während einer Feldumkehr. Im Gegensatz dazu weisen die Daten dieses Polaritätswechsels allerdings auf einen starken Beitrag sektorieller nicht-Dipol Anteile hin. Im Anschluß an den Übergang wird für kurze Zeit normale Polarität erreicht, bevor sich die VGPs wieder davon wegbewegen und einen neuen Cluster bilden, der von 14 Lavaflüssen aufgezeichnet wurde. Innerhalb dieses Clusters, der als Exkursion des Erdmagnetfeldes interpretiert wird, konnte keine charakteristische Variation der Paläointensität belegt werden (Mittelwert $14 \mu\text{T}$). Exkursionen des Erdmagnetfeldes im direkten Anschluß an eine Feldumkehr wurden auch schon häufig in Aufzeichnungen jüngerer Feldumkehrungen beobachtet. Eine Erklärung hierfür sind Instabilitäten im Strömungsmuster des Geodynamos als Folge der eigentlichen Feldumkehr. Gewöhnlich nehmen die VGPs solcher Exkursionen Positionen ähnlich zu denen ein, wie sie während der Umkehr beobachtet werden ("Rebound"-Effekt). Im vorliegenden Fall liegen sie auf dem durch die intermediären VGPs definierten Großkreis, überschießen allerdings den Pol normaler Polarität. Diese geometrischen Randbedingungen legen nahe, dass sektorielle nicht-Dipol Anteile des Feldes, ähnlich denen während des intermediären Zustandes, für dieses Verhalten verantwortlich sind.

Bemerkenswerterweise gibt es sehr viele Ähnlichkeiten zwischen dieser, der bisher bei weitem ältesten genau untersuchten Feldumkehr, und jüngeren, vornehmlich tertiären, Feldumkehrungen. Dazu gehören der intermediäre VGP Cluster, die scharfe Begrenzung der VGPs auf einen Großkreis, die Existenz einer Exkursion im Anschluß an die Feldumkehrung und generell niedrige Paläointensitäten in deren Verlauf. Es liegt daher nahe, dass die einer Feldumkehrung zugrundeliegenden Prozesse sowohl im Mesozoikum als auch im Känozoikum im Prinzip ähnlich waren.

Die Ergebnisse der auf die Exkursion folgenden 41 Lavaflüsse zeigen, dass erst in dieser Phase der Zustand stabiler normaler Polarität erreicht wird. Mittels Analyse dieses Teils der Sequenz können einige repräsentative charakteristische Parameter des Erdmagnetfeldes im frühen Mesozoikum bestimmt werden. So liegt die mittlere Paläointensität für diesen Bereich bei $19 \mu\text{T}$, was einem virtuellen geomagnetischen Dipolmoment (VDM) von $2.3 \times 10^{22} \text{ Am}^2$ entspricht. Damit kann belegt werden, dass sich die Phase niedriger VDMs während des Mesozoikums ("Mesozoic Dipole Low") zumindest bis an die Perm-Trias-Grenze erstreckt. Die Abschätzung der aufgezeichneten

Säkularvariation ergab vergleichbare Werte zu denen, wie sie für die letzten 5 Ma ermittelt wurden. In diesem Zeitraum herrschte allerdings im Mittel ein deutlich stärkeres VDM vor ($5.5 \times 10^{22} \text{ Am}^2$). Die Hypothese von verstärkter Säkularvariation während Phasen niedrigen Dipolmoments (und umgekehrt) kann daher nicht gestützt werden. Das Ausmaß der Säkularvariation und die Stärke des Dipolmoments scheinen - jedenfalls in der frühen Trias - komplexer gekoppelt zu sein als bisher angenommen.

Magnetostratigraphische Untersuchungen, die auch Basaltsequenzen des westsibirischen Beckens umfassen, belegen die Existenz von insgesamt sechs Polaritätsintervallen. Durch den Vergleich mit der globalen Polaritätszeitskala kann damit die Dauer der Platznahme der sibirischen Trap-Basalte mit maximal 3.2 Ma abgeschätzt werden. Der Großteil der Basalte (mit einer Mächtigkeit von mehr als 1700 m) wurde in der Region von Noril'sk gefördert. Innerhalb dieser Sequenz konnte allerdings nur ein Polaritätswechsel nachgewiesen werden. Dieser Befund wird auch durch Ergebnisse von Bohrlöchern in der Nähe der hier beschriebenen Aufschlüsse gestützt. Im Rahmen dieser Arbeit wurde gezeigt, dass die Existenz weiterer nicht identifizierter Polaritätsintervalle daher unwahrscheinlich ist. Es ist anzunehmen, dass die Lavasequenz in der Region von Noril'sk innerhalb wesentlich kürzerer Zeit als der oben genannten 3.2 Ma gebildet wurde. Radiometrische Daten begrenzen die Dauer der vulkanischen Aktivität auf etwa 1 Ma. Unter der Annahme ähnlicher Säkularvariationsraten in der frühen Trias und dem Holozän und einer mit jüngeren Polaritätswechseln vergleichbaren Dauer der Feldumkehr ergibt sich für die Platznahme der untersuchten Sequenz eine Gesamtdauer in der Größenordnung von 15000 Jahren. Dieser Wert ist allerdings als unterstes Limit aufzufassen. Angesichts der Mächtigkeit der Basaltabfolge würde dies enorme Eruptionsraten und -volumina voraussetzen. Eine vulkanische Aktivität solch katastrophalen Ausmaßes und die dadurch hervorgerufenen Änderungen des globalen Klimas kann die Ursache für das Massensterben an der Perm-Trias-Grenze gewesen sein.

Abstract

The Earth's magnetic field is generated by the motion of liquid iron-rich material in the outer core. One of the most drastic manifestations of the dynamics in the outer core are polarity reversals of the magnetic field. The processes controlling geomagnetic reversals, however, are still poorly understood. The mathematical formulation of the dynamics of the liquid outer core show such a degree of complexity that a universal numerical model still remains elusive. Given that the last reversal occurred about 780,000 years ago, direct observations of a reversal have never been possible. Thus we are left with records of ancient reversals recorded in sequences of sedimentary and igneous rocks. Documenting any systematics in reversal processes will provide substantial information about the outer core and core mantle boundary conditions. However, despite the advances in deciphering the behaviour of the field during polarity transitions, reversal records yield controversial results and thus answers to several key questions are still enigmatic.

Detailed studies of palaeodirectional and absolute palaeointensity patterns of geomagnetic reversals are scarce and are restricted to the Cenozoic so far. In order to verify or reject concepts developed on the basis of this dataset, reversal records which occurred in the more distant geological past of the Earth are needed. This work presents the results obtained from the Siberian Trap Basalts (Russia) which are coeval with the Permo-Triassic boundary (250 Ma). The sequence yields the by far oldest hitherto studied detailed record of a geomagnetic transition from reversed to normal polarity and provides new insights in transitional field behaviour.

Three sections (Talnakh, Listvjanka and Abagalakh) comprising a total of 86 lava flows have been sampled in the Noril'sk region, located at the northwestern rim of the Siberian Trap Basalt province. They provide a complete coverage of the lava pile outcropping in the area. The samples have been subjected to palaeomagnetic direction analysis and to Thellier-type palaeointensity experiments. Extensive rockmagnetic investigations and microscopical studies have been carried out to assess the reliability of the palaeomagnetic information recorded by the lava flows.

Magnetite and Ti-poor titanomagnetites were identified to be the carriers of the

characteristic remanent magnetisation. The reversibility of the thermomagnetic curves and the observation of exsolution lamellae by ore microscopy give clear evidence for a primary high-temperature oxidation of the titanomagnetite. It can thus be inferred that the measured palaeodirectional and intensity information obtained from these flows was acquired shortly after extrusion of each flow.

The demagnetisation of the natural remanence reveals only one direction of magnetisation for most samples. Thermal and alternating field demagnetisation methods are equally effective in isolating the characteristic remanent magnetisation. Occasional overprints have maximum unblocking temperatures of 350°C or remanence coercivities less than 20 mT. Reliable palaeointensity estimates were obtained for $\approx 50\%$ of the samples. The relatively high success rate can be attributed to the enhanced magnetic and thermal stability of high-temperature oxidised titanomagnetites.

In the lower part of the sequence reversed polarity of the Earth's magnetic field is identified. The associated palaeointensities yield values around 10 μT . The subsequent flows recorded transitional configurations. A tight cluster of virtual geomagnetic poles (VGPs) in mid northerly latitudes, comprising the results of 15 flows, is observed during the transition. Within the cluster the record shows a pronounced and well defined increase in intensity from around 6 to 13 μT . A doubling of local field intensity infers that large scale dynamic processes in the outer core are responsible for this feature, making a strong case for a reasonable temporal stability (several hundreds to a few thousand years) of the VGP cluster. Moreover, the VGP clustering is identified in two parallel sections (Talnakh and Listvjanka). This observation makes it unlikely that this feature is an artifact of a localised burst in volcanic activity and supports the concept of stabilised phases of the geomagnetic field during reversals. The VGPs of the overlying flows move towards the position expected for normal polarity. After rotating of the VGPs into the Late Permian/Early Triassic geographic reference system it is evident that most of the transitional VGPs are strongly confined to a narrow longitudinal band which is perpendicular to near- or far-sided VGP paths. Such near- or far-sided paths would be indicative for the dominance of zonal, and thus axis-symmetric, non-dipole fields. The VGP path of this transition suggests the contribution of strong sectorial components of the Earth's magnetic field. Following the transition itself, normal polarity is reached for a brief time interval. Subsequently, the VGPs depart from this position to form another well defined directional cluster recorded by 14 successive flows. During this clustering, which is interpreted as an excursion of the Earth's magnetic field, no characteristic variation in palaeointensity is identified (mean value 14 μT). Such post-transitional excursions are frequently observed in younger reversal records and are explained by instabilities of the geodynamo after the reversal. However, VGPs associated with post-

transitional excursions usually reach positions similar to those occupied by VGPs during the transition. In contrast to such "rebound" effects, the excursion-related VGPs of this record are still confined to the latitudinal band defined by the transition, but "overshoot" normal polarity. This geometrical constraint suggests that non-dipole components similar to those dominating the transitional VGP path are responsible for this observation.

Remarkably, the geomagnetic polarity transition described here shares many similarities – such as directional clustering, longitudinal confinement of the VGP path, the existence of a post-transitional excursion and generally low palaeointensities – with previously published reversal records of mainly Tertiary age. It may, therefore, be inferred that the underlying reversal processes are similar to those observed for the Cenozoic.

The results obtained of the superjacent 41 flows, which were extruded immediately after the reversal-related excursion, indicate that only at this stage of the record stable normal polarity is reached allowing to determine several characteristic parameters of the Early Triassic Earth's magnetic field. The mean palaeointensity for this part of the sequence is $19\ \mu\text{T}$, which corresponds to a virtual geomagnetic dipole moment (VDM) of $2.3 \times 10^{22}\ \text{Am}^2$. These findings confirm that the Mesozoic dipole low extends at least down to the Permo-Triassic boundary. Calculation of the recorded secular variation yields values similar to those averaged over the last 5 Ma, a period with distinctly higher mean VDM ($5.5 \times 10^{22}\ \text{Am}^2$) compared to the data presented here. The hypothesis of enhanced secular variation during phases of a low mean VDM can, therefore, not be substantiated by this study. Secular variation and the strength of the dipole moment seem to be – at least in the Early Mesozoic – more complexly coupled than previously assumed.

Magnetostratigraphic results of borehole samples obtained from basalts related to the Siberian Trap volcanism including the West Siberian basin yield in total 6 polarity intervals. Comparison to the global magnetostratigraphic scale indicates that the volcanic activity lasted no more than 3.2 Ma. However, the lava sequence in the Noril'sk area (more than 1700 m thick), representing the bulk of the erupted material, recorded only one polarity transition. This finding has been supported by data derived from boreholes in close vicinity to the surface sections which makes the presence of further undetected polarity transitions highly unlikely. It can be thus inferred that the emplacement of the sequence occurred much faster than the aforementioned 3.2 Ma. Radiometric ages suggest an upper limit for the duration of the emplacement of approximately 1 Ma. Based on the assumptions of similar rates of angular secular variation in the Early Triassic and in the Holocene and an average duration of the transition itself the time interval covered is estimated to be in the order of 15000 years. This value has to be regarded as a lowermost limit for the duration of the emplacement. Such a rapid development of the volcanic

province in the Noril'sk area would imply an enormous eruption rate making a strong case for the Siberian Trap basalts as cause for the Permo-Triassic crisis.

Chapter 1

Introduction

1.1 The Earth's magnetic field

The present geomagnetic field, disregarding fields of external origin (e.g. in the ionosphere), can be well approximated by a geocentric magnetic dipole with its axis tilted about 11° with respect to the axis of rotation of the Earth. Such a dipole accounts for roughly 80% of the magnetic field on the surface of the Earth [MERRILL ET AL., 1998]. Non-dipolar components of the field make up the remaining part of the field. The Earth's magnetic field is a conservative vector field. Thus, a scalar potential exists which is best described by spherical harmonics, whereby the Earth's magnetic field can be represented as the sum of hypothetical sources in terms of multipoles in the centre of the Earth. The potential is represented by Gauss coefficients g_l^m and h_l^m and their associated partially normalised Schmidt functions P_l^m ($l > m$, $l > 0$). The geocentric dipole is composed of the Gauss coefficient $l = 1$, whereas $l = 2$ describes a geocentric quadrupole, $l = 3$ an octupole, If $m = 0$ the surface harmonics are called *zonal harmonics*, if $l = m$ they are referred to as *sectorial harmonics*. In the general case they are termed *tesseral harmonics* (see MERRILL ET AL. [1998], JACOBS [1984]).

Usually, the field described by the harmonics of the degree $l \geq 15$ is attributed to sources within the Earth's crust due to remanent and also induced magnetisation. Fields of lower degrees have their sources in the Earth's core. The theory that the magnetic field is generated by a self-exciting dynamo due to the motion of conductive material in the interior of the Earth was first formulated by LARMOR [1919]. This concept was refined by ELSASSER [1946], BULLARD [1949] and others and is now known as the magneto-hydrodynamical (MHD) theory of the Earth's magnetic field.

The fluid pattern in the liquid outer core and its variations are responsible for certain observed features of the Earth's magnetic field such as secular variation, westward

drift of the non-dipole components, decrease of the field intensity, etc. The present Earth's magnetic field is constantly monitored by observatories, surveys and recently also satellites. Going back in time, however, the data become more scarce. The first continuous measurements started roughly 400 years ago in London. Beyond that, one relies on information recorded in rocks (or archeological material like pottery). Although most of the rock forming minerals are not ferro(i)magnetic, practically all rocks carry a magnetic remanence due to the presence of accessory iron oxides and/or iron sulphides. The remanent magnetisation carried by these minerals is called natural remanent magnetisation (NRM). During the formation of a rock it acquires a magnetisation parallel to the ambient field. In the case of a sedimentary rock the NRM is acquired during or shortly after the deposition of the material (detrital remanent magnetisation). The efficiency of the passive orientation of detrital magnetic minerals in the ambient field depends also on its intensity. Hence, records of relative palaeointensity variations can be derived from suitable sediments. Igneous rocks acquire a thermoremanent magnetisation (TRM) when cooling below the Curie-temperature of their magnetic minerals. The TRM is proportional to the intensity of the field. Extracting this information, using the THELLIER AND THELLIER [1959] method, is a time consuming task but has the advantage of providing information about the absolute palaeointensity of the Earth's magnetic field. A comprehensive review on magnetic minerals and remanence acquisition processes is given by DUNLOP AND ÖZDEMİR [1997].

Palaeomagnetism is the science of extracting and interpreting the magnetic information recorded by rocks. Analyses of palaeomagnetic data obtained from a multitude of rocks of different ages reveal another feature of the Earth's magnetic field. In the early 20th century DAVID [1904] and BRUNHES [1906] identified lava flows with reversed remanence directions, i.e. magnetisations antiparallel to the ambient field. These findings led to two different competing theories: (1) Self-reversal processes in the magnetic grains cause a net magnetisation of the rock to be antiparallel to the Earth's magnetic field. (2) The Earth's magnetic field changes its polarity. Although a few cases of self-reversal have been documented, palaeo- and rockmagnetic research has convincingly demonstrated that the magnetic field indeed has switched numerous times between two stable modes: reversed and normal polarity. In addition to polarity changes, the dipole axis of the magnetic field has frequently departed for short periods from its position near the rotation axis of the Earth and moved back to resume its near-axial position. This type of behaviour is described as a geomagnetic excursion.

1.2 Polarity transitions

Reversals of the geomagnetic field are recorded in sedimentary, intrusive and extrusive igneous rocks. However, despite great advances in numerical modeling the Earth's magnetic field using the MHD theory (e.g. GLATZMAIER AND ROBERTS [1995]) the processes responsible for reversals are still not understood. Detailed palaeomagnetic records can provide crucial information on behavioural and intensity characteristics of the transitional field during a polarity reversal constraining the plethora of numerically feasible models. Even though they take several thousands of years, transitional field configurations are not more than a glimpse on geological timescales. A main problem is to identify geological sequences with a sufficiently high temporal resolution of magnetisation acquisition.

1.2.1 Palaeomagnetic records of reversals

Sediments can provide continuous records of reversals and are frequently used to analyse transitional fields. There are some drawbacks, though. First of all, it is not possible to derive absolute palaeointensities from sediments. Moreover, remanence acquisition processes in sediments are relatively complicated and lock-in of the magnetic particles is not coeval with sedimentation, resulting in a filtering of the recorded signal. Additionally, diagenesis, viscous overprints and post-detrital reorientation of the magnetic grains can bias the magnetisation (e.g. TARDUNO AND WILKINSON [1996], KOK AND TAUXE [1996] and McMILLAN ET AL. [2002]).

Igneous intrusive bodies, formed during a polarity transition, may record the transitional field as the cooling front sweeps through. However, the generally poorly constrained cooling model of intrusives makes estimates of time of remanence acquisition speculative in most cases.

Subaerial lava flows have desirable rockmagnetic properties and the remanence acquisition is almost simultaneous with the extrusion and cooling of the volcanic material. A significant advantage is the possibility to determine absolute intensities of the Earth's magnetic field at the time of their extrusion. The sporadic nature of volcanic activity, however, leads to intermittent recordings of the field. Large sequences of lava flows and a high and preferentially more or less constant extrusion rate of the flows are hence needed to obtain reliable palaeomagnetic records of the transitional field.

1.2.2 Models of geomagnetic reversals

Two classical models for the geometry of the Earth's magnetic field during a reversal have been proposed based on early palaeomagnetic data:

1. CREER AND ISPIR [1970] suggested that the dipole decays and subsequently builds up in the opposite direction during a reversal. Another possibility would be a rotation of the dipole through 180° without changes in the overall dipole moment.
2. HILLHOUSE AND COX [1976] introduced the "standing field model" which assumes that the axial dipole component of the field diminishes and changes its orientation during the reversal. Non-dipolar components remain stable according to that model and, thus, dominate the transitional field.

Models (1) and (2) cover theoretically all possible mechanisms as the field must be either dominantly dipolar or non-dipolar during a reversal. Subsequent models are therefore refinements of these early models.

3. In the "flooding model" [HOFFMAN, 1977] the underlying idea is that the reversal process floods through the liquid core emerging from one region of initiation. Zonal, i.e. rotationally axial-symmetric, components would dominate throughout the reversal [FULLER ET AL., 1979]. This concept implies that the observed transitional VGPs would move along a great circle which is defined by the geographic poles and the sampling site.
4. In recent years, numerous detailed palaeomagnetic studies of reversals were published increasing the available dataset substantially. The analysis of these records yielded some remarkable similarities in the directional data of reversals. CLEMENT [1991] suggested on the basis of sedimentary data that the transitional field is non-dipolar and that transitional virtual geomagnetic poles (VGPs) are longitudinally confined to two antipodal longitude bands (along the Americas and along East Asia) of about 60° width.
5. LAJ ET AL. [1991] and RUNCORN [1992, 1996] sustained the notion of the preferred longitudinal bands but assumed a predominantly dipolar field during polarity transitions, i.e. a rotation of the dipole axis.
6. Using lava flow data, HOFFMAN [1992, 1996] observed directional clustering of transitional VGPs falling in the same longitudinal bands and that the same clusters are occupied during different reversals. He argues that these are "hang-up" points where the transitional field spends most of its time.

7. PRÉVOT AND CAMPS [1993] also analysed the data derived from volcanic sequences and dismissed the hypothesis of cluster and preferred VGP paths concluding that there is no consistent pattern for different reversals. A reassessment of the records including more datasets and using a different statistical approach led to the conclusion that the preferred VGP paths do indeed exist [LOVE, 2000c].

Another important constraint for reversal models is the duration of the transitional field configuration. Geological and theoretical considerations on this aspect are discussed in Section 6.7.

The variability of the models described above emphasise that interpretation of reversal records is not trivial. It has already been mentioned that volcanic and sedimentary records have both inherent advantages and disadvantages possibly causing artifacts (directional clustering in volcanic, smoothing in sedimentary sequences) which obscure the real transitional field behaviour. Moreover, the question arises if non-dipole contributions to the field can really be detected by analysing VGP movements. It has to be kept in mind that a VGP is calculated under the assumption of a geocentric axial dipole (the same holds true for the virtual dipole moment, VDM). In the case of dominating non-dipolar fields this description is inadequate. Thus, a multitude of observations of the same reversal obtained from different geographic sites is necessary to provide a insight in the morphology of transitional field behaviour. Locating many different sections which cover the same reversal, recorded in sufficient resolution, and which are geographically well distributed is a difficult task.

A feature relatively well documented, but not unchallenged (see also chapter 6), are preferred longitudinal reversal paths. LAJ ET AL. [1992] proposed that these bands correlate with zones of fast seismic longitudinal wave propagation in the lower mantle. They were identified by seismic tomography and are interpreted as anomalies with high density and low temperature [BLOXHAM AND JACKSON, 1991]. Zones with an exceptionally low seismic velocity at the base of the mantle, probably due to partial melting of mantle components, show strong anti-correlation to the VGP paths. According to GUBBINS AND RICHARDS [1986], these high and low velocity zones are presumably the result of mantle convection and accumulated subducted material at the core-mantle boundary (CMB). Coupling of mantle convection and fluid flow pattern in the liquid outer core of the Earth could therefore be responsible for the confinement of transitional VGP paths to discrete longitudinal bands.

Another approach to understanding reversal processes is to model fluid dynamics in the outer core numerically. Admittedly, difficulties involved in solving the geodynamo problem are immense and require extensive computational resources. Among others, one

major reason for that is the famous "Cowling Theorem". COWLING [1934, 1957] argued that non-steady axis-symmetric magnetic fields cannot be maintained by symmetric fluid motions. Thus, models have to be three dimensional and incorporate geometry of the outer and inner core and the properties of the core-mantle boundary (see also MERRILL AND MCFADDEN [1999] for a comprehensive review on dynamo models and theoretical constraints on the parameters involved). Another reason is the smallness of key parameters like the Rossby ($R_b \ll 1$ if rotation of the core is considered) and Ekman (relative importance of frictional effects) numbers which inhibit the exclusion of short timescales for realistic models. Despite of these problems GLATZMAIER AND ROBERTS [1995] could numerically simulate a reversal using a simplified model. During the reversal the dipole moment dominates the field geometry but is reduced to 10% of its normal value. Currently, significant advances are being made in this area and important new insights can be anticipated.

Up to now, the directional data on transitional fields is equivocal and constricted to times younger than the early Paleocene. Moreover, it is still a matter of debate whether dipolar or non-dipolar components are dominant during a reversal. Despite of the experimental difficulties in determining reliable palaeointensities a broader consensus among the scientific community exists regarding the intensity of the field during a reversal. Although datasets on absolute transitional palaeointensities are still scarce they indicate that the intensity is reduced to about 25% when compared to periods of stable normal or reversed polarity [MERRILL AND MCFADDEN, 1999].

1.3 The Mesozoic dipole low

Throughout the Mesozoic persistently low virtual dipole moment values (VDM, roughly 30% – 50% of present-day values) are observed. This feature, the Mesozoic Dipole Low (MDL), was first identified by BOL'SHAKOV AND SOLODOVNIKOV [1983] and PRÉVOT ET AL. [1990] and later confirmed by TANAKA ET AL. [1995]. PERRIN AND SHCHERBAKOV [1997] demonstrated that the morphology of the field was dominantly dipolar throughout this period, and that the MDL is unlikely to be an artifact of insufficient data. This was questioned by SELKIN AND TAUXE [2000] who included submarine basaltic glass (SBG) in their dataset and claimed that no significant variations can be detected. However, it has subsequently been shown that SBGs are not necessarily reliable recorders of palaeointensity information due to partial melting of the glass during Thellier-type experiments [SMIRNOV AND TARDUNO, 2003].

SHCHERBAKOV ET AL. [2002] analysed the evolution of the Earth's VDM from the past 400 Ma statistically and could show that the distribution of the VDMs over this period

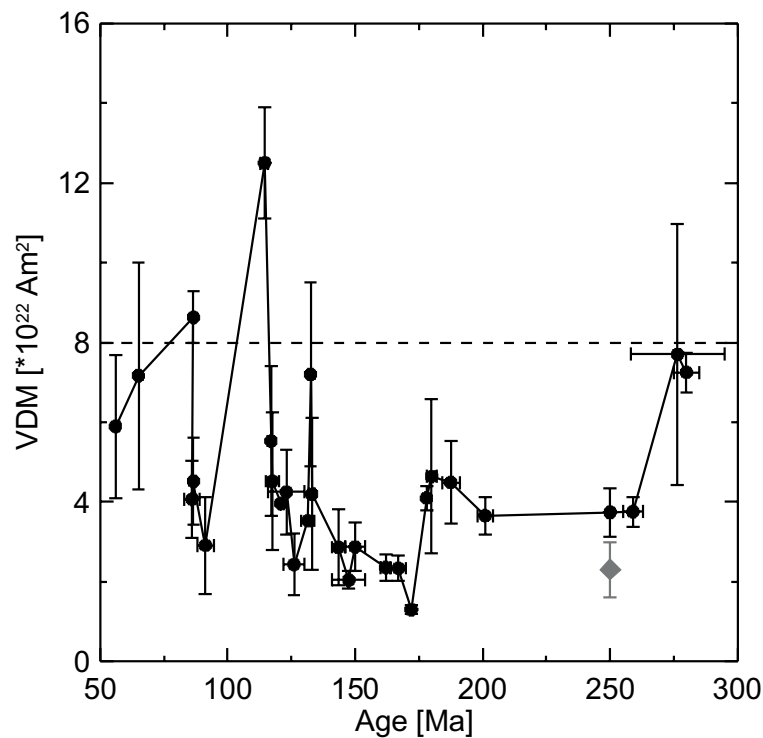


Figure 1.1: VDM against ages during the Mesozoic. For the data used and the applied selection criteria refer to appendix A. The broken line indicates the present day value; the grey diamond represents the mean VDM value obtained in this study (see chapters 5 and 6.4).

is bimodal. The distribution is described with 90% probability by a sum of two normal distributions reflecting the existence of two distinct regimes of field generations: a high intensity level with values close to today's VDM and a low intensity level (approximately half of it) as during the MDL. Their estimate for the upper and lower boundary of the MDL are 86 Ma and 276.5 Ma, respectively. However, during the MDL also high VDM values are reported (e.g. TARDUNO ET AL. [2001], GOGUITCHAICHVILI ET AL. [2002]). This suggests that long term features of the intensity record do not rule out brief periods of high or low intensity but rather reflect phases of relative dominance of either the high or the low intensity states of the Earth's magnetic field. HELLER ET AL. [2003] agree on the existence of the bimodality and propose that the relative occupancy of these states, which varies with time, is controlled by the evolution of CMB conditions. A model combining geodynamic cycles and the variation of the VDM since the early Devonian was proposed by BIGGIN AND THOMAS [2003]. They postulate that during the amalgamation of Pangea and its breakup avalanching events of subducted material from the 660 km discontinuity to the lower mantle are responsible for major mantle reorganisation processes. Subsequent accumulation of the subducted material at the CMB leads to differential thermal isolation and consequentially to changes in the convection pattern in the outer core. The variation of the VDM in this four-stage model is, therefore,

a result of a chain of geodynamic processes, beginning with plate reorganisation at the Earth's surface leading to fundamental changes in the dynamics of the outer core. An observation supporting the hypothesis of major mass rearrangement is a slowed despinning rate of the Earth's rotation between 250 and 100 Ma [DENIS ET AL., 2002]. Due to paucity of VDM data in key time periods, however, this model is still to be regarded as speculative.

1.4 Scientific aims

The Siberian Trap Basalts (STB) provide the possibility to address some of the problems outlined above. The short duration of the volcanic activity and the extremely high productivity makes this large igneous province (LIP) an excellent sequence for deciphering the fine structure of the Earth's magnetic field at the Permo-Triassic (P/T) boundary with high temporal resolution. The following aspects are the aims of this study:

1. Detailed investigations of polarity transitions are scarce and still limited to the Cenozoic. Therefore, a thick sequence of successive lava flows was sampled in order to gain new insights in reversal processes and to determine whether there are characteristic features of the palaeodirectional and -intensity records as observed in younger reversals.
2. The lower boundary of the Mesozoic dipole low is currently defined by palaeointensity studies which did not incorporate self-consistent quality checks during the course of the palaeointensity experiments. New accurate and reliable palaeointensity data are therefore urgently needed to study this important geomagnetic phenomenon.
3. Self-reversal of the remanent magnetisation was supposed to be widespread in the STB [METALLOVA AND FEINBERG, 1967]. Rockmagnetic investigations play thus an important role in assessing the reliability of the palaeomagnetic record. This holds especially true for palaeointensity studies.
4. The extrusion age of the STB straddles the P/T boundary and is thus coincident with the greatest extinction event in Earth's history. It has been proposed (e.g. CAMPBELL ET AL. [1992]) that the emplacement of this huge volume of volcanic rocks and the associated emissions of ashes and gases triggered catastrophic changes of the palaeoclimate. The biological impact of the volcanic activity, however, depends crucially on the duration of the volcanic activity. Absolute dating methods are unable to answer this question unequivocally. To provide further constraints on the duration of the record a reliable and complete magnetostratigraphy covering the whole volcanic sequence has to be established.

Chapter 2

The Siberian Trap Basalts

2.1 Geological Setting

The Siberian Trap Basalts (STB) on the north-western margin of the Siberian platform are the largest terrestrial continental igneous province (LIP) known on Earth. A tectonically deformed remnant of the traps, separated from the Siberian platform by the E-W trending Yeniseij-Khatanga trough, outcrops on the Taimyr peninsula (Fig. 2.1). The basalts unconformably overlie Proterozoic to Late Permian sediments (siltstone, sandstone, conglomerates and coal deposits). Today, the STB and the related tuffs and intrusions occupy roughly $1.5 \times 10^6 \text{ km}^2$ of the Siberian platform [ZOLOTUKHIN AND AL'MUKHAMEDOV, 1988]. The basalts alone are exposed over an area of $\approx 0.3 \times 10^5 \text{ km}^2$ [FEDORENKO ET AL., 1996] but their initial extent was probably much greater. Recently, KRAVCHINSKY ET AL. [2002] have shown that many of the basalts from the eastern part of the Siberian platform exhibit similar palaeomagnetic directions and ages as the bulk of the STB in the Tunguska basin. They correspond probably to an early, highly explosive phase of the Trap volcanism. Data from the Tyumenskaya (SG6) borehole [WESTPHAL ET AL., 1998] and results of REICHOW ET AL. [2002] show that the volcanic province extends far into the West Siberian Basin where the basalts are covered by Meso- and Cenozoic sediments thus increasing the area of the province even more (Fig. 2.1). Magmatic rocks from Central Kazakhstan studied by LYONS ET AL. [2002] have the same age as the STB and are assumed to be genetically linked to the STB. A maximum estimate for the whole STB-related volcanism yields an area in excess of $4 \times 10^6 \text{ km}^2$ (volume $> 3 \times 10^6 \text{ km}^3$, COURTILLOT AND RENNE [2003]).

The lava pile on the Siberian platform is up to 3 to 4 km thick in the NW and thins out to the SE, where the sequence is only tens of metres thick [ZOLOTUKHIN AND AL'MUKHAMEDOV, 1988]. No significant intercalated sedimentary rocks or palaeosols are present, providing prima facie evidence of the rapid formation of this volcanic province (e.g. SHARMA [1997]). Tuffs are distributed widely throughout the Tunguska basin. In the centre of the basin the pyroclastic deposits reach a maximum thickness of

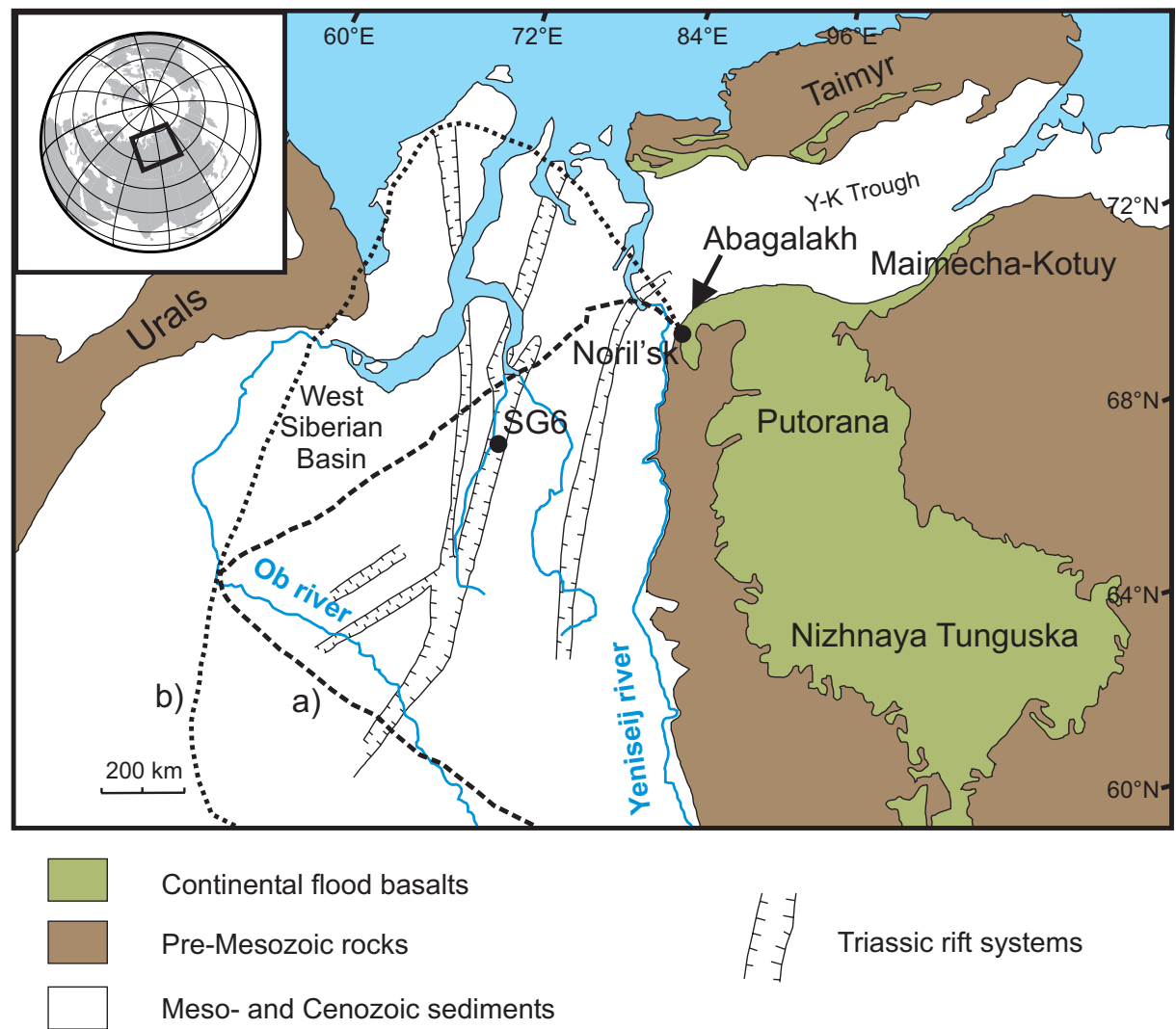


Figure 2.1: Geological outline of North-Western and Central Siberia (modified after WEST-PHAL ET AL. [1998]). a) and b) represent minimum and maximum estimates of the extent of the West Siberian Trap Basalts [REICHOW ET AL., 2002], respectively. The subprovinces, borehole SG6 and the sampling location Abagalakh are also indicated. Y-K denotes the Yeniseij-Khatanga Trough.

700 m, whereas lavas dominate the sequence in the north and in the west [SHARMA, 1997].

The province is generally subdivided broadly into distinct geographical regions shown in Figure 2.1: (1) Noril'sk, (2) Putorana, (3) Nizhnaya-Tunguska, (4) Maimecha-Kotuy and (5) Taimyr. The flood basalts in the Noril'sk area represent a particularly thick sequence with a high ratio of lavas to tuffs [FEDORENKO ET AL., 1996]. Due to the occurrence of rich Cu-Ni sulfide deposits in the Noril'sk region, the volcanic sequence has been studied extensively and good geochemical data are available. Lavas of the Noril'sk sequence vary in composition from trachybasalts and basaltic andesites to picritic basalts

and are divided into 11 suites (Tab. 3.1) on the basis of their chemical composition and texture (e.g. SHARMA [1997], LIND ET AL. [1994]). The lower part of the Siberian Trap Basalt province is nowhere else exposed with such a high resolution. The majority of the Putorana rocks are relatively homogeneous tholeiitic basalts, whereas in the Nizhnaya-Tunguska region tuffs are the dominating volcanic deposits. A wide variety of basic to ultrabasic volcanic rocks is found in the Maimecha-Kotuy region [FEDORENKO ET AL., 1996].

2.2 Age and duration of the Siberian Trap volcanism

CAMPBELL ET AL. [1992] dated zircons using the U-Pb method (SHRIMP ion microprobe) and obtained an age of 251.1 ± 3.6 Ma for an intrusion in the lower part of the volcanic sequence. Precise U-Pb zircon and baddeleyite ages (251.2 ± 0.3 Ma, KAMO ET AL. [1996]) and $^{40}\text{Ar}/^{39}\text{Ar}$ data (250.0 ± 1.6 Ma, RENNE ET AL. [1995]) place the onset of the volcanic activity, within margin of error, at the Permo-Triassic (P/T) boundary. An extensive compilation of STB $^{40}\text{Ar}/^{39}\text{Ar}$ dates (including also the results of RENNE AND BASU [1991], DALRYMPLE ET AL. [1995] and BASU ET AL. [1995]) is presented by REICHOW ET AL. [2002] (Fig. 2.2). The P/T boundary has been dated using ash layers in the reference sections of Meishan and Shangsi (both in South China) immediately above and below the palaeontological boundary. U-Pb ages on zircon of CLAUÉ-LONG ET AL. [1991] (251.2 ± 3.4 Ma) and BOWRING ET AL. [1998] (251.4 ± 0.3 Ma) of these ash layers agree very well. $^{40}\text{Ar}/^{39}\text{Ar}$ on sanidine yielded 250.0 ± 0.2 Ma for the P/T boundary [RENNE ET AL., 1995]. Comparison of ages derived from different radioisotopic systems is often quite problematic. It is therefore important to date both the Chinese ash layers and the STB samples with the same method and to refer them to the same standards. Doing so, RENNE ET AL. [1998] concluded that the difference between the two is in the order of 0 ± 0.4 Ma which puts beyond reasonable doubt that the peak activity of the Siberian Trap volcanism and the P/T boundary are synchronous.

Geological evidence and radiometric ages suggest that the Traps erupted during an extremely short time interval of only 0.9 ± 0.8 Ma [RENNE AND BASU, 1991]. CAMPBELL ET AL. [1992] estimates that the duration was even shorter (0.6 Ma). VENKATESAN ET AL. [1997] confirmed a short duration of less than 1 Ma (after recalibration to the same standard as the aforementioned $^{40}\text{Ar}/^{39}\text{Ar}$ dates [COURTILLOT AND RENNE, 2003]). Given the size, the short duration, and the simultaneity of this catastrophic volcanic activity and the P/T crisis it is very likely that this event triggered and certainly contributed to the greatest mass extinction in Earth's history. COURTILLOT AND RENNE [2003] demonstrate persuasive evidences for the correlation of LIP emplacement, like the Central Atlantic Magmatic Province (end of the Triassic) and the Viluy traps (end

Devonian), and major Phanerozoic mass extinctions. However, COURTILOT [1999] points out that the biological response to catastrophic events like the formation of the STB depends not only on the duration and violence of the volcanic activity but also on many factors as the palaeogeographic arrangement of the continents, the climate and the sea level at that time. Moreover, eruption volumes alone do apparently not correlate with extinction intensity. Thus, a critical volume is probably needed to trigger changes beyond the direct climatic consequences of the volcanic activity (like e.g. acid rain, drop in temperature followed by global warming due to the greenhouse effect). Such further changes could be the release of gas hydrates caused by global warming multiplying the climatic impact of the event [WIGNALL, 2001].

Another theory for the cause of the P/T crisis postulates the impact of a massive bolide such as that widely accepted for the Cretaceous/Tertiary boundary. BECKER ET AL. [2001] found in fullerenes from sediments at the P/T boundary trapped helium and argon with isotope ratios similar to the planetary component of carbonaceous chondrites. However, the search for iridium anomalies usually associated to such an event remains inconclusive so far (e.g. RETALLACK ET AL. [1998]). The idea that an impact caused the P/T mass extinction thus has yet to be substantiated.

2.3 Origin of the Siberian Trap Basalts

At present, no general model for the generation of the STB has been proposed that would satisfy all observation and inferences that must be accounted for [SHARMA, 1997]. Isotopic data suggest that all the magmatic rocks in Northern Siberia may have originated from the same part of the mantle [FEDORENKO ET AL., 2000]. Two fundamentally distinct classes of models are discussed in the literature. The idea that the LIPs form in response to the ascent of a deep mantle plume originating from the CMB was expressed by e.g. RICHARDS ET AL. [1989]. COURTILOT ET AL. [1999] refined this model for the STB. They drew attention to the close correlation between phases of (aborted) rifting in the Late Permian/Early Triassic at the western margin of the STB and the volcanic activity, and suggested that this rifting was triggered by an upwelling mantle plume. NIKISHIN ET AL. [2002] agreed on the interpretation of a short lived (less than 10 Ma) plume as a source of the erupted and intruded material. Yet, they reverse the causality of the events and claim that global plate kinematics, i.e. the assembly of Pangea, was associated with a reorganisation of the global mantle convection system. This would have had a bearing on the development of major mantle plumes and, to a degree, also on the pattern of related flood basalt magmatism. Their model favours a preexisting rift system which was later penetrated by a plume. CZAMANSKE ET AL. [1998] dismiss the existence of

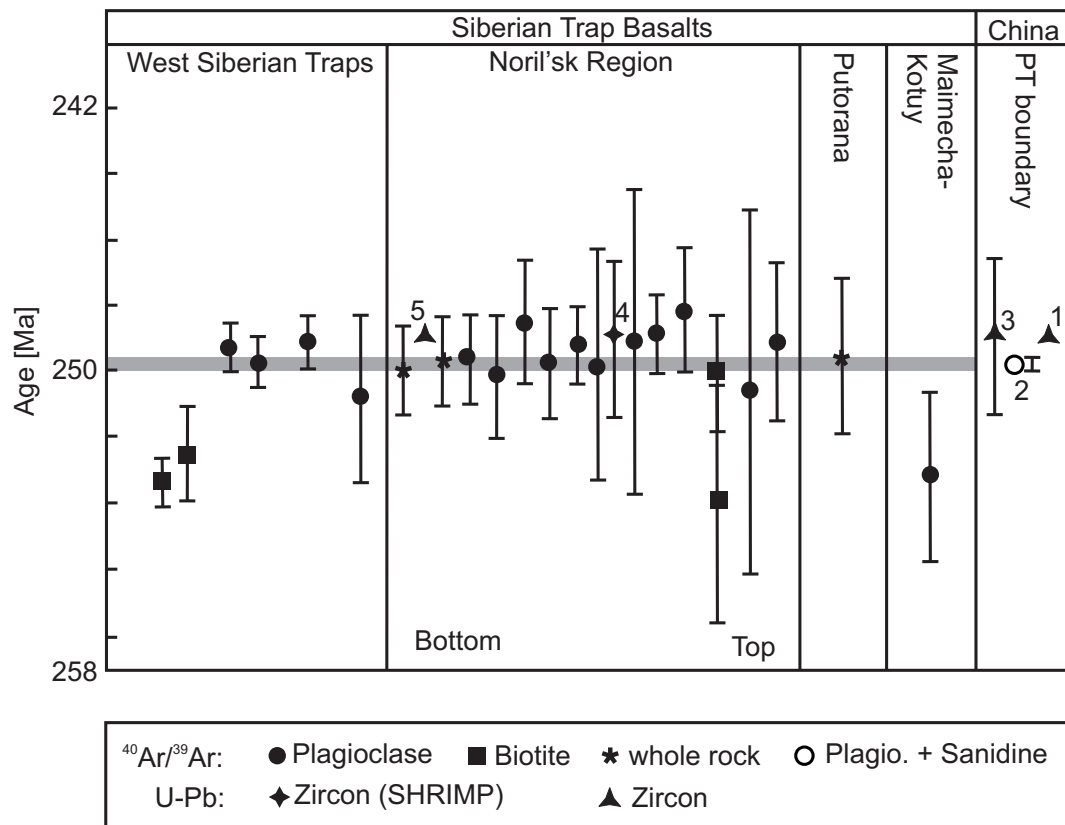


Figure 2.2: Compilation of published $^{40}\text{Ar}/^{39}\text{Ar}$ ages of the Siberian Traps (modified after REICHOW ET AL. [2002]). Numbers 1 [BOWRING ET AL., 1998], 2 [RENNE ET AL., 1995] and 3 [CLAOUÉ-LONG ET AL., 1991] refer to age determinations of ash layers immediately above and below the palaeontological Permo-Triassic boundary in the reference sections of Meishan and Shangsi (South China). The grey bar is the proposed age window of the P/T boundary according to RENNE ET AL. [1995]. 4 denotes an U-Pb SHRIMP age of CAMPBELL ET AL. [1992], whereas 5 refers to the age determination (error smaller than symbol size) of an intrusion in the lower part of the Traps [KAMO ET AL., 1996].

this plume. Their line of argument is based on very moderate uplift observed at the sedimentary/volcanic interface at the base of the lava pile. Hot, plume-related material in the upper mantle, however, would lead to significant uplift at the surface due to thermal expansion. Hence, they postulate that the magma derived from convective partial melting which was subsequently released by lithospheric shear and related, localised extension.

Chapter 3

Palaeomagnetic Results

3.1 Sampling

Three sections have been sampled in order to obtain a complete stratigraphic coverage of the STB in the Noril'sk area (see also HEUNEMANN ET AL. [2003]). The Talnakh section, located approximately 9 km E of Talnakh (Fig. 3.1), was sampled in 2000. It comprises 7 flows of the Ivakinsky suite and the lowermost part of the Syverminsky suite (Fig. 3.3 and 3.4). The Ivakinsky suite, being the oldest suite of the STB in the Noril'sk area, directly overlies Late Permian sediments of the Tunguska Series. A parallel profile in the Listvjanka river valley close to the Talnakh section was studied in the following year. Here, 20 consecutive flows from the Ivakinsky up to the top of the Gudchikhinsky suite were sampled (Fig. 3.2). Outcrops along the Listvjanka river are of excellent quality and boundaries between flows could be easily identified. The Abagalakh and its directly underlying continuation, the Icon section, both about 130 km NE of Noril'sk, were sampled during the Summers of 2000 and 2001. The combined Abagalakh/Icon section is referred to below as Abagalakh section. It is situated at the northern rim of the Putorana Plateau. Here a total of 59 flows was sampled from the Tuklonsky up to the top of the Kunginsky suite (Tab. 3.1). Stratigraphically lower suites are present in the Abagalakh section but were not sampled due to unclear bedding and very poor outcrop quality. The composite section covers practically the whole pile of volcanics in the Noril'sk area. Minor stratigraphic gaps (some tens of meters) are present in the Abagalakh section. The only significant stratigraphic gap (max. 130 m) is the Khakanchansky suite which is absent in both the Listvjanka and the Abagalakh section. The lava flows are mainly tholeiitic or alkaline to subalkaline basalts with a thickness from 3 to 45 m. A compilation of the suites sampled is given in Table 3.1.

Table 3.1: Volcanic suites in the Noril'sk area and sections sampled^a.

Suite	Petro.	bedding (DD/D) [†] [°/°]	thickn. [m]	Section (number of flows)		
				Talnakh (69°28'N, 088°32'E)	Listvjanka (69°28'N, 088°43'E)	Abagalakh (70°22'N, 090°04'E)
Samodsy (Sm)	Th	—	—	—	—	—
Kumginsky (Km)	Th	145/09	192	—	—	7
Kharaelakhsky (Hr)	Th, ASA	145/10	291	—	—	8
Mokulaevsky (Mk)	Th	145/13	380	—	—	13
Morongovsky (Mr)	Th, ASA, Tf	152/14	297	—	—	11
Nadezhdinsky (Nd)	Th, ASA, Tf	152/14	369	—	—	15
Tuklonsky (Tk)	Th	152/14	42	—	—	5
Khakanchansky (Kh)	Tf	—	—	—	—	—
Gudchikhinsky (Gd)	Th, P	009/12	92	—	5	—
Syverminsky (Sv)	Th, ASA	009/12	66	3	11	—
Ivakinsky (Iv)	ASA, Th	009/12	66–97	4	4	—

^a Given are the names of the suites in the Noril'sk area, their main petrographical composition (Th: tholeiitic basalts, ASA: alkaline to subalkaline basalts, Tf: Tuff, P: picrites), the approximate thickness (thickn.) of the suites as observed in the field, and number of flows sampled per suite.

[†]bedding data used for bedding correction is specified by the direction of dip (DD) and the dip angle (D).

At least six samples were taken per flow with a petrol-powered portable drill. Cores were oriented using a magnetic, and whenever possible, a sun compass ($\approx 75\%$ of the cores). Outcrop situation permitting, samples were taken in the lower or middle part of the lava flows. The upper parts were avoided to prevent sampling of units which were reheated by the following flow. Several flows consisted of individual blocks separated by erosional debris. Here, at least three independent blocks were sampled in order to check the internal consistency of the palaeodirectional results. Tuff layers, mostly less than a few tens of centimetres thick, are generally poorly exposed and were not sampled due to the bad quality of these outcrops. Some flows, identified as independent units, were not sampled as they consisted merely of debris, or were not accessible. Minor tilts of the basalt flows, not exceeding 15° and dipping to the north (Talnakh and Listvjanka) or southeast (Abagalakh), were determined directly in the field or using aerial photographs (V. RAD'KO, personal communication and own observations). In some cases bedding could be measured at contacts between individual lava flows. Dip angles decrease with increasing stratigraphic height. This observation is consistent with subsidence during emplacement due to the load of the accumulating lava pile. This in turn results in a slight burial metamorphism which does not exceed zeolite facies [LIGHTFOOT ET AL., 1990].

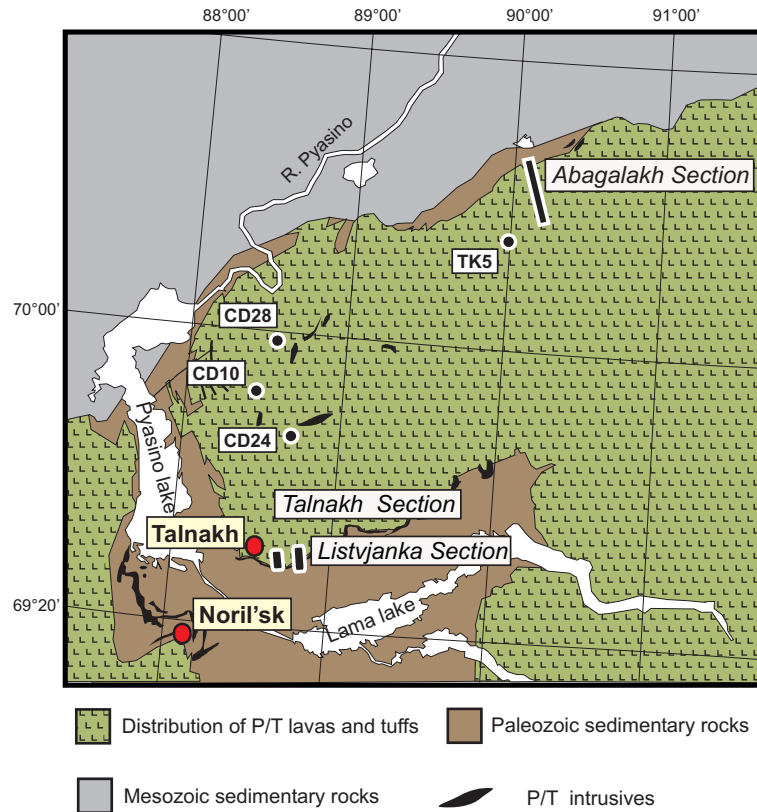


Figure 3.1: Simplified geological map of the Noril'sk area (modified after GUREVITCH ET AL. [2003]). The Listvjanka and Talnakh sections are close to the town of Talnakh NE of Noril'sk. Another section was sampled along the northern rim of the STB the Abagalakh and Icon river valley. The dots indicate the location of boreholes. Magnetostratigraphic results of these boreholes are presented in chapter 3.6.

3.2 NRM demagnetisation

All samples measured (almost 700) have been demagnetised stepwise either thermally (TH) up to their respective Curie-temperature or by alternating field (AF) up to 200 mT with an average of 15 steps. About 150 of these samples were measured in the palaeomagnetic laboratory of the VNIGRI in St. Petersburg (Russia) by Evgenii Gurevitch using a JR5 spinner magnetometer. The rest of the samples was studied in the palaeomagnetic laboratory of the Department of Earth and Environmental Sciences (Geophysics Section, Ludwig-Maximilians-Universität München) in Niederlippach. Demagnetisation (Schoenstedt and ASC TD48 furnaces, 2G AF system) and measurement (2G cryogenic and Molspin magnetometers) equipment is housed in a magnetically shielded room. Inter-laboratory comparison prove the very good coherence of the results. AF and thermal demagnetisation showed to be equally effective in determining the characteristic

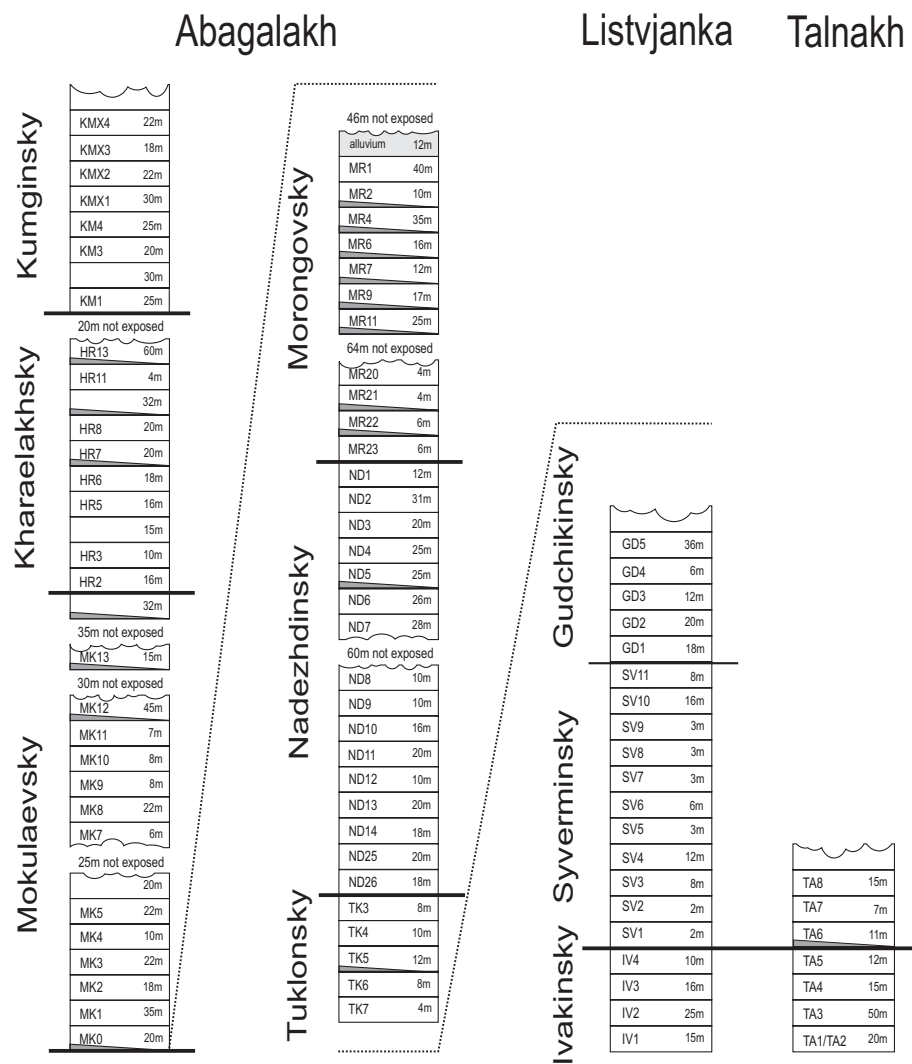


Figure 3.2: Stratigraphy of the sampled sections. Shown are the name of the individual flows and their approximate thickness. Grey wedges denote tuff layers (not sampled). Some flows could be identified but were not accessible.



Figure 3.3: Outcrop of the Ivakinsky suite in the Talnakh section. The waterfall cuts through the lowermost two flows of the section. Palaeozoic sedimentary rocks are found below.



Figure 3.4: Well preserved surface of flow TA1-2 (Talnakh section). Clearly visible are the typical surface structures of a Pahoehoe-flow.

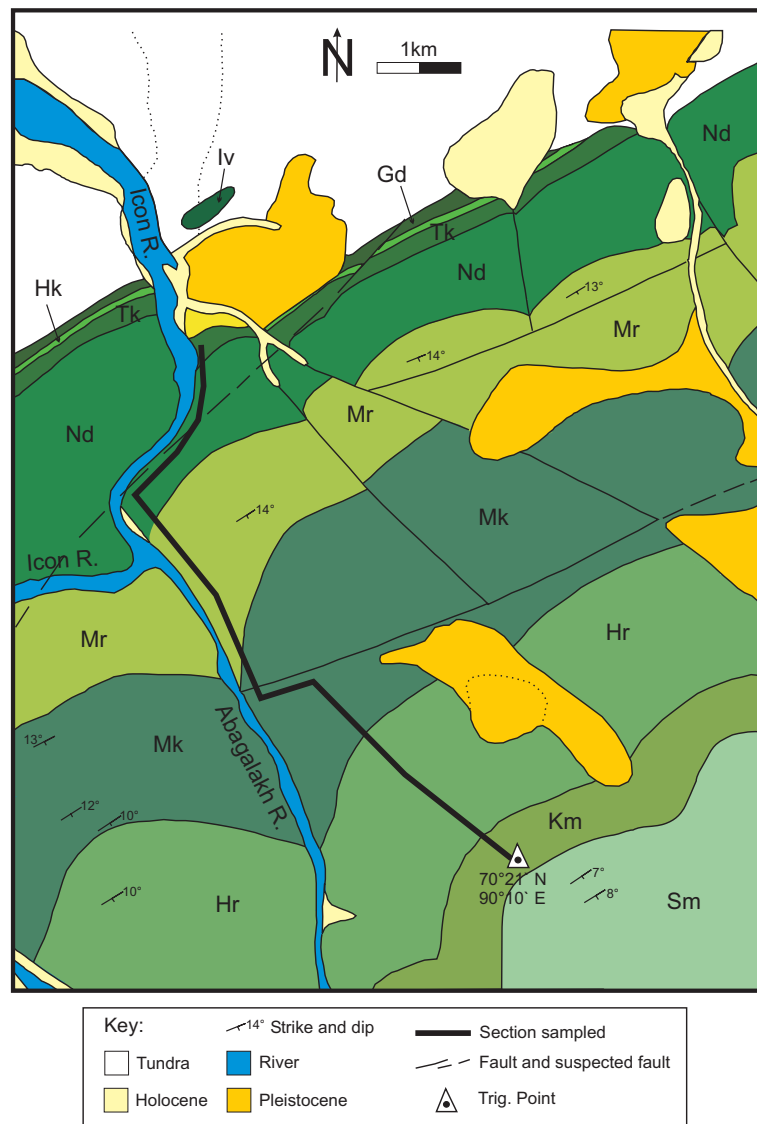


Figure 3.5: Geological map of the Abagalakh/Icon river valley (modified after V. RAD'KO, personal communication). Green colours denote the different suites of the P/T volcanics. Abbreviation of the individual suites is given in Tab. 3.1.

remanent magnetisation (ChRM). During stepwise thermal demagnetisation, mineral alteration was monitored by measuring the low field susceptibility at room temperature with a KLY-2 kappa bridge. Results of the stepwise demagnetisation experiments were plotted using equal area stereographic and orthogonal projections [ZIJDERVELD, 1967]. Linear trajectories were identified by eye and subjected to principal component analysis [KIRSCHVINK, 1980]. A few samples yielded no stable endpoints and were, therefore, analysed using the great-circle technique [MCFADDEN AND MCELHINNY, 1988]. FISHER [1953] statistics was used to calculate flow mean directions and the associated statistical parameters.

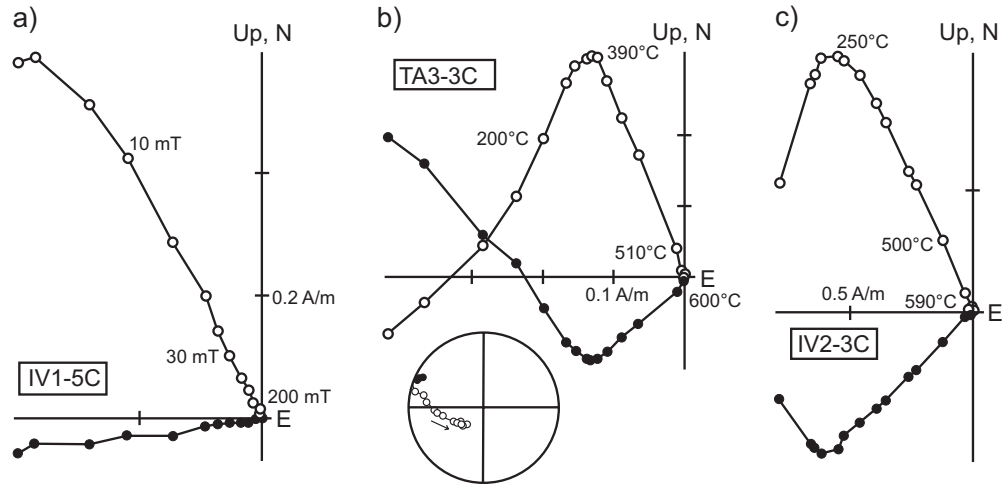


Figure 3.6: ZIJDERVELD [1967] plots of representative samples of reversed polarity (bedding corrected). Open symbols correspond to the projection onto the vertical plane, solid symbols onto the horizontal plane. Typically, the overprint is moderate and is easily removed. In (a) the ChRM is defined by the linear segment between 10 and 70 mT. Figure (b) shows a sample with relatively strong overprint up to 390°C. The stereographic projection reveals that the direction of the magnetisation moves along a great circle before reaching a stable endpoint. This is indication for an overlap of the ChRM and the overprint in T_{ub} at lower temperatures. Usually, the overprint, if present, is removed between 250 and 350°C (see c).

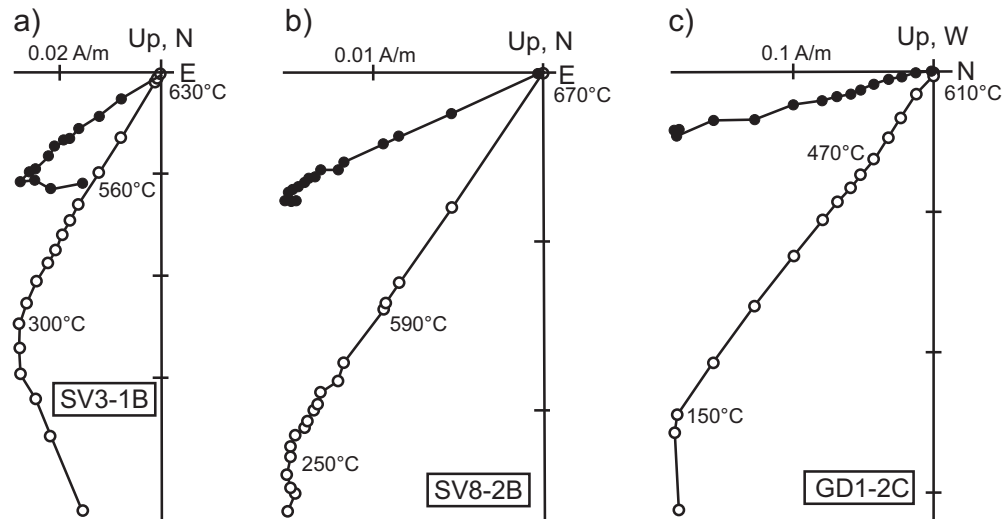


Figure 3.7: Demagnetisation behaviour of samples which recorded transitional field configuration (bedding corrected). As already shown in Fig. 3.6 a secondary overprint can be removed and the ChRM isolated. Note the high T_{ub} of the NRM (670°C) in sample SV8-2B (b). In this case two different magnetic phases, magnetite and hematite, carry identical directions which are both primary (see also Fig. 3.8 and chapter 4).

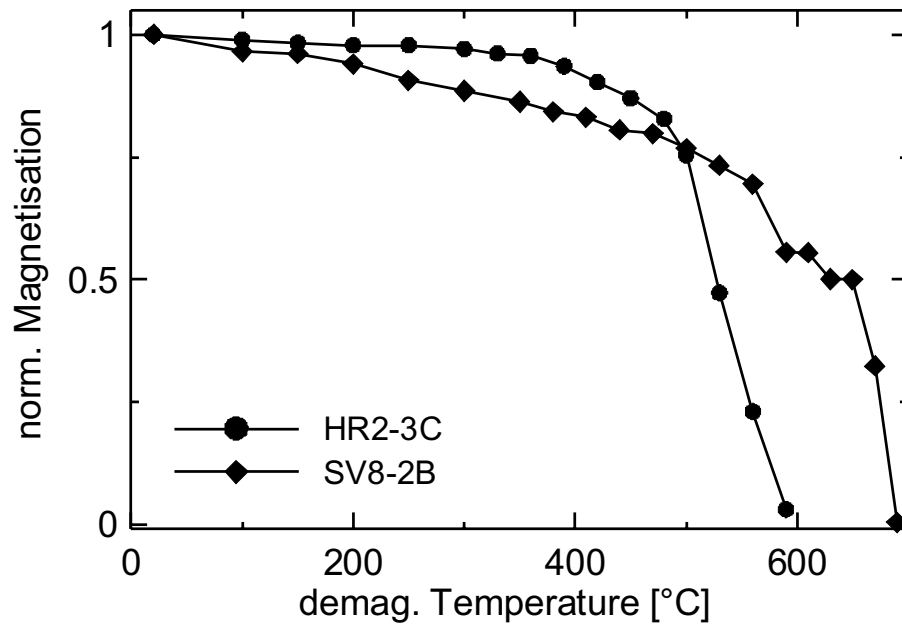


Figure 3.8: Intensity of NRM versus peak temperature of the thermal demagnetisation step. Sample SV8-2B exhibits two different magnetic phases with maximum T_{ub} of 590°C and $\approx 670^{\circ}\text{C}$. Both phases carry identical ChRM directions (Fig. 3.7). The results of a sample containing solely magnetite are depicted for comparison.

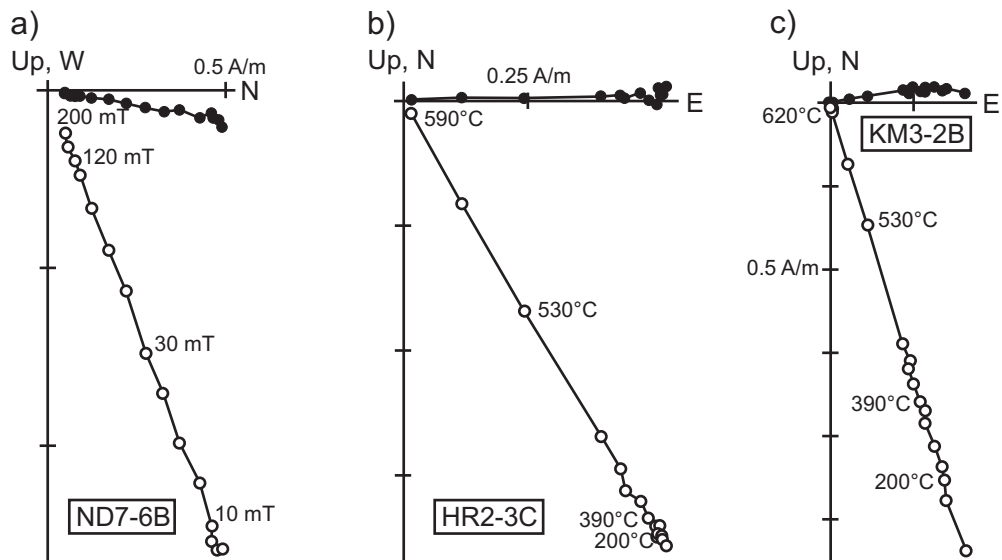


Figure 3.9: (a) Example of a sample with a direction related to group C (excursion). (b) and (c) belong to flows of the stable normal part of the section. Overprints are rarely observed in the higher stratigraphic levels of the section. All results are bedding corrected.

Table 3.2: (continued)

Site	n/N	Geogr.		Strat.		k	α_{95} [°]	VGP		Gr.
		Dec [°]	Inc [°]	Dec [°]	Inc [°]			Long. [°]	Lat. [°]	
KM3	7 / 9	44	73	75	73	510	2.7	162	59	D
KM1	7 / 8	41	72	69	72	273	3.7	169	59	D
HR13	9 / 9	9	77	59	81	148	4.2	146	72	D
HR11	8 / 8	19	71	50	75	156	4.4	179	69	D
HR8	0 / 6	—	—	—	—	—	—	—	—	—
HR7	8 / 10	62	77	96	73	71	6.6	148	51	D
HR6	6 / 8	92	71	109	64	1071	2.0	146	36	D
HR5	7 / 9	84	72	105	66	114	5.8	148	40	D
HR3	9 / 9	72	57	85	53	166	4.0	172	33	D
HR2	8 / 9	77	66	94	61	476	2.5	160	38	D
MK13	8 / 8	56	76	95	71	466	2.6	150	49	D
MK12	8 / 8	64	76	100	70	108	5.5	148	46	D
MK11	7 / 8	34	78	90	76	306	3.7	146	58	D
MK10	10 / 10	59	70	89	66	53	6.7	161	45	D
MK9	9 / 9	39	66	68	67	233	3.4	178	53	D
MK8	10 / 10	27	82	106	79	161	3.8	131	57	D
MK7	7 / 7	31	80	95	77	218	4.1	140	58	D
MK5	10 / 10	358	84	123	82	94	5.0	117	59	D
MK4	8 / 9	26	72	66	74	316	3.1	169	62	D
MK3	10 / 10	43	76	84	72	455	2.3	157	54	D
MK2	9 / 9	208	85	161	75	344	2.8	102	42	D
MK1	9 / 9	21	89	141	78	152	4.2	113	50	D
MK0	10 / 10	57	81	110	75	353	2.6	135	50	D
MR1	9 / 9	37	82	117	77	512	2.3	127	53	D
MR2	7 / 8	29	82	115	78	285	3.7	127	55	D
MR4	8 / 9	23	73	73	76	252	3.6	157	63	D
MR6	7 / 10	44	76	96	74	390	3.1	147	53	D
MR7	10 / 10	28	76	89	77	306	2.8	144	59	D
MR9	7 / 9	298	82	187	82	441	2.9	87	54	D
MR11	9 / 10	355	84	136	81	676	2.0	111	56	D
MR20	6 / 6	26	78	98	78	1064	2.1	137	59	D
MR21	6 / 6	19	78	91	80	325	3.7	137	62	D
MR22	6 / 6	22	74	77	77	619	2.7	152	63	D
MR23	4 / 4	30	76	91	77	253	5.8	144	58	D
ND1	8 / 9	48	76	100	73	1412	1.5	144	51	D
ND3	7 / 7	359	71	40	81	802	2.1	153	77	D
ND4	8 / 8	25	72	72	75	156	4.4	159	62	D
ND5	7 / 7	21	66	54	72	1110	1.8	183	64	D
ND6	7 / 7	359	58	14	69	778	2.2	242	72	C
ND7	8 / 8	351	59	4	72	611	2.2	261	76	C
ND8	8 / 8	12	60	35	69	401	2.8	212	66	C
ND9	8 / 9	8	58	28	67	389	2.8	223	66	C
ND10	7 / 8	1	58	18	69	281	3.6	237	70	C
ND11	6 / 6	355	54	7	66	444	3.2	258	68	C

Table 3.2: (continued)

Site	n/N	Geogr.		Strat.		k	α_{95} [°]	VGP		Gr.
		Dec [°]	Inc [°]	Dec [°]	Inc [°]			Long. [°]	Lat. [°]	
ND12	8 / 9	0	55	14	66	464	2.6	245	67	C
ND13	8 / 8	356	57	10	69	191	4.0	251	71	C
ND14	10 / 10	5	54	20	65	94	5.1	238	64	C
ND25	6 / 6	13	55	31	64	54	9.2	222	61	C
ND26	10 / 11	19	54	38	62	310	2.7	215	57	C
TK3	8 / 8	6	59	26	69	60	7.2	223	69	C
TK4	8 / 8	359	64	23	75	230	3.7	210	78	C
TK5	8 / 8	11	61	35	70	90	5.9	208	68	C
TK6	9 / 10	22	72	67	75	143	4.3	164	63	–
TK7	10 / 10	21	74	76	77	542	2.1	152	63	–
GD5	5 / 5	129	71	94	73	538	3.3	146	52	–
GD4	5 / 7	97	53	82	51	109	7.4	174	33	–
GD3	7 / 7	129	53	114	58	172	4.6	143	28	–
GD2	7 / 7	147	61	127	69	225	4.0	127	37	–
GD1	8 / 8	154	46	145	55	91	5.9	118	18	B
SV11	6 / 7	161	48	153	58	174	5.1	111	20	B
SV10	6 / 6	158	43	151	53	491	3.0	114	15	B
SV9	4 / 5	166	40	161	50	147	7.6	105	11	B
SV8	6 / 6	162	46	155	56	128	5.9	110	18	B
SV7	6 / 6	156	46	148	56	240	4.3	116	18	B
SV6	7 / 7	159	45	152	54	116	5.6	113	16	B
SV5	5 / 6	157	44	149	54	448	3.7	116	16	B
SV4	8 / 8	161	46	153	55	107	5.4	111	17	B
SV3	7 / 7	155	39	148	48	122	5.5	117	12	B
SV2	5 / 6	157	48	148	58	129	6.8	115	20	B
SV1	8 / 8	160	46	152	55	136	4.9	112	17	B
IV4	0 / 10	–	–	–	–	–	–	–	–	–
IV3	5 / 5	291	-71	258	-70	318	4.4	343	-51	A
IV2	8 / 8	258	-68	236	-62	143	4.6	12	-52	A
IV1	6 / 6	287	-66	261	-65	396	3.4	346	-46	A

^aThe results are in stratigraphic order from top (KMX4) to bottom (IV1). n/N denotes the success rate, which is the number of samples used for calculation of the mean flow direction (n) versus the number of samples demagnetised (N); Geogr.: geographic coordinates, Strat.: stratigraphic coordinates, Dec. and Inc. denominate declination and inclination, respectively; k is the precision parameter and α_{95} the aperture angle of the 95% confidence cone [FISHER, 1953]. k and α_{95} are identical for geographic and stratigraphic coordinates as there is no within site variation of bedding parameter. Given also are also the associated VGP longitude/latitude values. Gr. Indicates the group of directions the individual flow belongs to (see text).

Table 3.3: Mean characteristic directions of the Talnakh section^a

Site	n/N	Geogr.		Strat.		k	α_{95} [°]	VGP		Gr.
		Dec [°]	Inc [°]	Dec [°]	Inc [°]			Long. [°]	Lat. [°]	
TA8	8 / 9	156	49	146	58	104	5.4	116	21	B
TA7	8 / 8	158	39	152	49	71	6.6	113	11	B
TA6	6 / 7	171	45	166	56	25	13.8	100	16	B
TA5	4 / 4	198	-72	195	-61	5891	1.2	65	-62	–
TA4	8 / 9	322	-73	280	-78	57	7.5	314	-56	A
TA3	7 / 8	263	-72	236	-66	99	6.2	7	-56	A
TA1-2	0 / 14	–	–	–	–	–	–	–	–	–

^a For the legend and the description of the given values see Table 3.2

3.3 Palaeomagnetic Record

Bedding corrected inclination and declination data are plotted versus stratigraphic position in Figure 3.10. The composite Listvjanka/Abagalakh section (black dots) is characterised at its bottom by steep negative inclinations around -68° (declination 251°) recorded by the flows of the Ivakinsky suite (group A). Following group A, a succession of 11 flows (flows SV1 to GD1) have positive inclinations. Their directions are evidently not antipodal to those of the Ivakinsky suite, having inclinations around $+54^\circ$ and declinations of 151° . The same pattern, i.e. the departure from a reversed to a intermediate direction, is observed in the Talnakh section (open red symbols). Remarkably, the results of the Talnakh section resemble the directional clustering very well. This reproducibility makes a good case for a geomagnetic origin of the feature and not for an artifact due to insufficient removal of secondary components. The intermediate cluster (group B) is formed by SV1 to GD1 and TA6 to TA8, in total 14 flows. Flow TA5 plots between group A and group B. Following the directional clustering the directions of the next flows shift towards those expected for normal polarity (GD2 to GD5). No data are available for the Khakanchansky suite. However, palaeomagnetic results from boreholes situated close to the surface section indicate that no major variation in inclination is to be expected for the period covered by this suite (see chapter 3.6). The directions of the first two flows of the Tuklonsky suite superjacent to the Khakanchansky suite, are also similar to values of normal polarity. The following 14 flows from TK5 to ND6 form a well defined group (C, Dec.: 22° , Inc.: $+68^\circ$) which differs significantly from directions of normal polarity. All flows from flow ND5 to KMX4, the stratigraphically topmost unit sampled, are of normal polarity and are referred to as group D. The mean direction of this group yields a declination of 88.5° and an inclination of $+75.4^\circ$. The four groups are also readily identified when all flow mean directions are plotted in a

stereogram (Fig. 3.11). Individual flows not included in one of the groups are identified by their name. Including GD2 to GD5, and TK6 and TK7 yields no significantly different mean direction for group D (Dec.: 89.3° , Inc.: $+74.2^\circ$, k : 65.3, α_{95} : 2.6°). Moreover, the mean of these six flows (Dec.: 95.2° , Inc.: $+68.2^\circ$, α_{95} : 11.4°) is at a 95% confidence level indistinguishable from group D, admittedly due to the large α_{95} . Therefore, it is likely that between group B and the group C the Earth's magnetic field established normal polarity for a brief period. It is preferred, however, not to add these individual flow means to group D but rather adhere to a sequential interpretation of the data in a stratigraphical sense. In this interpretation these six flows represent a movement towards normal polarity (GD2 to GD4) followed by a movement in direction towards the excursions cluster. The declination and inclination values of the individual groups, the associated statistical parameters and their VGPs are listed in Table 3.4.

Table 3.4: Mean directions of the observed directional groups^a

Group	N	Dec [$^\circ$]	Inc [$^\circ$]	k	α_{95} [$^\circ$]	VGP _{Long} [$^\circ$]	VGP _{Lat} [$^\circ$]	d_p/d_m [$^\circ/^\circ$]	polarity
D	41	88.5	75.4	78	2.5	148.2	57.1	4.3 / 4.7	normal
C	14	21.9	68.4	233	2.6	230.4	68.7	3.7 / 4.4	excursion
B	14	151.9	54.4	325	2.1	114.3	16.6	2.2 / 3.1	transitional
A	5	250.9	-68.1	106	8.4	7.1	-53.7	12 / 14	reversed

^a For each group the number of sites (N), the bedding corrected mean declination (Dec) and inclination (Inc) with their respective 95% confidence cones (α_{95}) and precision parameter k are shown. Also given are the associated VGP positions (longitude/latitude) and the parameters of the confidence oval.

According to the directional pattern described above, the record can be divided into three phases. The first phase, from the bottom to the studied sections to flow TK6, represents a geomagnetic transition from reversed to normal polarity. Several flows recorded strongly clustering intermediate directions. It remains to be checked whether the directions of group B were possibly acquired during a remagnetisation event long after the emplacement of the STB. For this purpose the associated VGP has been calculated in geographic (Long: 109°E , Lat: 7°N) and stratigraphic coordinates (Long: 114°E , Lat: 17°N). A query of the global Palaeomagnetic Database (GPMDB, McELHINNY [1998], version 4.3 released July 2002) yields no similar palaeomagnetic poles of the Siberian platform for the last 250 Ma. Moreover, palaeogeographic reconstructions (e.g. SMETHURST ET AL. [1998]) place the Siberian platform at high latitudes throughout the last 250 Ma, which is obviously incompatible with the VGP of group B, both in geographic and stratigraphic coordinates. It can therefore be ruled out that this remanence is related to an overprint acquired between 0 and 250 Ma. Consequentially,

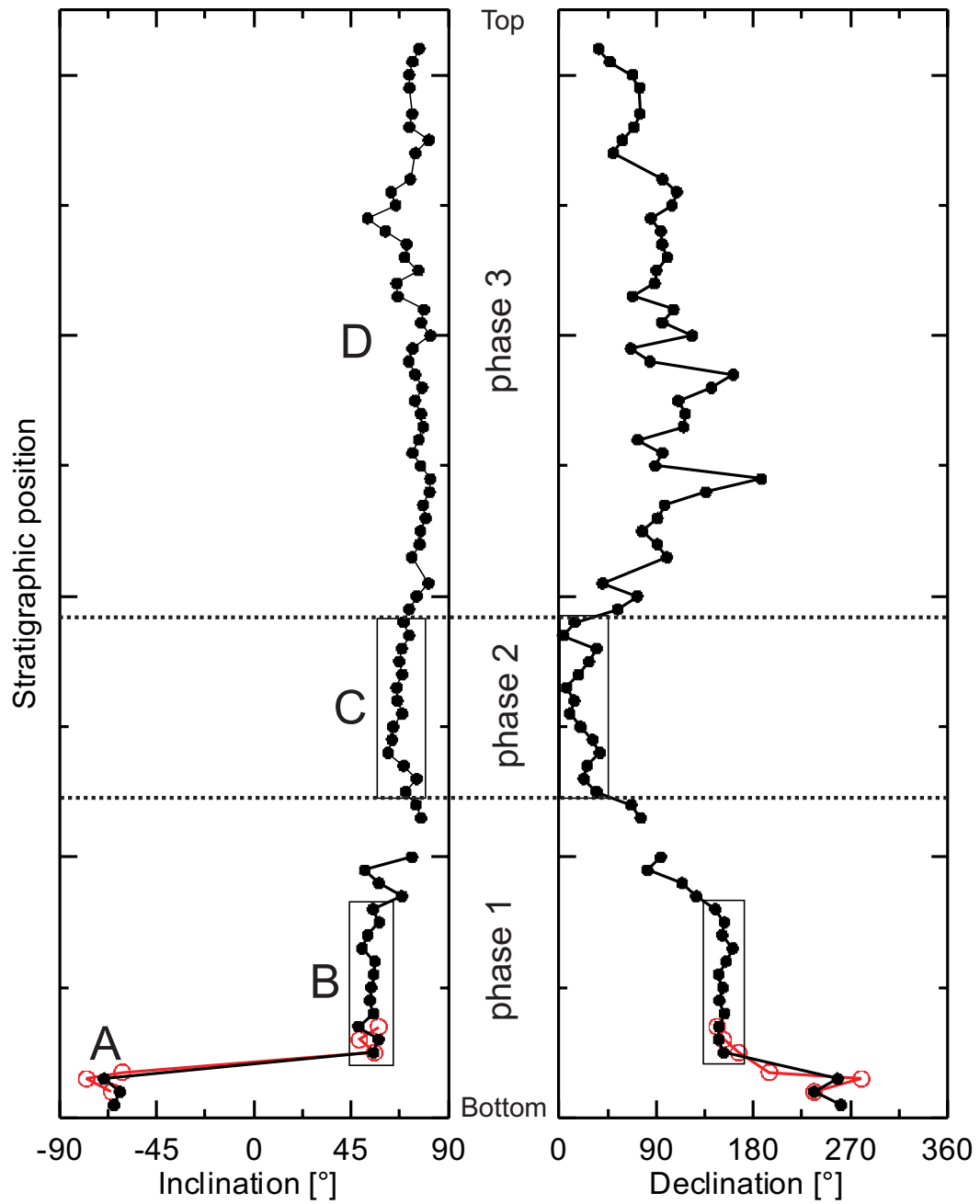


Figure 3.10: Inclination and declination record of the Listvjanka and Abagalakh section (black dots) and the Talnakh section (red open symbols) after bedding correction. Indicated are also the phases of the record and the groups of directions as defined in the text. The gap comprises the Khakanchansky suite, which is absent in all the sections studied.

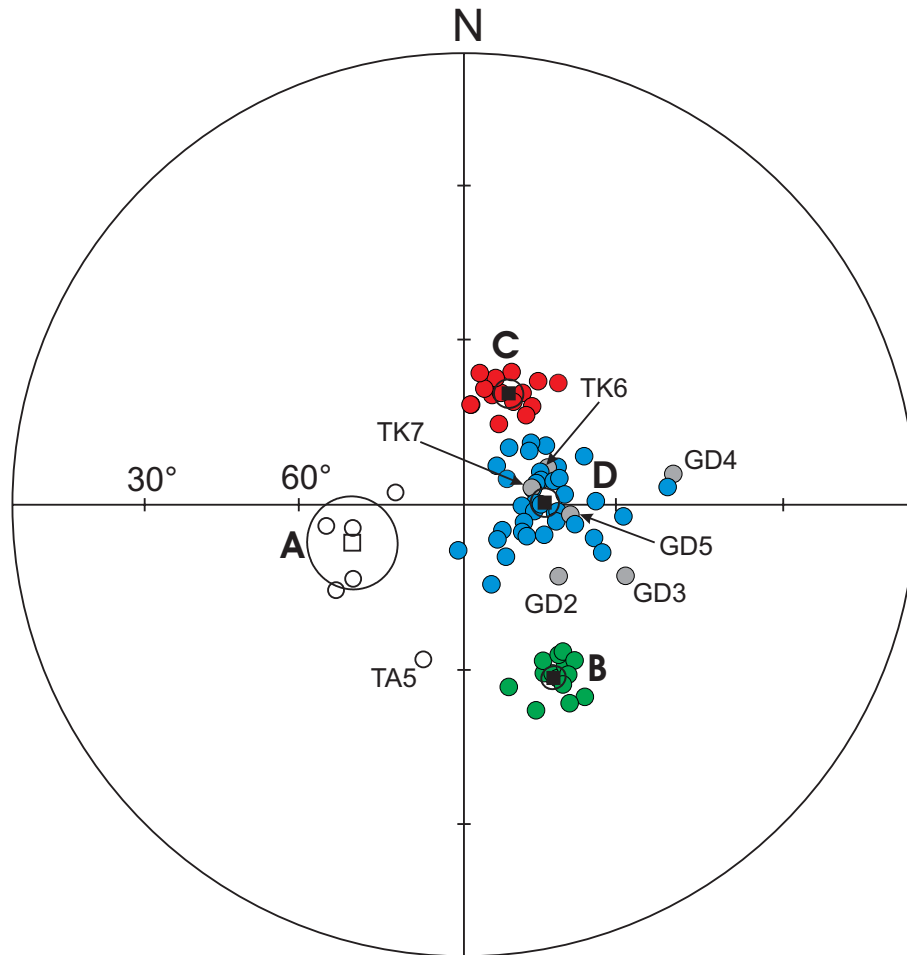


Figure 3.11: Site mean directions after bedding correction in stereographic projection (open symbols: negative inclinations, full symbols: positive inclinations). Flow mean directions which belong to group B, C or D (as defined in the text) are shown in green, red or blue, respectively. Squares indicate the mean directions of the those groups. Individual flow means which were not included in one of the groups are identified by their site name (apart from TA5 grey dots).

the directions can be regarded as primary and transitional.

The second phase comprises group C. The considerable number of successive flows displaying inclinations around $+68^\circ$ and declinations around 22° suggest that this feature is relatively stable. Conventionally, geomagnetic excursions are defined by departure of the VGP from its time averaged position by more than 40° (e.g. VANDAMME [1994]). In a strict sense, phase 2 would not be classified as an excursion as it lies at only 37° great circle distance compared to group D. However, interpreting the record sequentially its position has to be compared with the short normal period preceding it. It has been shown before that this period has at a 95% confidence level statistically undistinguishable mean pole from the mean pole of group D. But using the mean pole of the short normal period, the distance to group C is of about 44° . These considerations make clear that the 40° criteria is somewhat arbitrary – particularly as there is no physical constraint defining this threshold – and can, therefore, lead to ambiguous interpretations. Remarkably, there is no overlap in the population of directions of preceding or following flows or groups with the directions of group C. Together with the considerations made above, this observation is therefore evidence for an excursion of the field. Whether this excursion is independent from the reversal itself or a post-transitional effect as consequence of an unsuccessful attempt to establish stable normal polarity (e.g. HOFFMAN [1992]; MERRILL ET AL. [1998]) will be discussed in chapter 6.3.

The third phase (group D) is interpreted to represent stable normal polarity and hence to be representative of the Early Triassic. Scatter in the declination during this phase arises from secular variation and is discussed in chapter 3.5. Comparing the mean VGP of group D to published palaeomagnetic poles derived from the STB allows to check the consistency of the results. A compilation of selected palaeomagnetic poles from STB (see Tab. 3.5) is shown in Figure 3.12. Some poles, however, have to be regarded as not reliable. SOLODOVNIKOV [1995] included in the calculation of his VGP data derived from the Syverminsky suite. It was demonstrated above that flows of this suite erupted during the reversal and thus recorded transitional directions. The corresponding VGP is consequently biased and shifted to lower latitudes. The same applies to the data of LIND ET AL. [1994]. These samples were also demagnetised incompletely, so that it cannot be ruled out that secondary overprints were not fully removed. Moreover, the palaeomagnetic pole of GUSEV ET AL. [1967] has to be regarded as unreliable as only the NRM was measured and used for calculation of the VGP. The results of the Western Taimyr P/T volcanics [GUREVITCH ET AL., 1995] and Eastern Siberian trap basalts [KRAVCHINSKY ET AL., 2002] agree, apart from their relatively large confidence ovals, very well with the data presented here. In order to check if stable normal polarity was really reached the mean pole for the Siberian platform between 248 and 253 Ma,

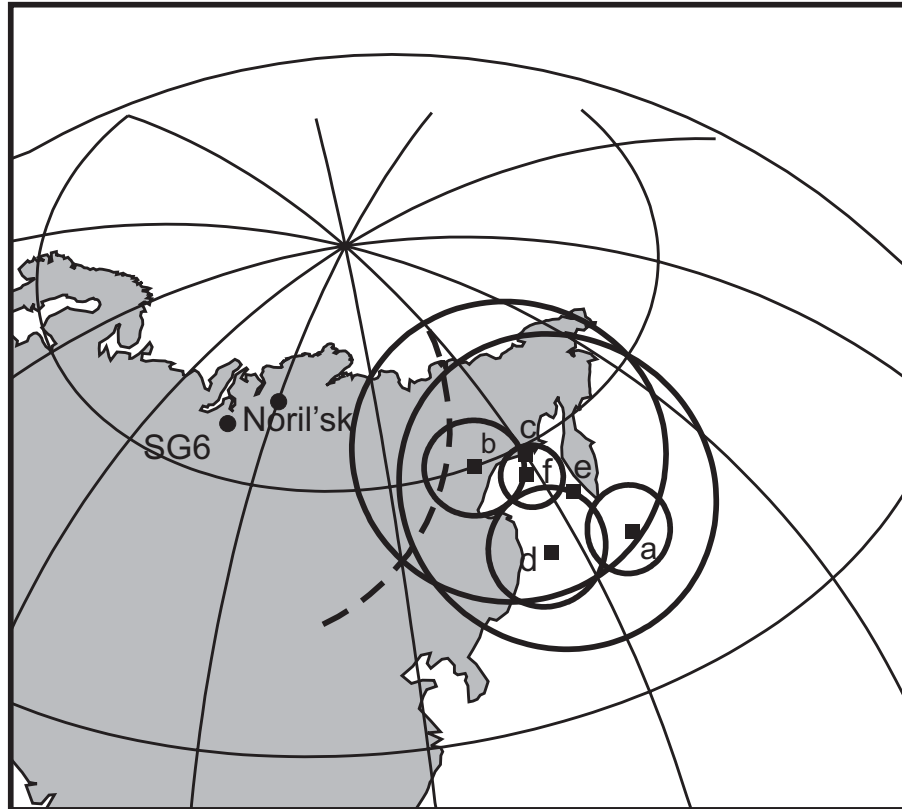


Figure 3.12: Compilation of palaeomagnetic poles obtained from the STB. (a) refers to results of the Maimecha-Kotuy region [GUSEV ET AL., 1967], (b) Noril'sk area [LIND ET AL., 1994]; (c) specifies the mean pole of the Western Taimyr traps [GUREVITCH ET AL., 1995]; (d) SOLODOVNIKOV [1995], Noril'sk area; (e) KRAVCHINSKY ET AL. [2002], Eastern STB. The mean pole (group D) obtained in this study is denoted by (f). Mean inclination derived from borehole SG6 constrain VGP positions to lay on a circle (broken line) centred at the site location. Error estimates for SG6 are omitted for clarity.

excluding poles obtained from the STB or related units, was calculated (VGP longitude: 151°N, latitude: 52°E, k : 97, A_{95} : 8.8°; compilation of SMETHURST ET AL. [1998], see also Table 3.5 for the individual poles). Evidently, the VGP of the stable normal period of the STB record is at a 95% confidence level undistinguishable from the mean non STB-related mean pole proving that indeed normal polarity was recorded by the uppermost 41 flows of the Abagalakh section.

Table 3.5: Selected poles for the STB and the Siberian platform around the P/T boundary^a

Rock unit	Age [Ma]	Site _{Long} [°]	Site _{Lat} [°]	Dec [°]	Inc [°]	α_{95} [°]	VGP _{Long} [°]	VGP _{Lat} [°]	GPDB
Lena River sediments	253	125	75	164	75	19	136	145	1964 ¹
STB, Maimecha Koty	253	102	71	102	70	3	158	46	— ²
STB, Noril'sk area	250	91	69.5	100	72	4	145	48	3044 ³
STB, Noril'sk area	250	88	69	88	78	3	139	60	3269 ⁴
STB, Abagalakh	250	90	70	88.5	75.4	2.5	148	57	—
Eastern STB	250	111	66	101	77	10	154	53	3486 ⁵
STB, West Taimyr	250	84	73	84	75	10	150	58	2832 ⁶
Upper Vilyui intr.	248	108	66	81	75	4	168	56	1986 ⁷
Markha region intr.	248	112	66	102	75	5	158	51	1997 ⁷
Upper Markha intr.	248	111	66	106	75	6	154	48	968 ⁸
Ygyattin region intr.	248	115	64	103	82	4	141	55	968 ⁸

^a GPDB: Global Palaeomagnetic Database Reference Number (MCELHINNY [1998], version 4.3 released July 2002), ¹PISAREVSKY [1982], ²GUSEV ET AL. [1967], ³SOLODOVNIKOV [1995], ⁴LIND ET AL. [1994], ⁵KRAVCHINSKY ET AL. [2002], ⁶GUREVITCH ET AL. [1995], ⁷KAMYSHEVA [1971], ⁸Kamysheva, quoted in KHRAMOV [1984]

Using VGPs to visualise transitional field behaviour has several pitfalls, though. In the presence of strong non-dipolar components this representation fails as a multitude of field configurations can generate an observed local field vector. Geographically well distributed observation on the same geomagnetic feature are therefore essential in order to describe at least lower harmonics of the Earth's magnetic field. However, the VGP concept is the only tool available to provide a generalised view of a reversal. Figure 3.13 shows the individual phases of the record. A description of the palaeomagnetic record integrating results of the palaeointensity experiments is given in chapter 6. The combination of the datasets provides deeper insight in the stability of the observed directional groups.

3.4 Fold and reversal test

Given the age of the sequence it is especially important to prove that the extracted palaeomagnetic information was really recorded during the emplacement of the flows.

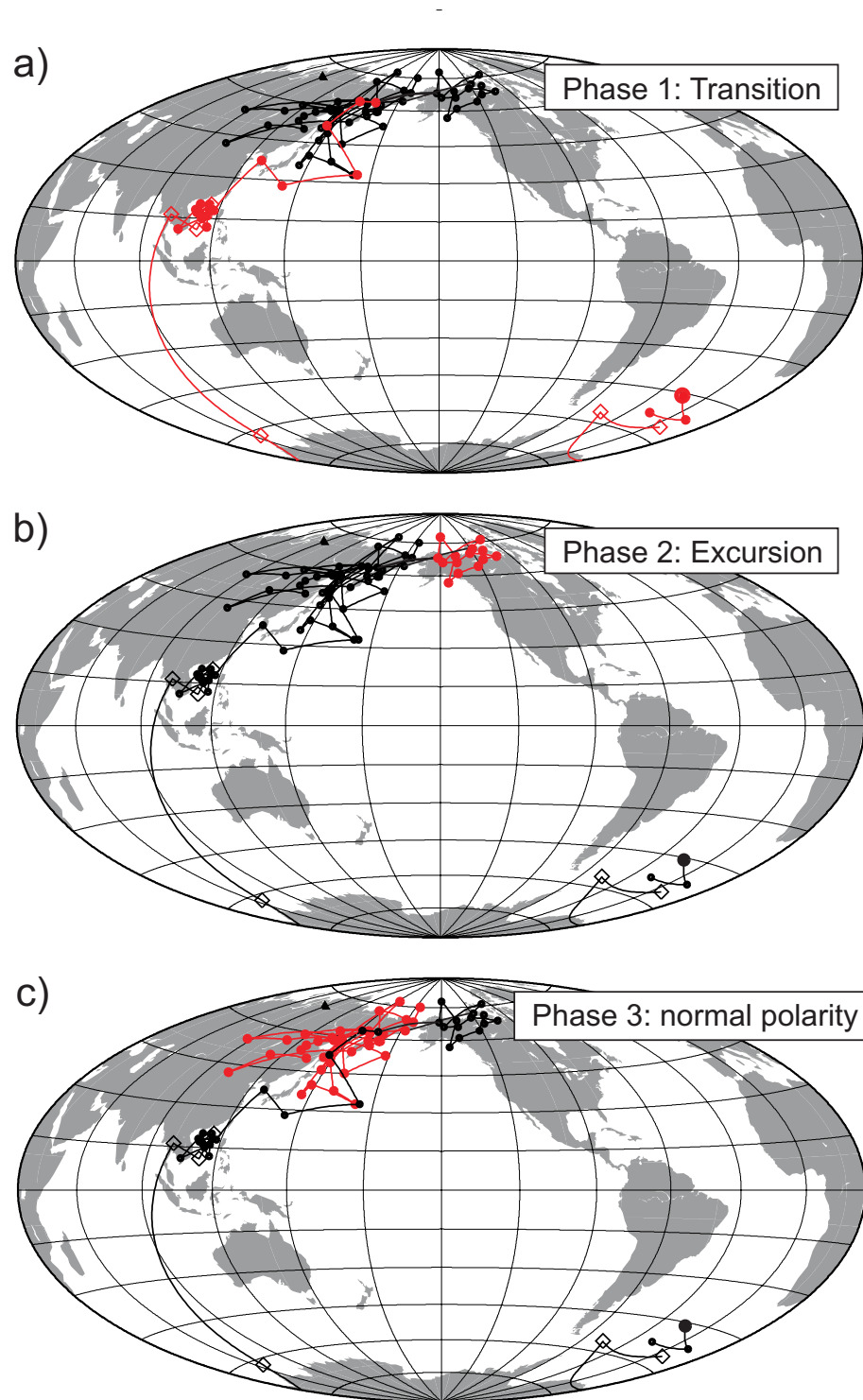


Figure 3.13: Movement of the VGPs during the emplacement of the flows. Continents are shown in their present position. (a) Phase 1: The record starts with reversed polarity. Dots denote results of the Listvjanka/Abagalkh section (larger dot: bottommost flow), open diamonds VGPs obtained from the Talnakh section. Noticeable is the clustering of VGP at low latitudes (group B). Afterwards the VGPs move towards the pole position of normal polarity. (b) Phase 2: A sudden shift of the poles is observed subsequently. This clustering (group C) is well defined and has a significantly different mean pole compared to stable normal polarity. (c) Phase 3: This phase represents stable normal polarity. VGP scatter arises from secular variation.

In order to test if the ChRM was acquired before or after subsidence of the lava pile an internal fold test was carried out using parametric resampling [WATSON AND ENKIN, 1993] with the ENKIN [1990] software package (version 3.9, released April 1995). Reversed, transitional and excursional directions were excluded. This test yields inconclusive results as differences in bedding are too small using flow mean directions of phase 3 only. Therefore, the mean direction of the Ivakinsky suite flows, having a distinctly different bedding as the flows of the Abagalakh section, were inverted to normal polarity and added to the dataset. In order to circumvent statistical overestimation of normal directions (41 to 5 reversely magnetised flows) all flow means of phase 3 with the same bedding (see Tab. 3.1) were merged. Optimal unfolding after WATSON AND ENKIN [1993] yields a maximum k , which is a measure of the dispersion of a population of directions [FISHER, 1953], of 195 at ca. 76% of unfolding. The associated lower and upper 95% confidence limits are 40% and 105%, respectively. Figure 3.14 shows the variation of k versus the degree of unfolding for 20 randomly resampled datasets (black lines). The distribution of maximum k values for 1000 simulations with 5% increments of unfolding is represented by the grey histogram. For these calculations the data of the reversed flows play a key as they represent the opposing limb to the Abagalakh section. Slight variation of the dip of their bedding plane have a great effect on the overall result of the fold test. Reducing the dip angle of the Ivakinsky suite slightly from 11.5° to 10° the same simulations yield a maximum unfolding of 84%. Assuming that the geological model of progressive subsidence due to the load of the accumulated lava pile and the deflation of the underlying magma chamber is valid (e.g. LIGHTFOOT ET AL. [1990]), the dip of the Ivakinsky would have been overestimated by the measurements of the bedding plane in the field.

Another method to test for reliability of the directional record is the reversal test. Group A and D are nearly antipodal but do not pass the reversal test of MCFADDEN AND MCELHINNY [1990] ($\gamma_{observed} = 9.2^\circ$; $\gamma_{critical} = 7.7^\circ$). However, the small number of flows of reversed polarity limits the significance of the statistical test. Moreover, if assuming that the dip of the Ivakinsky suite was overestimated, like the results of the fold test suggest, and using a smaller dip angle for the bedding correction (10°), $\gamma_{observed}$ reduces to 7.2° . In this case the reversal test is positive and of category B.

Both tests evidence that the ChRM was acquired, within the accuracy of the measurement of the dip angle and the 95% confidence of the statistical analysis, prior to subsidence. Shortcomings arise due to the strong asymmetry in the number of flows of reversed to normal polarity and the small differences in the bedding. Furthermore, both tests also depend critically on the directional results obtained from the Ivakinsky suite. The influence of dip overestimation in the Ivakinsky suite has already been

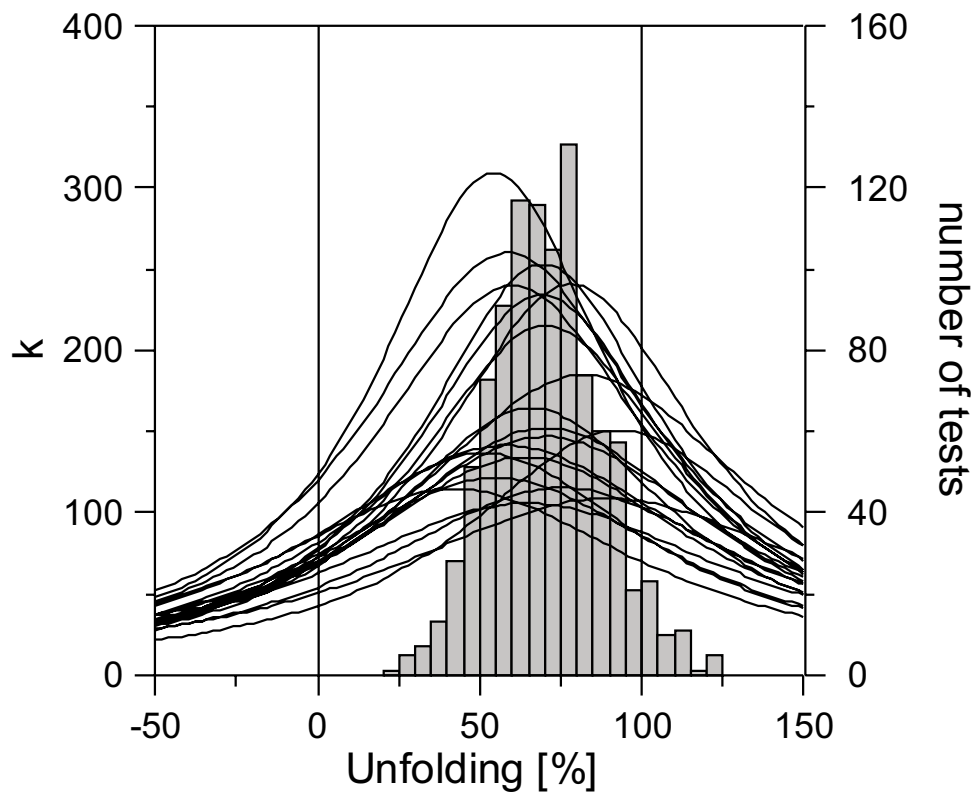


Figure 3.14: Results of the fold test according to WATSON AND ENKIN [1993]. The black lines show the precision parameter k [FISHER, 1953] versus unfolding for 20 examples of parametric resampling. Maximum k value distribution of 1000 trials in groups of 5% is given by the histogram.

discussed above. Remarkably, the results of the reversal and the fold test are consistent in this point. Another explanation may be that the VGPs of the group A are very close to the reversal and already show directions which are slightly deviant to the stable reversed pole. With the data at hand it cannot be decided which alternative is more likely.

3.5 Palaeosecular Variation

In order to estimate the palaeosecular variation (PSV), the VGP dispersion for the stable normal part of the section (phase 3) and the associated cut-off angle A was calculated according to VANDAMME [1994]. This procedure yields $A = 32^\circ$. No results had to be disregarded using this iterative method. The data were corrected for the within-site scatter [MCELHINNY AND MCFADDEN, 1997]. This correction is a function of the latitude which was in our case defined as the palaeolatitude obtained from the mean pole of the phase 3 assuming a geocentric axial dipole. The VGP dispersion (S_F) yielded a value of 15.4° with upper and lower 95% confidence limits [COX, 1969] of $S_u = 18.2^\circ$ and $S_l = 13.3^\circ$,

respectively. The high number of flow mean directions used in this calculation suggests that this S_F value can be regarded as reliable. Palaeosecular variation averaged over the last 5 Ma yields values of approximately $S_F = 20^\circ$ [MCELHINNY AND MCFADDEN, 1997] for the corresponding latitude (Table 3.6). It has to be noted that this discrepancy is caused by the larger cut-off angle (42.6°) used in this study. Applying the same cut-off angle all of the flow means above the transitional cluster contribute to the calculation of PSV. The resulting $S_F = 21.4^\circ$ is closer to that of MCELHINNY AND MCFADDEN [1997] exceeding it slightly. However, as demonstrated, only phase 3 represents a reliable record of stable normal polarity. Therefore, only data with similar cut-off angles applied to the original dataset can provide comparable results.

Table 3.6: Comparison of the geomagnetic VGP dispersion of the 0–5 Ma time interval with the results of this study^a

Age	A	N	$\bar{\alpha}_{95}$	Plat	S_P	S_F	S_u	S_l	comment
0–5	42.6	643	4.6	64.7	20.9	20.3	21.1	19.6	McE. & McF. (1997)
250	43.6	61	3.7	62.4	21.4	21.4	24.5	19.0	all above group B
0–5	32	472	–	64.4	18.2	17.4	18.2	16.7	PSVRL database
250	32	41	3.5	62.4	15.4	15.3	18.1	13.3	group D
250	20.1	14	2.6	51.6	8.4	8.1	10.8	6.4	excursion, group C
250	13.0	12	2.0	34.9	4.5	4.4	5.9	3.4	transitional, group B

^a A: VGP cutoff angle, N: number of sites used for calculation, $\bar{\alpha}_{95}$: mean 95% confidence limit for the sites used in each S_F determination, Plat: mean palaeolatitude, S_P , S_F , S_l , S_u : PSV parameters as defined in the text. McE. & McF. refers to MCELHINNY AND MCFADDEN [1997]

A query of the PSV from lavas database (PSVRL, version 4.1, released May 2001), designed by MCELHINNY AND LOCK [1996] and currently maintained by S. Pisarevsky, using a cut-off angle of 32° (0–5 Ma, 472 datasets, $\alpha_{95} < 10^\circ$) yields S_F of 17.4° ($S_u = 18.2^\circ$, $S_l = 16.2^\circ$). Thus, our results indicate that the palaeosecular variation in the earliest Triassic was somewhat but not significantly lower. Results of LYONS ET AL. [2002] obtained from 15 cooling units of the early Triassic Semeitau igneous series (Kazakhstan), likely to be genetically related to the Siberian traps, showed also to be indistinguishable from the secular variation averaged over the past 5 Ma at the 95% confidence level. For comparison VGP dispersion was also calculated for the transitional phase and the excursion. Significantly lower values could prima facie suggest that secular variation was suppressed during the transitional cluster ($S_F = 4.4^\circ$, $S_u = 5.9^\circ$, $S_l = 3.4^\circ$) and the excursion ($S_F = 8.1^\circ$, $S_u = 10.8^\circ$, $S_l = 6.4^\circ$). But these values have to be considered with caution as the time interval sampled by the eruptions was probably too short to record PSV in its full extent.

3.6 Magnetostratigraphic correlation

Constraining the duration of the STB activity is (see chapter 1) critical before considering whether they are ultimately the cause for the P/T crisis or not. Magnetostratigraphy can give at least estimates on the maximum duration.

A detailed study comparing palaeomagnetic results obtained from borehole cores to the results of the outcrop section studied here was carried out recently [GUREVITCH ET AL., 2003] to provide a continuous coverage of the lava pile in the Noril'sk region. Four wells were drilled in the proximity to Noril'sk and the Abagalakh section (see Fig. 3.1). Figure 3.15 summarises the variation of the inclination as a function of the stratigraphic position of the composite outcrop section and the results obtained from boreholes. Above the Ivakinsky suite almost all samples have positive, normal (N) inclinations. It has to be emphasised that data points in the borehole inclination plots depict results of individual samples. Levels of reversed (R) polarity above the Ivakinsky suite can not be correlated among the boreholes and might, therefore, be an artifact of mishandling during sampling or storage. Other samples may also originate from unrecognised intrusions of younger age. Borehole CD 10 only penetrated the Kumginsky suite. The results obtained are inconclusive. There is no significant succession of consistently positive or negative inclinations allowing for the definition of polarity intervals. The flows of the Kumginsky suite sampled in the Abagalakh river valley do not show any indication of reversed polarity. Borehole results of the Ivakinsky suite are also ambiguous. Both polarities are found. As demonstrated in chapter 3.2, overprints in the Ivakinsky are more persistent and led in two cases to the rejection of the results as they exhibited both polarities within one site. Not having the possibility to check if adjacent samples of a borehole core derive from the same cooling unit, internal consistency remains unverified. The palaeomagnetic analyses of flows of the Ivakinsky suite of both the Talnakh and Abagalakh section yields no evidence for normal polarity. Thus, combining the findings of outcrop sections and borehole samples it can be assumed that the magnetostratigraphic succession for the whole Noril'sk area comprises only one reversal from reversed to normal polarity (R-N). Further undetected reversed polarity intervals are highly unlikely.

The magnetostratigraphic results of the different regions of the STB are displayed in Figure 3.16. GUREVITCH ET AL. [1995] studied the volcanic sequence on Taimyr and came to the conclusion that the R-N succession is overlain by a short period of reversed polarity. The lower part of the sequence is coeval with the first volcanics of the Noril'sk area. Therefore, volcanism on Taimyr lasted slightly longer. The stratigraphy of the West Siberian Basalts displays 5 polarity intervals (N-R-N-R-N, WESTPHAL ET AL. [1998]). Borehole SG6 (Fig. 2.1) penetrates the full thickness of the sedimentary

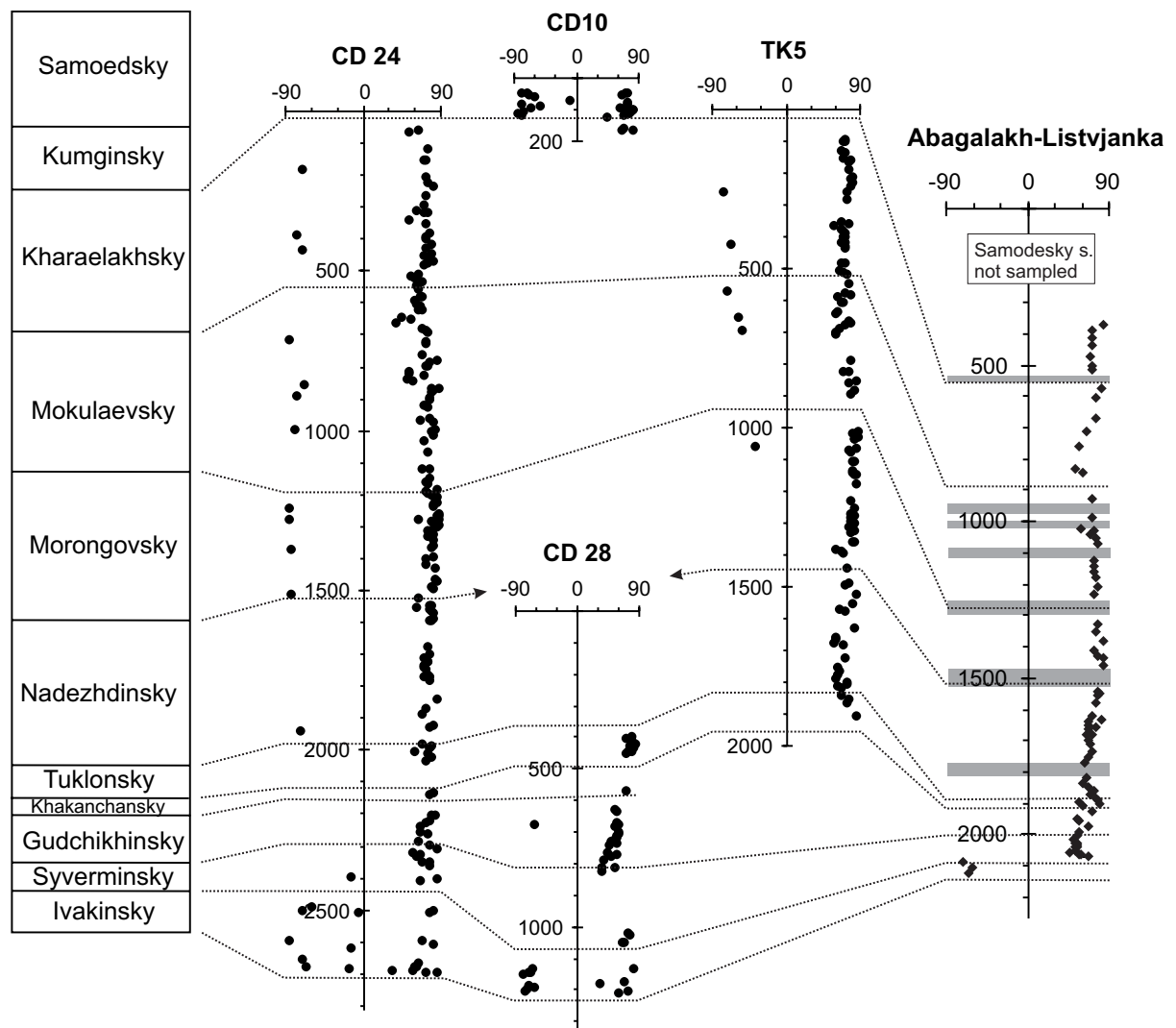


Figure 3.15: Magnetostratigraphic correlation of borehole and outcrop data (inclination only, modified after GUREVITCH ET AL. [2003]). For boreholes, individual sample inclinations are shown, whereas data points of the Abagalakh-Listvjanka section represent flow mean directions. Grey shaded stratigraphic levels were not exposed. The correlation of the suites is based on geochemical analyses (V. RAD'KO, personal communication).

Mesozoic-Cenozoic cover before reaching the volcanics. Below this thin basalt layer (20 m) a 60 m thick sedimentary sequence of Induan age follows. The rest of the drilled core consists of basalts. The Palaeozoic basement was not reached and, therefore, no information about the onset of the volcanic activity in the West Siberian basin could be gained. However, the data shows clearly that eruption ceased around the end of the Induan. Probably, the lowermost zone of normal polarity corresponds to that of the Norli'sk area. The interpretation of the data available for the Maimecha-Kotuy (M-K) is more complicated. Based on geochemical comparisons FEDORENKO AND CZAMANSKE [1997] concluded that the top of the M-K section must be younger than the top of the

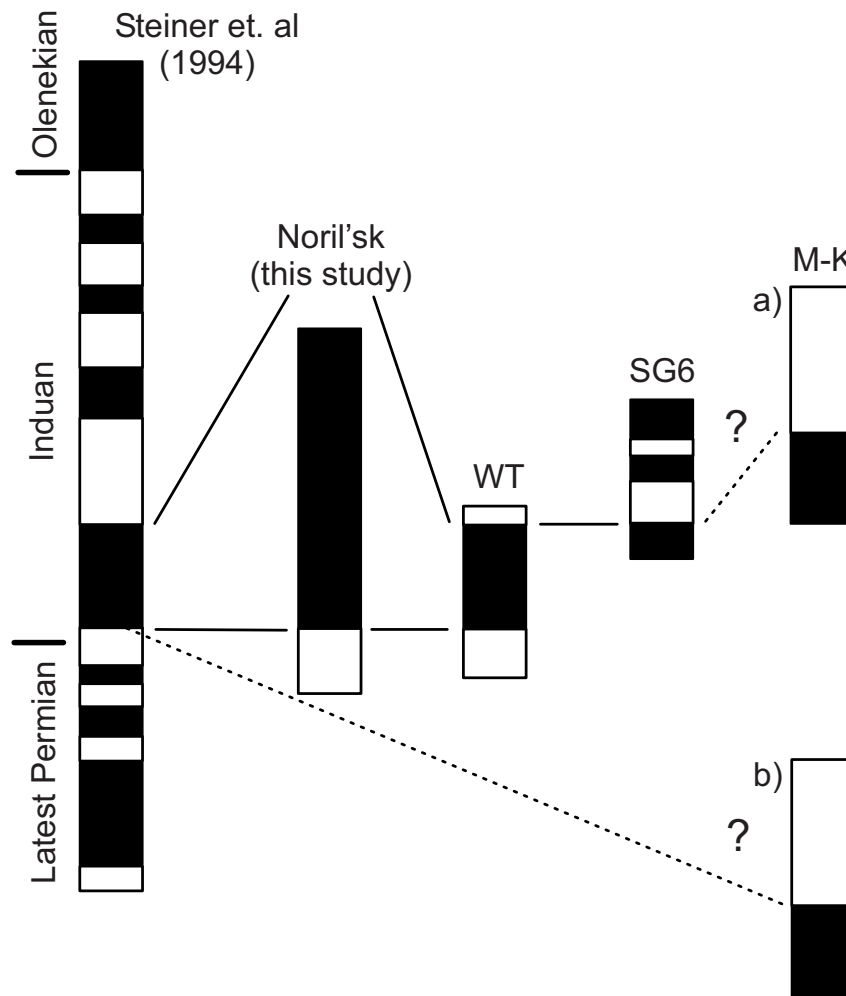


Figure 3.16: Magnetostratigraphic correlation between the STB and the global P/T magnetostratigraphic scale [STEINER ET AL., 1993]. black: normal polarity, white: reversed polarity, WT: Western Taimyr [GUREVITCH ET AL., 1995], SG6: results of the Tyumenskaya borehole [WESTPHAL ET AL., 1998], M-K (a) and (b): alternative correlations for the magnetostratigraphy [GUSEV ET AL., 1967] of the Maimecha-Kotuy region. For this northeastern and least studied part of the STB only one radiometric age (253.3 ± 2.6 Ma) is available making alternative (b) more plausible. The height of the columns (except for the global scale) indicates the approximate relative thickness of the volcanic sequences. This Figure was modified after GUREVITCH ET AL. [2003].

basalts in the Noril'sk region. Radiometric ages contradict this correlation. BASU ET AL. [1995] obtained $^{40}\text{Ar}/^{39}\text{Ar}$ plateau ages of 253.3 ± 2.6 Ma. This would place the onset of the volcanic activity significantly prior to the P/T boundary and in turn the N-R succession observed by GUSEV ET AL. [1967] would be one of the Illawarra reversals. In order to solve the ambiguities outlined above more radiometric data are necessary. This holds also true for palaeomagnetic data that do not meet modern reliability criteria and, hence, have to be regarded as unreliable.

Excluding the still unsolved correlation of the M-K basalts, some fundamental duration constraints can be derived from the magnetostratigraphic data at hand. It is undisputed that the reversed polarity interval coincides with the P/T boundary. The upper limit for the volcanic activity is defined up to now by the palaeomagnetic results of borehole SG6. GRADSTEIN ET AL. [1995] estimate the duration of the Induan to be about 3.2 Ma. That would also be the maximum duration in which the whole volcanic sequence accumulated. The bulk of the basalts, however, was erupted certainly in a considerably shorter time. The findings make a strong case for a scenario of initially violent and voluminous eruptions causing the P/T crisis. Subsequently, somewhat more quiet volcanic activity may have hindered the recovery of the ecosystem.

Chapter 4

Rockmagnetic Studies

Early studies of the rockmagnetic properties of intrusive and extrusive rocks related to the Siberian Trap volcanism concluded that partial self-reversal is a commonly observed feature [METALLOVA AND FEINBERG, 1967]. Furthermore, the authors suspected that self-reversal mechanisms are the cause for the occurrence of reversely magnetised units of the Traps. In this chapter rockmagnetic studies are presented in order to check for this hypothesis and to assess the reliability of the palaeomagnetic results. Moreover, these investigations also provide valuable information for selecting suitable samples for palaeointensity experiments.

4.1 Microscopy: Evidence for high-temperature oxidation

One polished section was prepared for each lava flow. Optical-microscope (Leitz Orthoplan) observations under polarised light (crossed Nicols) revealed the presence of the optically anisotropic mineral hemoilmenite ($\text{Fe}_{2-y}\text{Ti}_y\text{O}_3$, $0 < y < 1$) within the titanomagnetite ($\text{Fe}_{3-x}\text{Ti}_x\text{O}_4$, $0 < x < 1$) grains in most of the samples studied (Fig. 4.1). Additional scanning electron-microscopical (Zeiss DSM 960) observations and energy dispersive X-ray (EDX) analyses confirm this interpretation qualitatively on the basis of the iron/titanium (Fe/Ti) ratios of the two different phases (Fig. 4.1c). These titanomagnetite/ilmenite intergrowths are a clear indication of a primary high-temperature oxidation of the ore grains which occurs deuterically during cooling of subaerial basalts above 500°C to 600°C [LINDSLEY, 1962; DUNLOP AND ÖZDEMİR, 1997]. The process is characterised by progressive formation of hemoilmenite lamellae separating progressively Ti depleted titanomagnetite, ultimately yielding on the one hand oxyexsolved Ti-poor titanomagnetites with a near magnetite composition. On the other hand hemoilmenite at that stage has a composition close to ilmenite ($y = 1$). In cases of incomplete oxidation two different titanomagnetite phases may be present and the samples exhibit two Curie-temperatures. When the oxidation is carried to

completion magnetite and ilmenite are replaced by higher oxidised phases such as hematite, pseudobrookite (Fe_2TiO_5) and rutile (TiO_2), which are often very fine grained [O'REILLY, 1984]. Magnetite and hematite may also coexist in highly oxidised basalts.

Ilmenite intergrowth in titanomagnetites can be divided into three different textural forms [BUDDINGTON AND LINDSLEY, 1964], all observed in the samples studied here:

- Trellis-type (Fig. 4.1a): Oxyexsolved ilmenite lamellae show well defined contacts with the surrounding titanomagnetite and are usually very thin (up to a few μm). They are oriented parallel to the $\{111\}$ plane or to all sets of octahedral planes of the host mineral. Terminations of the lamellae at the grain boundary and intersections are often tapered.
- Composite type (Fig. 4.1b): Characteristic for this form are inclusions partially or totally included in the titanomagnetite. Trellis lamellae are usually also present.
- Sandwich-type (Fig. 4.1c): The number of lamellae is much smaller compared to the Trellis-type. They are often thicker than Trellis lamellae and have rarely parallel sides. Sandwich lamellae that coexist with Trellis laths predate those.

All three types can coexist. Trellis lamellae are clearly a result of oxidation exsolution whereas sandwich and composite ilmenite are either products of oxidation or primary crystallisation from the melt [HAGGERTY, 1976]. The intrinsic properties of the intergrowth and their development depends on factors like the composition of the original titanomagnetite, oxygen fugacity and the cooling history of the individual lava flows. Slow cooling, for example, fosters the development of larger lamellae compared to structures observed in rapidly cooled flows. High-temperature oxidised titanomagnetites usually have very high magnetic stability due to the exsolution texture. The lamellae act like elongated subgrains, reducing the effective grain size of the original titanomagnetite grain. As a whole the grain behaves more like an ensemble of interacting single domain (SD) grains with high shape anisotropy and hence high coercivity and remanence stability [O'REILLY, 1984]. Moreover, high-temperature oxidised grains are less susceptible to alteration during heating. This fact is explained by the higher equilibrium oxygen fugacity of magnetite or Ti-poor titanomagnetite compared to Ti-rich titanomagnetite [BUDDINGTON AND LINDSLEY, 1964].

Trellis-type lamellae dominate in the vast majority of the cases of the studied samples which is evidence for at least intermediate degrees of high temperature oxidation. Two flows of the Syverminsky suite (SV8 and SV9) exhibit a slightly deviant rockmagnetic behaviour. Their NRM is carried by two magnetomineralogical phases, one unblocking around 580°C , the other having maximum blocking temperatures of up to 640°C or even

670°C. In addition to magnetite these samples also contain a hematite component. Both components carry identical palaeomagnetic directions (Fig. 3.7b). Polished sections reveal tiny reddish specular hematite grains arranged around larger (titano-)magnetite grains. In these flows oxidation processes proceeded to a high degree.

The question now is if the NRM carried by high-temperature oxidised basalts is a real thermoremanent magnetisation (TRM). This is a vital prerequisite to obtain reliable palaeointensity estimates which resemble the strength of the Earth's magnetic field during cooling of the lava flow. In reality, however, in many cases volume growth of the magnetic phase still proceeds below its Curie-temperature and a thermochemical remanent magnetisation (TCRM) is acquired [DUNLOP AND ÖZDEMİR, 1997]. The NRM is therefore the sum of the TRM and the TCRM. Since this grain growth happens during initial cooling the directional fidelity is guaranteed. For palaeointensity determinations rockmagnetic constraints are stricter, though. But, excluding cases of extremely slow cooling like in lava lakes, KELLOGG ET AL. [1970] showed that TCRM serves as a reasonable analog of TRM in palaeointensity experiments.

4.2 Rockmagnetic parameters

Magnetic hysteresis loops at room temperature of at least one sample of each lava flow (about 110 in total) were measured using a Variable Field Translation Balance (VFTB, maximum field of 0.9 T). The paramagnetic content was estimated by a linear fit between 0.6 and 0.9 T and subtracted from the loop prior to calculation of the hysteresis parameters. The results are summarised in Table 4.1. Besides samples GD3, MK1, MR21 and MR22 all results plot in the pseudo single domain (PSD) grain size range using the H_{cr}/H_c and M_{rs}/M_s ratios according to DAY ET AL. [1977]. Although these so called Day-plots are frequently used in the literature to estimate the domain states of titanomagnetite, this approach is in a strict sense not valid as these ratios were defined in the original publication for magnetite only. Moreover, recent results of DUNLOP [2002a,b] show convincingly that these ratios can be helpful for titanomagnetite but should not be used uncritically as diagnostic granulometric tool. Compositional variations of the (titano-)magnetite, different mixtures of superparamagnetic (SP), SD, PSD and MD particles and different stress regimes in the samples can make the interpretation of hysteresis parameters and their ratios ambiguous [TAUXE ET AL., 1996].

Strong field thermomagnetic curves, measured in fields between 350 and 700 mT (usually sufficient to magnetically saturate the samples), are in most cases reversible. The dominant minerals are magnetite as well as Ti-poor titanomagnetite with Curie-

temperatures (T_C) typically between 530°C and 590°C (Fig. 4.2a). A few samples exhibit relatively low T_C , down to 440°C which corresponds to a titanium (Ti) content $x \simeq 0.2$ [DUNLOP AND ÖZDEMİR, 1997]. 10 samples have two Curie-temperatures (Fig. 4.2b). The cooling curves of these samples lack the lower T_C . These samples always exhibit evidence for oxidation during heating, even if using different heating rates. Cause for this behaviour is that initially incomplete (non-equilibrium) oxidation is driven toward completion by heating during the experiment [KONO, 1985].

Table 4.1: Results of the rockmagnetic investigations^a

Site	H_c [mT]	H_{cr} [mT]	M_{rs} [Am ² /kg]	M_s [Am ² /kg]	H_{cr}/H_c	M_{rs}/M_s	$T_{C,1}$ [°C]	$T_{C,2}$ [°C]	T_{ub} [°C]
KMX4	16.9	32.2	0.13	0.85	1.90	0.15	587		590
KMX3	17.4	38.6	0.15	0.97	2.22	0.16	588	–	
KMX2	4.7	13.3	0.09	1.01	2.84	0.09	415	514	
KMX1	17.6	40.9	0.11	0.73	2.33	0.15	598	–	580
KM4	8.3	22.2	0.09	0.81	2.67	0.12	410	535	410/540
KM3	10.2	30.9	0.11	0.80	3.03	0.13	506	588	
KM1	5.3	15.9	0.07	0.82	3.02	0.09	420	526	500
HR13	15.5	37.8	0.10	0.78	2.45	0.13	591	–	
HR11	15.7	29.0	0.11	0.53	1.85	0.20	572	–	
HR8	8.5	19.4	0.08	0.65	2.27	0.12	540	–	
HR7	18.2	36.7	0.14	0.76	2.02	0.18	590	–	590
HR6	18.5	39.6	0.09	0.57	2.14	0.16	588	–	
HR5	3.7	10.2	0.04	0.60	2.76	0.07	462	–	
HR3	24.4	57.3	0.18	0.87	2.35	0.20	585	–	
HR2	18.8	39.8	0.10	0.64	2.11	0.16	587	–	590
MK13	11.2	27.0	0.05	0.45	2.40	0.12	582	–	
MK12	5.2	12.1	0.05	0.57	2.33	0.09	445	485	
MK11	10.8	30.4	0.04	0.31	2.83	0.13	590	–	580
MK10	6.4	14.4	0.12	0.82	2.27	0.14	524	–	
MK9	4.7	12.5	0.05	0.64	2.65	0.08	452	–	
MK8	4.8	13.9	0.06	0.79	2.93	0.08	524	–	
MK7	14.3	39.6	0.06	0.59	2.77	0.11	587	–	
MK5	3.6	10.6	0.02	0.32	2.98	0.07	440	–	420
MK3	18.6	39.5	0.09	0.55	2.13	0.16	585	–	590
MK2	45.7	108.0	0.28	0.80	2.37	0.35	605	–	
MK1	2.5	13.1	0.06	2.06	5.29	0.03	555	–	350/580
MK0	19.4	39.2	0.002	0.01	2.02	0.16	590	–	
MR1	17.9	35.2	0.06	0.44	1.97	0.13	549	590	
MR2	5.6	20.1	0.02	0.23	3.61	0.09	500	–	
MR4	3.3	12.0	0.04	0.64	3.69	0.06	485	–	
MR6	18.3	38.6	0.09	0.55	2.11	0.16	586	–	
MR7	9.4	23.8	0.04	0.39	2.53	0.11	532	590	470
MR9	21.5	40.3	0.05	0.23	1.88	0.21	586	–	580

Table 4.1: (continued)

Site	H_c [mT]	H_{cr} [mT]	M_{rs} [Am ² /kg]	M_s [Am ² /kg]	H_{cr}/H_c	M_{rs}/M_s	$T_{C,1}$ [°C]	$T_{C,2}$ [°C]	T_{ub} [°C]
MR11	21.3	52.4	0.05	0.33	2.46	0.16	580	—	200/500
MR20	7.8	24.9	0.10	0.82	3.18	0.12	520	—	
MR21	2.2	20.1	0.011	0.31	9.06	0.03	501	—	
MR22	2.6	18.8	0.05	1.68	7.29	0.03	500	—	
MR23	5.6	18.0	0.03	0.42	3.20	0.08	500	—	590
ND1	13.0	31.8	0.08	0.54	2.44	0.14	585	—	
ND3	6.7	17.0	0.08	0.74	2.56	0.11	490	—	
ND4	16.2	43.3	0.05	0.03	2.68	0.15	590	—	
ND5	18.2	44.1	0.05	0.30	2.42	0.16	595	—	≈ 580
ND6	14.2	33.2	0.04	0.30	2.34	0.14	586	—	
ND7	12.6	29.4	0.06	0.41	2.33	0.15	585	—	
ND8	16.3	33.9	0.17	0.79	2.08	0.21	585	—	
ND9	7.7	18.4	0.04	0.33	2.38	0.11	588	—	580
ND10	12.7	30.4	0.34	2.54	2.39	0.14	581	—	
ND11	3.4	14.3	0.02	0.33	4.25	0.05	575	—	
ND12	8.4	25.4	0.04	0.39	3.03	0.10	587	—	
ND13	10.5	27.0	0.03	0.24	2.57	0.11	585	—	580
ND14	25.3	49.3	0.02	0.07	1.95	0.30	385	580	
ND25	9.4	26.6	0.02	0.16	2.84	0.10	585	—	
ND26	11.3	27.0	0.03	0.25	2.39	0.12	589	—	
TK3	54.2	94.1	1.88	4.76	1.74	0.39	500	590	580
TK4	9.7	24.5	0.14	1.33	2.53	0.11	550	—	
TK5	9.1	23.8	0.20	1.89	2.62	0.11	535	—	
TK6	16.7	36.8	0.97	5.23	2.20	0.19	495	585	
TK7	15.4	33.1	1.24	6.74	2.15	0.18	587	—	580
GD5	37.4	52.3	3.63	9.62	1.40	0.38	585	—	
GD4	41.6	83.9	0.63	1.71	2.02	0.37	590	—	
GD3	11.8	50.6	0.22	1.76	4.30	0.13	580	—	
GD2	5.6	18.3	0.02	0.24	3.27	0.07	550	—	weak
GD1	12.2	31.7	0.01	0.03	2.60	0.16	580	—	
SV11	11.7	26.6	0.37	2.23	2.27	0.17	595	—	
SV10	6.4	21.9	0.10	1.49	3.40	0.07	590	—	
SV9 [†]	—	—	—	—	—	—	≈ 670	—	weak
SV8 [†]	—	—	—	—	—	—	≈ 670	—	
SV7 [‡]	31.1	46.6	0.03	0.8	1.50	0.36	≈ 590	—	
SV6	15.7	37.9	0.03	0.14	2.41	0.21	585	—	
SV5	8.4	26.0	0.03	0.23	3.07	0.11	590	—	≈ 580
SV4	14.9	39.2	0.17	1.10	2.63	0.15	590	—	
SV3	14.3	30.9	0.02	0.08	2.15	0.20	590	—	
SV2	14.6	40.6	0.01	0.04	2.79	0.19	597	—	
SV1	19.1	43.0	0.01	0.02	2.25	0.22	590	—	540
IV4	3.8	12.2	0.04	0.85	3.21	0.05	540	—	
IV3	18.5	36.5	0.62	2.85	1.97	0.22	524	—	
IV2	14.5	33.8	0.55	3.08	2.34	0.18	584	—	

Table 4.1: (continued)

Site	H_c [mT]	H_{cr} [mT]	M_{rs} [Am ² /kg]	M_s [Am ² /kg]	H_{cr}/H_c	M_{rs}/M_s	$T_{C,1}$ [°C]	$T_{C,2}$ [°C]	T_{ub} [°C]
IV1	5.7	16.6	0.05	0.72	2.90	0.07	585	–	
TA8	10.0	24.5	0.02	0.15	2.46	0.13	587	–	
TA7 [†]	–	–	–	–	–	–	≈ 590	–	
TA6	13.3	27.8	0.0008	0.005	2.09	0.16	580	–	
TA5	9.1	23.3	0.08	0.70	2.57	0.11	550	–	
TA4	19.5	37.6	0.60	2.51	1.93	0.24	534	–	
TA3	15.7	32.9	0.23	1.17	2.10	0.20	535	–	
TA1-2	4.8	14.6	0.1	1.05	3.03	0.08	530	–	

^aGiven are the characteristic hysteresis parameter coercive force (H_c), remanence coercive force (H_{cr} , measured with backfield curves), remanent saturation magnetisation (M_{rs}), saturation magnetisation and their respective ratios. $T_{C,1}$ and, if present $T_{C,2}$, indicate the Curie-temperature(s) of the samples. The maximum blocking temperature T_{ub} of the natural remanent magnetisation (NRM) was determined by continuous thermal demagnetisation with the HOTSPIN-magnetometer [MATZKA ET AL., 2003]. "weak" denotes that measurements of the respective properties was performed but fell below the sensitivity of the instrument.

[†] Available field strength of the VFTB was not sufficient to saturate the samples. Strong paramagnetic contribution and low magnetisation of the samples allowed only approximate or no estimation of T_C .

[‡] Sample SV7 exhibits a strongly wasp-waisted hysteresis loop indicating the presence of two phases with distinctly different coercivities. T_C was, in contrast to rest of the samples, determined with measurements in weak magnetic fields due to a high content of paramagnetic minerals.

4.3 Continuous thermal demagnetisation of the NRM

For a subset of 24 flows continuous demagnetisation curves were measured with a high temperature spinner magnetometer (HOTSPIN, MATZKA [2001], MATZKA ET AL. [2003]). Samples are heated and cooled in zero field to monitor the unblocking of the NRM. When heated successively to different maximum temperatures (e.g. 200°C, 400°C, 550°C and 600°C), these measurements provide a test for self-reversal or partial self-reversal. The data indicates that the largest part of the primary remanence unblocks close to T_C (see Tab. 4.1 and Fig. 4.3a), which proves that the carriers of the remanence are indeed magnetite or Ti-poor titanomagnetites. Figure 4.3b depicts a sample with two blocking temperatures. Both components exhibit identical primary remanence directions. Oxidation processes in this flow were probably incomplete.

In one case (flow KM4) an increase of the magnetisation between 420°C and 540°C is clearly visible (Fig. 4.4a). The direction of the NRM switches its direction at 420°C (Fig. 4.4b) and is at 500°C still antiparallel to the NRM at lower temperatures. Hence, it can be inferred that this sample carries two antiparallel components recorded by two magnetomineralogical phases with different T_C (see Fig. 4.4a inset). Stepwise thermal demagnetisation experiments yield only one stable component with well defined directions for individual samples. However, the overall palaeomagnetic result of the flow is highly inconsistent. Ore microscopic investigations of this sample reveals clear indication for high-temperature oxidation (see also chapter 4.1). NÉEL [1951] proposed for such systems of two phase intergrowth a mechanism of self-reversal due to magnetostatic interaction. A classical case of this mechanism was reported by HELLER AND PETERSEN [1982]. According to Néels model the phase with lower T_C ($T_{C,1}$) acquires its remanence in the external stray field of the higher T_C ($T_{C,2}$) phase between cooling from $T_{C,2}$ to $T_{C,1}$. This remanence is consequently antiparallel to the TRM (and the ambient magnetic field) of the high T_C phase. In the laboratory a self-reversing sample should, therefore, exhibit reversible changes of the magnetisation direction during heating and cooling if $T_{C,2}$ is not exceeded. Evidently, the reversible behaviour is observed during cooling the sample from 500°C to room temperature (T_0 , Fig. 4.4a and b). In the case of heating the sample above $T_{C,2}$ (Fig. 4.4c and d) the original magnetisation is erased completely and the magnetic phase with $T_{C,1}$ does not acquire a TRM. It has to be noted that only 2 components (z and one arbitrary orthogonal horizontal axis of the sample) of the NRM are measured by the HOTSPIN. Therefore, Figures 4.4b and d) depict the angle between the z axis of the sample and the projection of the NRM vector on plane defined by the sensor. The initial value of the angle is arbitrary. However, a reversible 180° shift of this angle is diagnostic for antiparallel coupling of two remanence components resulting in self-reversal of the NRM (Fig. 4.4b).

Close spatial arrangement of the two phases (intergrowth) is imperative for this mechanism. The occurrence of two T_C alone is not diagnostic for self-reversal. The above described findings represent strong evidence for magnetostatic interaction as the most probable mechanism responsible for the observed self-reversal in flow KM4. This effect, however, could only be satisfactorily shown for some samples of the flow. Others lack the feature. A plausible explanation for this fact is that different samples derive from different regions of the flow. It has been shown that the degree of oxidation and thus the composition of the magnetic minerals can display remarkable vertical (e.g. PETERSEN [1976]) or even lateral variation [YAMAMOTO ET AL., 2003] within one flow. Conditions for the development of ore grains exhibiting self-reversal is then restricted to only certain regions of the flow.

4.4 Summary

Most of the lava flows sampled show clear indications for high-temperature oxidation supported by optical and electron-microscopical observations. Evidence for low-temperature oxidation is absent. Hence, the measured palaeodirectional and intensity information obtained from these flows was acquired during or shortly after extrusion of the basalts. The minerals carrying the remanence are magnetite or Ti-poor titanomagnetite identified by T_C . The reversibility of the thermomagnetic curves indicate that most of the samples are not susceptible to oxidation during heating experiments. Samples with two T_C display slight signs of oxidation at elevated temperatures. Continuous thermal demagnetisation experiments showed that maximum unblocking and Curie-temperatures are in most cases similar. Only one flow exhibits self-reversal. It can be ruled out that self-reversal is a common feature in the Siberian Trap Basalts as proposed by METALLOVA AND FEINBERG [1967]. Summarising the findings, it can be concluded that the rockmagnetic studies substantiate the reliability of the palaeomagnetic results.

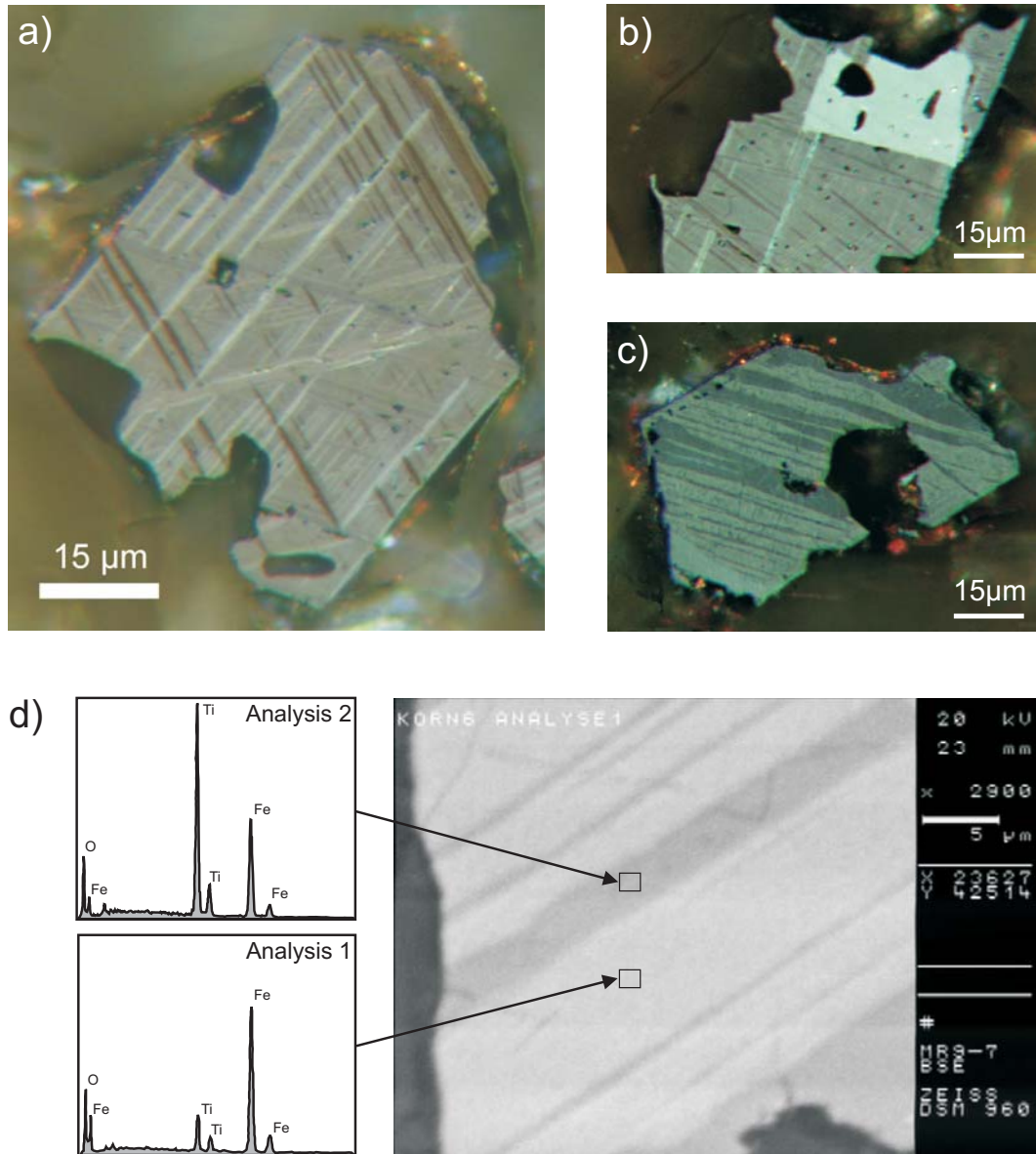


Figure 4.1: Optical-microscopical observation of polished sections under crossed Nicols show ilmenite exsolution lamellae of (a) Trellis-type (sample HR2-3), (b) composite type (sample MK3-7) and (c) Sandwich-type (sample HR7-2). Ilmenite/(titano-)magnetite exsolution lamellae are clear evidence for high-temperature oxidation of titanomagnetite. (d) shows an electron-microscopical picture (in BSE-mode) of an ore grain in sample MR9-7. Again, exsolution lamellae are clearly visible. EDX analyses confirm qualitatively on the basis of the Fe/Ti ratios that the lamellae are indeed Ti-poor titanomagnetite (analysis 1) and Ti-rich hemoilmenite (analysis 2).

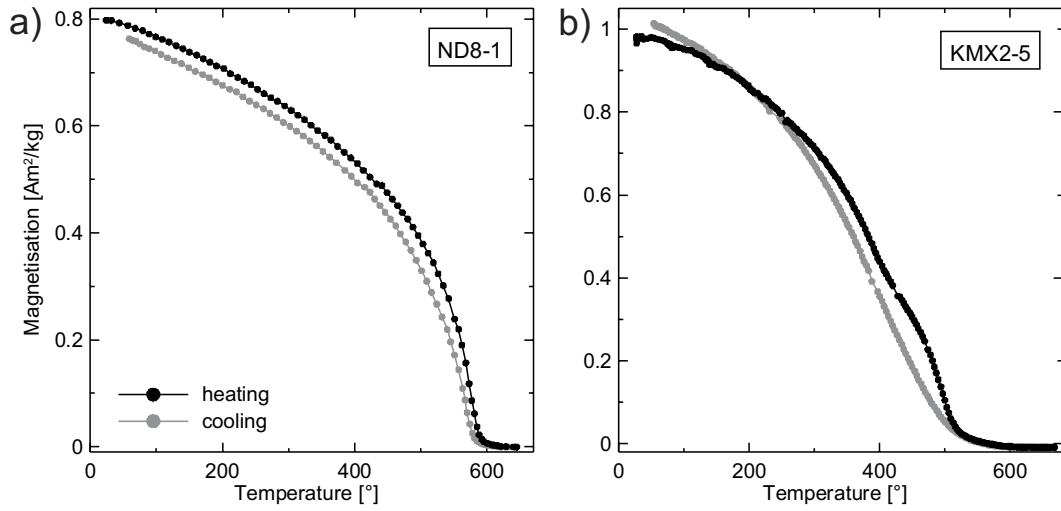


Figure 4.2: Examples for thermomagnetic curves ($M_s(T)$ -curves) measured with the VFTB. (a) Most curves have only one Curie-temperature (T_C) and are reversible. (b) 10 samples have two T_C . The cooling curve lacks the lower T_C due to oxidation during laboratory heating.

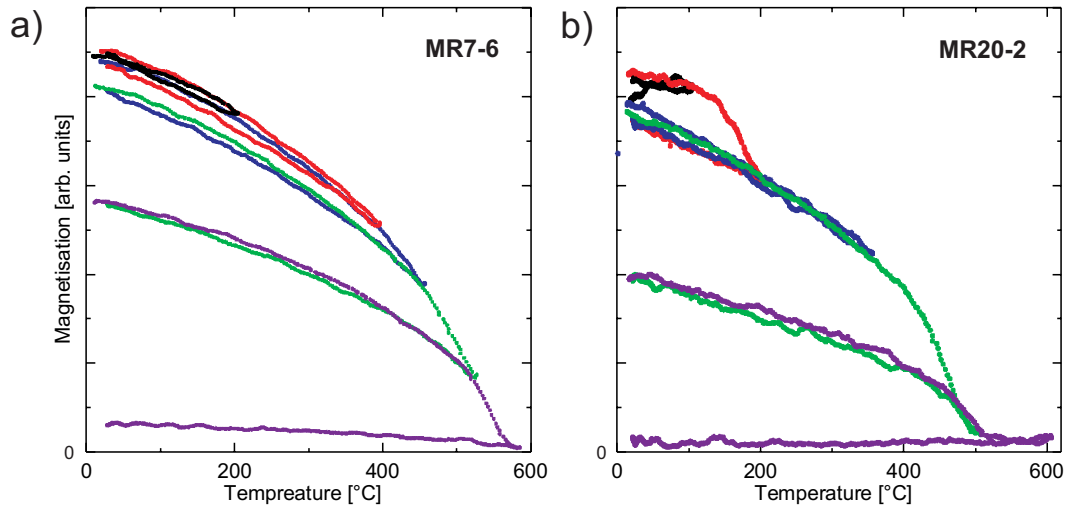


Figure 4.3: (a) Representative example of a HOTSPIN measurement. Samples were heated to a peak temperature and then cooled again to T_0 . Different colours indicate experimental runs with different peak temperatures. (b) Continuous demagnetisation of sample MR20-2 indicates two blocking temperatures (200°C and 500°C). The low T_{ub} component can be attributed to an overprint.

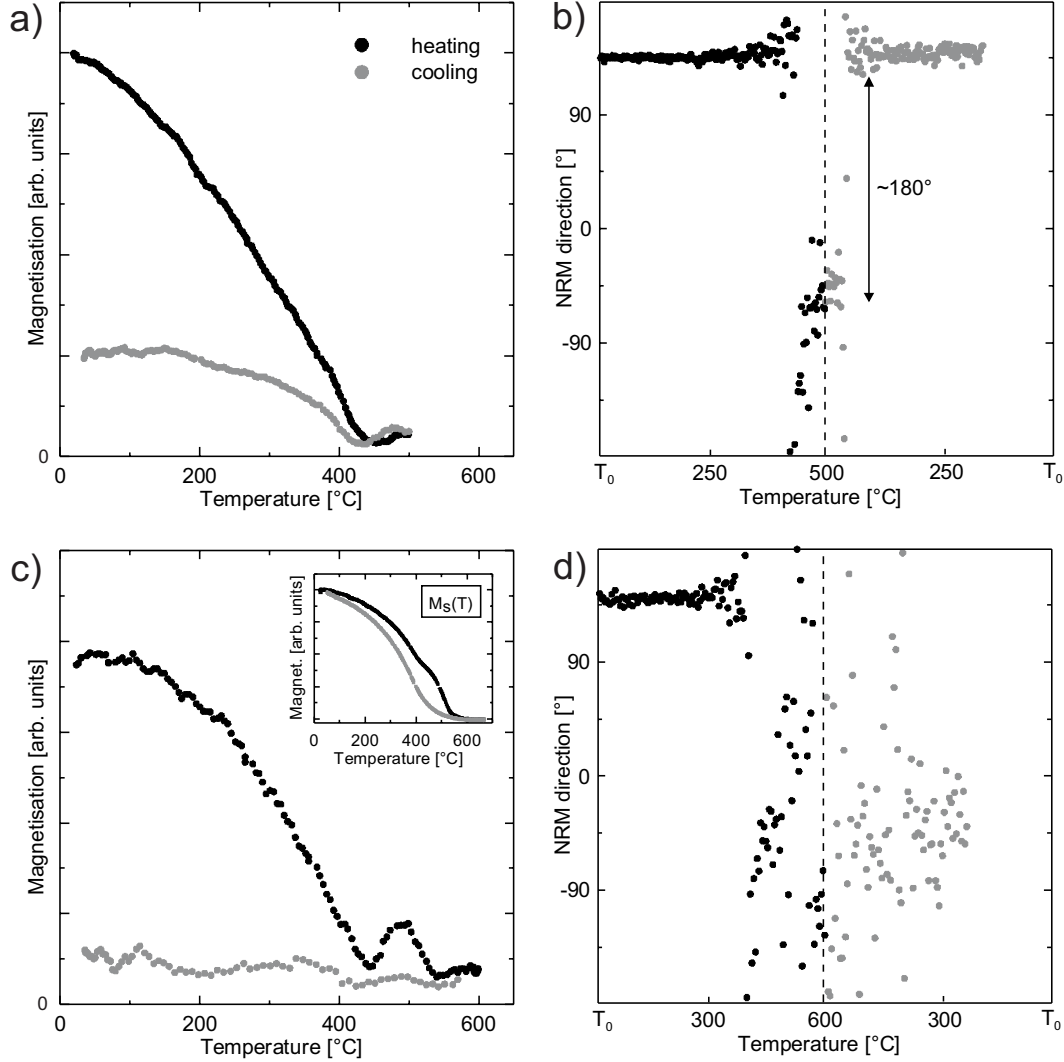


Figure 4.4: (a) Continuous demagnetisation of sample KM4 shows an increase in magnetisation between 420°C and 500°C due to self-reversal. Previous runs to lower peak temperatures indicate a second T_b around 410°C (see also Table 4.1). (b) Shown is the direction of the NRM as a function of temperature. Around 420°C the remanence switches to a antiparallel direction. This behaviour is reversible, a clear evidence for self-reversal. (c) The next experiment with a maximum temperature of 600°C again reveals the peak in magnetisation. This curve is not reversible as the sample was heated above $T_{C,2}$ erasing the magnetic information stored in the high T_C phase. The inset depicts its thermomagnetic curve revealing the presence of two different phases, probably titanomagnetite. (d) The direction of the magnetisation displays large scatter during cooling as result of the complete demagnetisation of the NRM.

Chapter 5

Palaeointensity determinations

5.1 Sample selection

The first step in selecting samples for the palaeointensity experiments was to analyse their NRM-demagnetisation behaviour. As shown in chapter 3 almost all of the specimens exhibit a single stable component. Only in few cases a weak secondary overprint was observed. Sites with inconsistent palaeomagnetic results were excluded. Determinations of the viscosity index [PRÉVOT ET AL., 1985] for one sample of each flow generally yield values below 5%. The reversibility of the thermomagnetic curves and the limited variation of susceptibility during thermal demagnetisation indicates also that all flows are, fortunately, in principle well suited for palaeointensity experiments.

5.2 Methods

A modified THELLIER AND THELLIER [1959] technique was used to determine absolute palaeointensities. This method relies on the linearity between applied field and TRM acquired by the sample. Moreover, a partial TRM (pTRM), i.e. a TRM acquired in a given temperature interval, has to be independent from a pTRM acquired in any other temperature interval. Another prerequisite is that individual pTRMs have to be additive. If these conditions are fulfilled a TRM acquired in a well defined magnetic field in the laboratory can then be compared to the NRM, allowing to estimate the strength of the Earth's magnetic field during the emplacement and cooling of the igneous rock. Modifications of the original experiment include several checks to guarantee the reliability of the results. COE [1967] added pTRM checks (CK) to the original experiment in order to monitor alteration processes of the magnetic minerals. These already routinely used CKs were performed every second heating step over the whole temperature spectrum. A further problem that can lead to wrong palaeointensity determinations is the presence of MD particles. SHASHKANOV AND METALLOVA [1972] showed that a pTRM of MD particles acquired at a given temperature interval is not fully removed if the sample is heated again to the same maximum temperature of pTRM acquisition and subsequently cooled

in zero field. This so called "tail" is caused by higher unblocking (T_{ub}) than blocking temperatures (T_b) of the pTRM of MD particles. SD particles, in contrast, have identical T_{ub} and T_b . MCCLELLAND AND BRIDEN [1996] proposed a check to identify thermal stabilisation of the MD particles. It was later implemented by LEONHARDT ET AL. [2000] and RIISAGER AND RIISAGER [2001] to monitor tails of the pTRM. Basically, this check (MD check) introduces a repeated demagnetisation step to a temperature T_i after a pTRM acquisition between T_i and room temperature T_0 (pTRM(T_i, T_0)). The NRM(T_i) after a first demagnetisation step measured before imparting the pTRM is then compared to the repeated demagnetisation (NRM_{re}(T_i)). The difference is normalised to the total NRM (NRM_t) which is graphically represented in the NRM-TRM plot [ARAI, 1963] by the intersection of the extrapolated best linear fit of the data with the ordinate. If this value exceeds a given threshold (10% to 15% in this study) the results are considered to be not reliable. Differences between the two measurements may have two causes which both severely bias the result of the experiment: (1) Changes in direction between NRM(T_i) and NRM_{re}(T_i) are interpreted as evidence for formation of alteration products with higher blocking temperatures. (2) Significant differences in intensity without directional variations are an indication for either destruction of remanence carrying minerals or changes in the domain structure of MD particles during repeated heating such as those observed by HEIDER ET AL. [1988]. This check was performed roughly at every third temperature step (e.g. 200°C, 380°C, 480°C and 520°C).

Beyond this NRM-TRM plots of samples dominated by MD particles display a characteristic concave up trend, although it can be masked by other effects and is thus not always easily detected. It has been shown by DUNLOP AND ÖZDEMİR [2000] and FABIAN [2001] that this behaviour is caused by MD remanences with $T_{ub} < T_b$. During the experiment NRM with low T_{ub} is easily removed, whereas pTRM acquisition is delayed by the presence of high T_b . A check sensitive to such spurious MD remanences (additivity check, AC) was introduced recently by KRÁSA ET AL. [2003]. It consists of an additional demagnetisation step (up to a temperature T_2) after a pTRM acquisition (pTRM(T_1, T_0), with $T_2 < T_1$). If the law of additivity is fulfilled, a prerequisite essential for a reliable palaeointensity estimate, the remaining magnetisation after this additional demagnetisation should equal the difference pTRM(T_1, T_0) – pTRM(T_2, T_0). As the difference of two pTRMs is analysed, it has to be normalised to the total TRM (TRM_t, intersection of the extrapolated linear best fit with the abscissa). As proposed by KRÁSA ET AL. [2003] the threshold for an acceptable AC error is 7%.

A total of 300 samples was subjected to the experiments described above. Additivity checks were applied to about half of the sample collection. Most samples have a diameter and length of 5 mm ('mini'-specimens). 40 samples with a diameter/length of 9 mm were

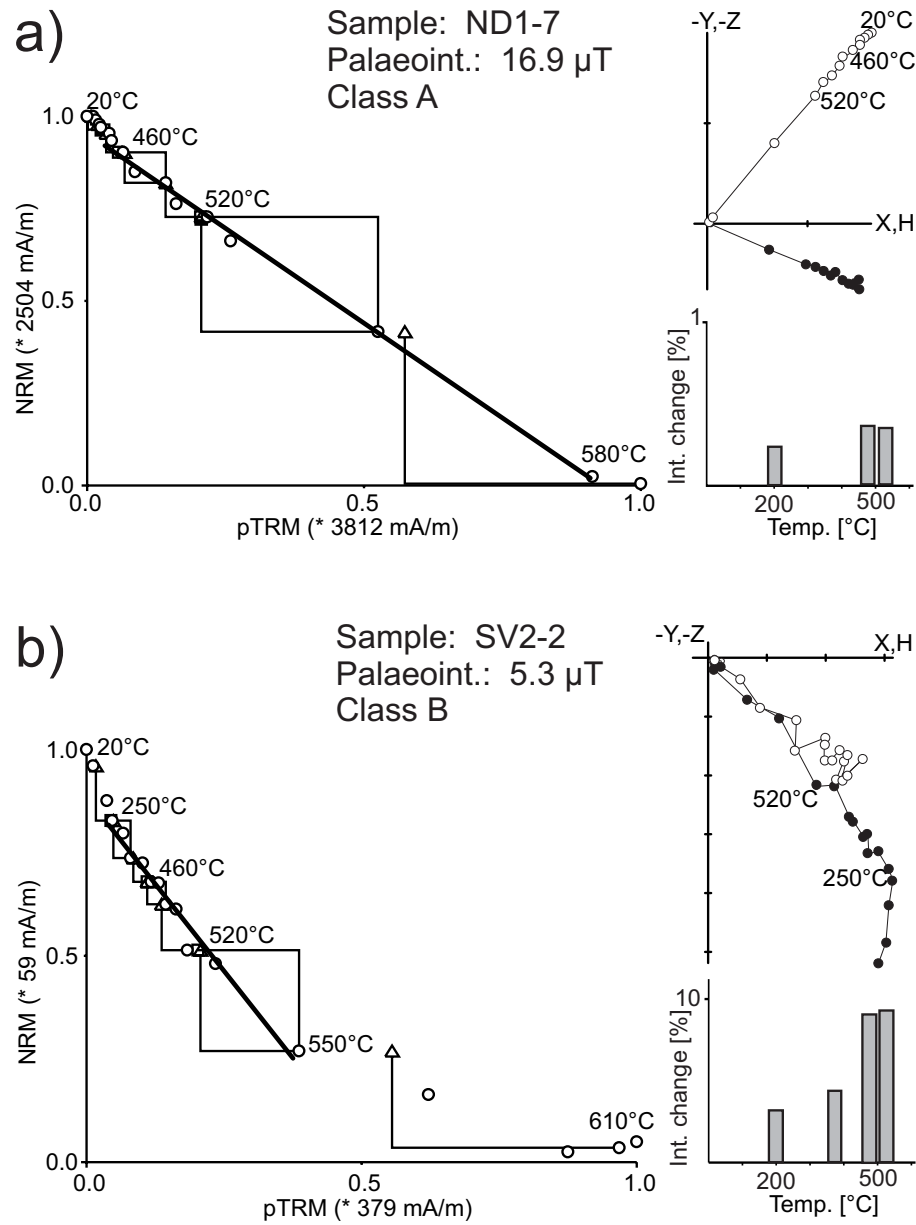


Figure 5.1: Representative examples for class A and B palaeointensity determinations. The thick black line represents the linear fit used for calculation of the palaeointensity. pTRM checks [COE, 1967] are indicated by open triangles, additivity checks [KRÁSA ET AL., 2003] by open squares. Lines display the temperature interval covered by the individual checks. Also shown are the associated ZIJDERVELD [1967] plots in core-coordinates and the results of the MD tail checks [LEONHARDT ET AL., 2000].

used. All these daughter samples were obtained from the lower part of standard inch-sized samples and not oriented with respect to the original core. To ensure the primary character of the magnetisation the mother sample (inch core) was stepwise thermally demagnetised and its demagnetisation behaviour compared to that of the respective daughter sample of the same drill core. Only 'mini'-samples which showed similar behaviour as the inch-specimens were analysed with respect to their palaeointensity information. All samples

were heated in a MMTD20 thermal demagnetiser and measured with a 2G cryogenic magnetometer housed in a shielded room. The applied field intensity during pTRM acquisition ranged between 18 and 35 μT . 45 specimens were heated and cooled in a quartz-glass tube in an inert argon atmosphere, all others in air. Results for all accepted palaeointensity determinations are independent of the sample size, applied field intensity or the atmosphere to which the samples were exposed during heating and cooling.

5.3 Reliability criteria

The data were analysed using NRM-TRM [ARAI, 1963] plots. The criteria listed below were used to assess the quality of the experimental palaeointensity data:

1. In order to ensure that the magnetisation is of primary origin the temperature range of the linear fit has to match the temperature range of the characteristic remanent magnetisation of the respective inch sample. The maximum mean angular deviation in this interval must not exceed 5° .
2. A minimum of 5 consecutive data points is required for a linear fit.
3. Less than 10% standard deviation of the linear fit.
4. At least 30% of the NRM (fraction f) has to be covered by the linear fit.
5. The difference between pTRM check and pTRM acquisition (CK error), normalised to the total TRM, has to be less than 5% before and within the linear segment to ensure that the effect of chemical alteration does not bias the results.
6. Within the linear segment, the remanence of the NRM in core coordinates or after a MD tail check should not move towards the direction of the applied field.
7. The limit for a successful MD tail check is 10% ($\frac{|\text{NRM}(T_i) - \text{NRM}_{re}(T_i)|}{\text{NRM}_t} < 0.1$) and the difference in direction should not exceed 9° .
8. The critical threshold for an acceptable AC is 7% ($\frac{|p\text{TRM}(T_1, T_0) - p\text{TRM}(T_2, T_0)|}{\text{TRM}_t} < 0.07$). This criterion could be applied only to 50% of the samples.

If conditions (1) to (7) are fulfilled, the result is classified as class A determination (63 samples). Violation of criteria (1) or (2) leads to immediate rejection. If only one of the other criteria is not fulfilled the result is a class B determination (80 samples). The upper limits for a B result are: standard deviation of the linear fit $< 15\%$, $f < 20\%$, CK error $< 7\%$, MD checks $< 15\%$, $\angle(\text{NRM}(T_i), \text{NRM}_{re}(T_i)) < 15^\circ$ and AC $< 10\%$. All other results were rejected.

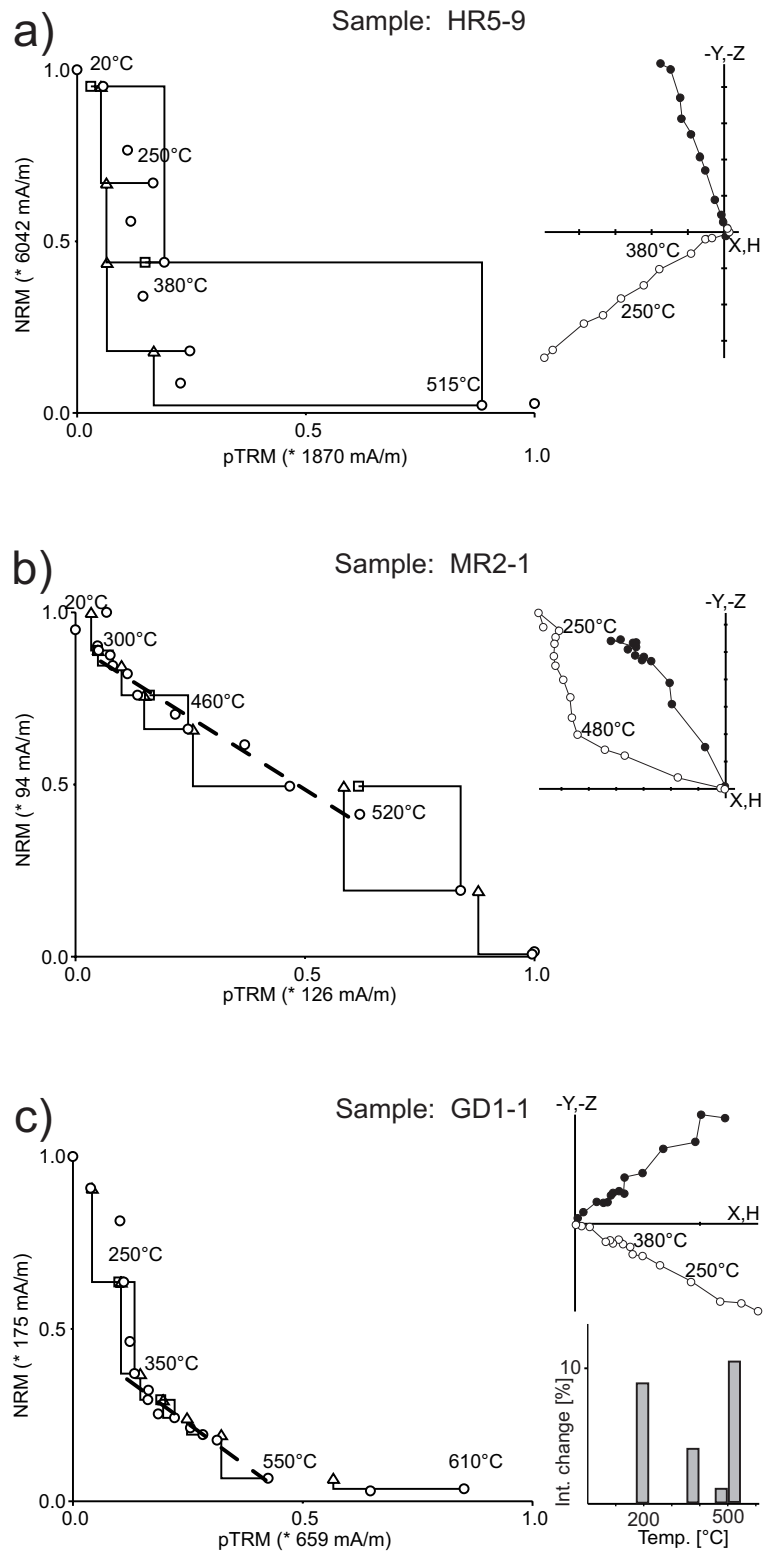


Figure 5.2: Typical examples of rejected palaeointensity results due to: (a) alteration, (b) mismatch of temperature range of the characteristic remanent magnetisation (ChRM) and the temperature range of the linear segment. In some cases the reliability criteria are exceeded in several parameters and were thus excluded from further interpretation. (in example (c) CK error > 8%, MD-check > 10%). ZIJDERVELD [1967] plots are shown in core coordinates.

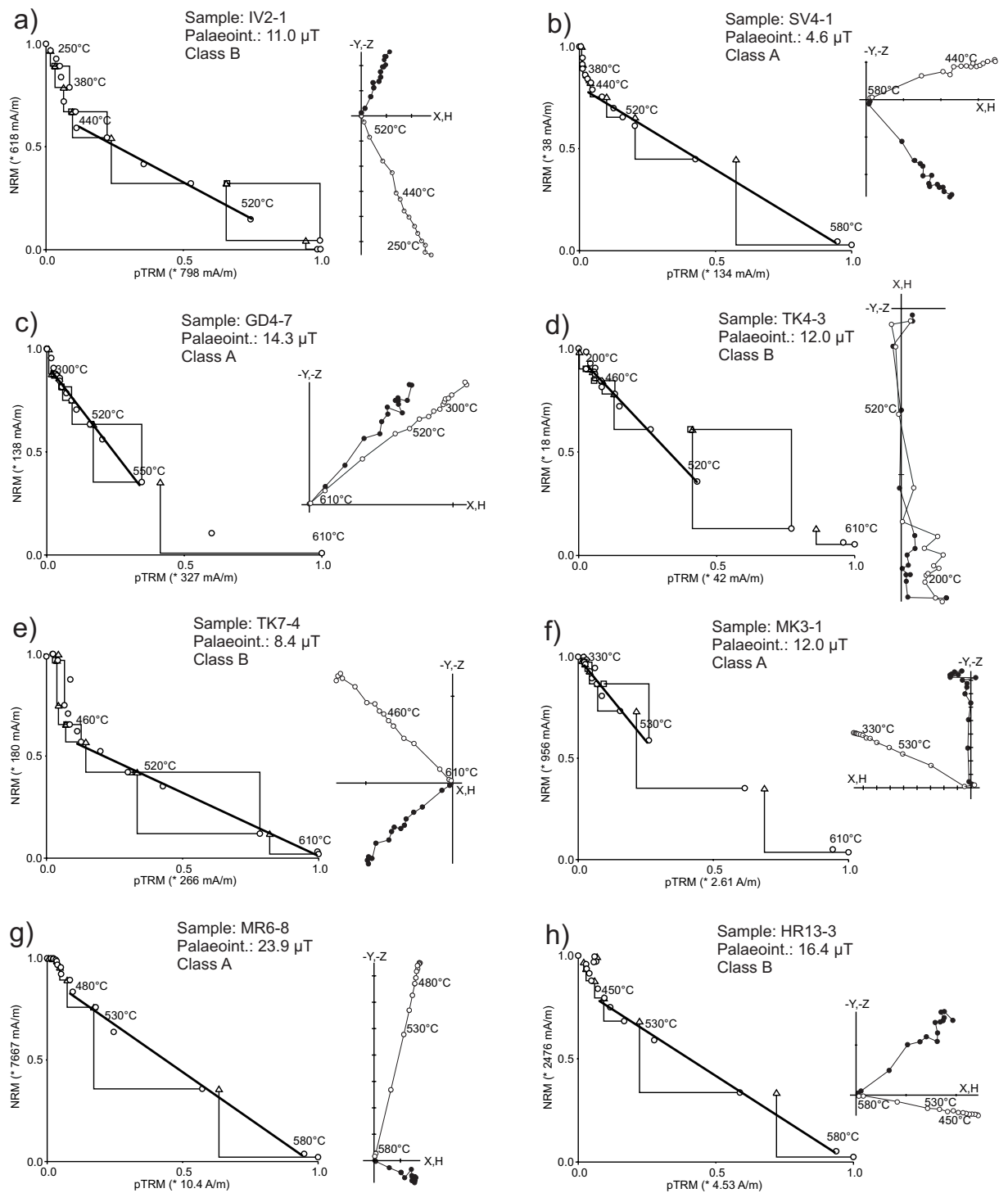


Figure 5.3: Examples of successful palaeointensity determinations (Zijderveld [1967] plots in core coordinates) of samples from different suites.

5.4 Interpretation of the Arai-plots

Representative examples for palaeointensity determinations and their associated Zijderveld-plots (ZIJDERVELD [1967], in core coordinates) of the two quality classes are shown in Figure 5.1. Figure 5.2 depicts some rejected results. In most cases of rejected results, alteration caused the destruction or formation of the remanence carrying material in the course of the experiment (Fig. 5.2a). Some samples show a clear concave curvature of the NRM-TRM plot which is indicative of the dominating role of MD particles (Fig. 5.2c). The presence of this MD tail gives estimates of the palaeointensity in the high temperature range which are systematically too low and where therefore excluded from further interpretation. In the lower temperature range the direction of the remanence does not resemble the primary component of the magnetisation (Fig. 5.3b), as could be shown for the respective sister specimens (inch cores). These specimens were also rejected.

Reliable palaeointensity estimates were obtained for $\approx 50\%$ of the samples (Table 5.1). The relatively high success rate can be attributed to the fact that high-temperature oxidised titanomagnetites, demonstrated to be dominant in the flows studied, are less susceptible to alteration during laboratory heating (see chapter 4). Figures 5a) to f) show representative results of the experiments for different stratigraphic levels. Most of the determinations cover a fraction of the NRM between 40% and 80% and have a quality factor q , as defined by COE ET AL. [1978], of 5 to 15. The weighted mean palaeointensity was calculated according to PRÉVOT ET AL. [1985]. No reliable palaeointensity estimates were obtained for samples of the Talnakh section. Most of these samples exhibit strong alteration during the experiment. In the cases of flows SV8 and SV9, a hematite component in addition to magnetite is identified (see also chapter 4). The palaeomagnetic direction carried by the hematite is identical to that of the magnetite component. Moreover, if analysing the palaeointensity information carried by magnetite and the information carried by both components only minor differences in the results are observed (1-2 μT). Similar behaviour obtained from samples containing magnetite and hematite was also observed by SOLODOVNIKOV [1995]. Two scenarios can account for these results: (1) Assuming that the hematite formed well after the emplacement of the flow by e.g. chemical processes it should carry a different ChRM. To explain the fact that the palaeodirectional and -intensity information stored in both phases are almost identical would require that the whole flow was reheated above the Curie-temperature of both magnetic phases by the following flow erasing any pre-existing NRM and imparting a new one. (2) An alternative interpretation is that the formation of the hematite is coeval with the emplacement of the flow. In this case high-temperature oxidation proceeded to higher degree than in the other flows. The NRM of both components would therefore be primary and was acquired soon after the extrusion of the flows during cooling down to ambient temperatures. Alternative

(2) is preferred as it is very unlikely that the heat input from above affected the flows (more than 3 m thick) as a whole. In order to reduce any effects from reheating, great care was taken to sample the lower part of the flows. The palaeointensity estimates for the two flows in question were determined solely for the temperature range of the magnetite component.

5.5 Results

The results of all accepted determinations are summarised in Table 5.1. Most of the flows show relatively high consistency. In the literature, a threshold of 25% variability of individual results compared to the mean value is regarded as still acceptable in-site scatter. Applying this criteria would lead to the exclusion of 6 site mean results (SV3, SV4, GD3, TK5, ND5 and KMX1). However, most of these results have small absolute standard deviations but low mean values. Therefore, the 25% threshold does not seem to be sensibly applicable in these cases and was, hence, not used in assessing the reliability of the data. Figure 5.4 shows the flow mean palaeointensity values and the calculated VDMs. Some flows only yielded one result which is indicated by open symbols. Such flows were not included in the VDM plot. The range of individual palaeointensity results is represented by the grey band in Figure 5.4b which demonstrates that the main features of the record are not an artifact of using weighted flow mean values. Moreover, there is no correlation between the palaeointensity results and their respective quality factor q or quality class proving that both high and low palaeointensity values were extracted with comparable reliability.

Unfortunately, the success rate of palaeointensity determinations of flows from the Ivakinsky suite is low and only two results satisfy the reliability criteria. They yield low palaeointensities around $10 \mu\text{T}$. During the clustering of transitional directions the intensity decreases further down to ≈ 5 to $7 \mu\text{T}$. A sudden increase ($13 \mu\text{T}$) is observed above flow SV6 which remains stable throughout the adjoining flows of this group. Just before and after the stratigraphic gap palaeointensities are around $9 \mu\text{T}$. No characteristic variation as for group B is detected in group C. The mean palaeointensity of this group is $13.7 \pm 2.9 \mu\text{T}$. The remaining part of the section displays greater variation in palaeointensity but are all significantly higher than during the transition. Averaging the results yields a value of $19.3 \pm 7.2 \mu\text{T}$. The associated VDM values, assuming a dipolar field, are shown in Fig. 5.4c. The line indicates a spline fit using the flow mean VDM to guide the eye. Intensity variations are not correlated with changes in the petrological composition or variations of rockmagnetic parameters. Hence, the record is interpreted to reflect real changes of the intensity of the Earth's magnetic field. Deciding whether these changes are only effects of locally observed non-dipolar

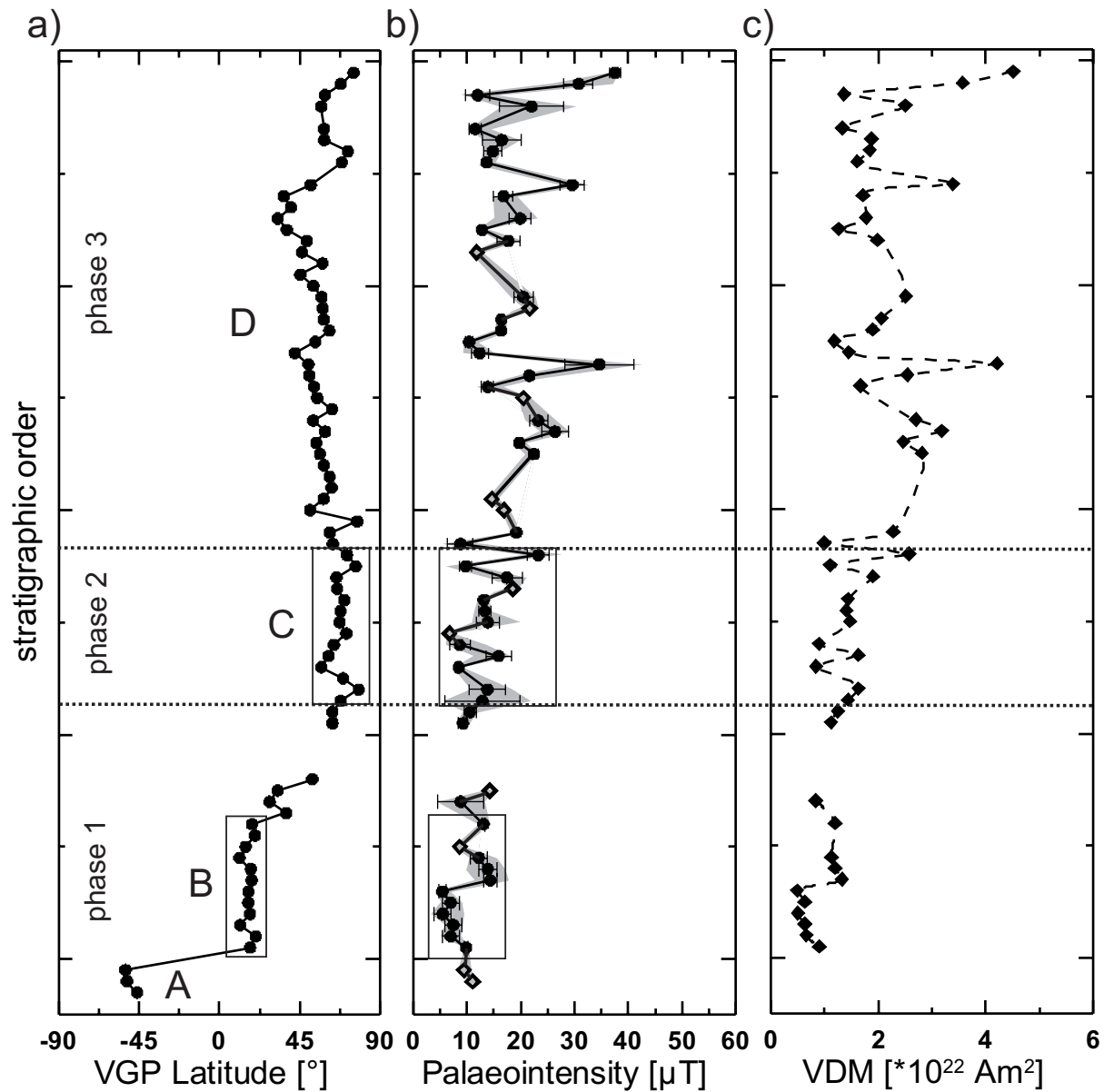


Figure 5.4: VGP latitude (a), palaeointensity (b) and VDM (c) across the studied sections. Open symbols in (b) denote results of lava flows with only one successful Thellier-Thellier-determination. Also given are the directional groups (A to D) and the phases as defined in chapter 3. Error bars correspond to the standard deviation of the weighted mean palaeointensity of the respective cooling unit. All individual palaeointensity results plot within the grey shaded areas.

components of the field, or are real changes of the dipole moment is impossible, though. The same applies to the transition and the excursion. Throughout the record VDM values are well below today's value ($\approx 8 \times 10^{22} \text{ Am}^2$). The mean VDM of the stable normal part of the section (phase 3) is $2.3 \pm 0.7 \times 10^{22} \text{ Am}^2$. Compared to this value the transitional VDMs are reduced by about 50% to 80%.

Table 5.1: Results of the palaeointensity experiments^a

Site	VGP Lat./Long.	Pol.	n/N	Sample	Cl.	ΔT	N_p	f	g	q	w	$F_p \pm \sigma_{F_p}$ [μT]	$\widetilde{F}_p \pm \sigma_{\widetilde{F}_p}$ [μT]	VDM [$\times 10^{22}$ Am ²]
Abagalakh section														
KMX4	75/185	N	2/4	KMX4-3	B	545-590	5	0.63	0.64	10.85	6.26	38.1 \pm 1.4	37.6 \pm 1.0	4.51
KMX3	68/186	N	4/4	KMX4-6	B	420-530	5	0.40	0.61	4.79	2.77	36.3 \pm 1.9		3.57
				KMX3-1	B	420-580	7	0.83	0.80	26.12	11.68	32.1 \pm 0.8	30.8 \pm 2.7	
				KMX3-2	B	420-610	8	0.87	0.81	14.33	5.85	36.9 \pm 1.8		
				KMX3-3	B	535-590	6	0.46	0.77	14.01	7.01	26.4 \pm 0.7		
KMX2	59/170	N	2/5	KMX3-6	A	300-530	9	0.44	0.69	10.62	4.01	25.4 \pm 0.7		1.36
				KMX2-4	B	250-420	6	0.36	0.75	6.62	3.31	10.9 \pm 0.5	12.0 \pm 2.2	
				KMX2-5	B	250-420	6	0.33	0.73	2.31	1.16	15.0 \pm 1.5		
KMX1	57/165	N	2/3	KMX1-2	B	360-530	7	0.54	0.61	8.64	3.87	18.6 \pm 0.7	22.0 \pm 6.1	2.51
				KMX1-4	A	390-530	6	0.36	0.67	3.27	1.64	29.9 \pm 2.2		
KM4	—	—	—	—	—	—	—	—	—	—	—	—	—	—
KM3	59/162	N	3/5	KM3-2	B	250-530	10	0.71	0.76	7.27	2.57	11.5 \pm 0.9	11.5 \pm 1.2	1.33
				KM3-4	B	200-530	11	0.69	0.80	10.83	3.60	10.6 \pm 0.5		
				KM3-5	B	20-440	9	0.45	0.80	3.19	1.21	14.1 \pm 1.6		
KM1	59/169	N	2/6	KM1-2	A	260-510	6	0.50	0.58	2.91	1.46	12.4 \pm 1.2	16.5 \pm 3.6	1.87
				KM1-5	A	370-520	6	0.33	0.54	3.68	1.84	19.6 \pm 0.9		
HR13	72/146	N	2/4	HR13-1	B	515-590	8	0.78	0.79	19.23	7.85	12.9 \pm 0.4	14.8 \pm 1.7	1.84
				HR13-3	B	450-580	6	0.87	0.69	17.94	8.97	16.4 \pm 0.6		
HR11	69/179	N	2/4	HR11-2	A	200-480	9	0.50	0.74	6.22	2.35	14.0 \pm 0.8	13.7 \pm 0.3	1.61
				HR11-6	B	535-590	6	0.22	0.65	5.71	2.85	13.4 \pm 0.3		
HR8	—	—	—	—	—	—	—	—	—	—	—	—	—	—
HR7	51/148	N	2/4	HR7-5	B	515-590	8	0.40	0.81	8.09	3.30	32.3 \pm 1.3	29.6 \pm 2.2	3.39

Site	VGP Lat./Long.	Pol.	n/N	Sample	Cl.	ΔT	N_p	f	g	q	w	$F_p \pm \sigma_{F_p}$ [μT]	$\widetilde{F}_p \pm \sigma_{\widetilde{F}_p}$ [μT]	VDM [$\times 10^{22} \text{ Am}^2$]
HR6	36/146	N	2/4	HR7-6 HR6-1 HR6-4	B A A	300-530 20-610 420-530	9 16 5	0.64 1.00 0.36	0.77 0.81 0.65	16.08 23.85 2.95	6.08 6.37 1.71	28.1 \pm 0.9 16.1 \pm 0.6 19.2 \pm 1.5	16.8 \pm 1.8	1.72
HR5	40/148	N	0/3	—	—	—	—	—	—	—	—	—	—	—
HR3	33/172	N	4/4	HR3-2 HR3-3 HR3-4 HR3-7	A A A A	200-580 510-610 515-590 20-580	13 5 8 15	0.88 0.81 0.73 0.97	0.74 0.70 0.83 0.81	13.73 12.34 15.23 27.89	4.14 7.13 6.22 7.74	14.9 \pm 0.7 22.9 \pm 1.1 22.8 \pm 0.9 17.6 \pm 0.5	19.9 \pm 2.0	1.77
HR2	38/160	N	3/3	HR2-3 HR2-4 HR2-5	A A A	300-530 20-610 20-580	9 16 15	0.45 1.00 0.98	0.69 0.85 0.75	5.22 18.28 19.08	1.97 4.89 5.29	13.0 \pm 0.8 12.0 \pm 0.6 13.4 \pm 0.5	12.8 \pm 0.4	1.27
MK13	49/150	N	2/3	MK13-6 MK13-9	B B	360-530 360-530	7 7	0.64 0.62	0.69 0.68	5.66 5.63	2.53 2.52	19.9 \pm 1.5 15.5 \pm 1.2	17.7 \pm 2.2	1.99
MK12	46/148	N	1/3	MK12-2	B	300-450	6	0.57	0.68	9.42	4.71	11.8 \pm 0.5	—	—
MK11	58/146	N	0/3	—	—	—	—	—	—	—	—	—	—	—
MK10	45/17	N	0/5	—	—	—	—	—	—	—	—	—	—	—
MK9	53/178	N	0/4	—	—	—	—	—	—	—	—	—	—	—
MK8	57/131	N	2/5	MK8-6 MK8-7	B B	250-420 420-610	6 8	0.36 0.91	0.65 0.78	2.30 17.99	1.15 7.35	18.0 \pm 1.9 20.9 \pm 0.8	20.5 \pm 1.8	2.51
MK7	58/140	N	1/5	MK7-7	A	200-580	13	0.83	0.73	9.41	2.84	21.7 \pm 1.4	—	—
MK5	59/117	N	2/5	MK5-3 MK5-4	B B	200-420 200-420	7 7	0.81 0.77	0.65 0.68	5.43 4.16	2.43 1.86	16.4 \pm 1.6 16.4 \pm 2.1	16.4 \pm 0.03	2.06
MK4	62/169	N	2/3	MK4-5 MK4-6	B B	20-610 450-610	16 7	0.99 0.95	0.63 0.62	23.16 16.05	6.19 7.18	16.5 \pm 0.5 16.1 \pm 0.6	16.3 \pm 0.2	1.89
MK3	54/157	N	3/3	MK3-1 MK3-3 MK3-4	A A A	330-530 100-530 360-530	8 12 7	0.38 0.39 0.42	0.73 0.74 0.65	3.01 4.52 5.29	1.23 1.43 2.37	12.0 \pm 1.1 10.4 \pm 0.7 9.5 \pm 0.5	10.4 \pm 0.8	1.18
MK2	42/102	N	4/4	MK2-2	B	510-610	5	0.86	0.61	25.69	14.83	14.7 \pm 0.3	12.4 \pm 1.5	1.45

Site	VGP Lat./Long.	Pol.	n/N	Sample	Cl.	ΔT	N_p	f	g	q	w	$F_p \pm \sigma_{F_p}$ [μT]	$\widetilde{F}_p \pm \sigma_{\widetilde{F}_p}$ [μT]	VDM [$\times 10^{22} \text{ Am}^2$]
MK1	50/113	N	2/4	MK2-4	A	420-580	7	0.92	0.68	8.64	3.86	9.3 \pm 0.7		
				MK2-5	A	515-590	8	0.62	0.83	8.21	3.35	9.2 \pm 0.6		
				MK2-6	B	390-550	7	0.56	0.63	13.35	5.97	10.4 \pm 0.3		
MK0	50/135	N	2/4	MK1-1	B	510-610	5	0.83	0.66	7.05	4.07	42.2 \pm 3.3	34.6 \pm 6.4	4.21
				MK1-3	B	420-610	8	0.87	0.83	15.26	6.23	29.6 \pm 1.4		
				MK0-3	B	300-610	12	1.00	0.75	12.41	3.93	21.9 \pm 1.3	21.6 \pm 0.3	2.54
MR1	53/127	N	4/5	MK0-5	B	420-580	7	0.96	0.70	7.45	3.33	21.3 \pm 1.9		
				MR1-1	B	330-530	8	0.76	0.78	9.44	3.85	12.7 \pm 0.8	13.8 \pm 1.1	1.67
				MR1-2	B	200-530	11	0.68	0.79	9.27	3.09	14.7 \pm 0.9		
MR2	55/127	N	1/4	MR1-5	B	330-530	8	0.75	0.77	9.83	4.01	11.8 \pm 0.7		
				MR1-6	A	300-550	9	0.79	0.73	9.18	3.47	16.6 \pm 1.0		
				MR2-2	B	360-510	6	0.65	0.76	8.37	4.18	20.4 \pm 1.2		
MR4	63/157	N	0/4	-	-	-	-	-	-	-	-	-		
MR6	53/147	N	3/3	MR6-2	A	420-580	7	0.91	0.77	11.38	5.09	20.6 \pm 1.3	23.3 \pm 1.7	2.70
				MR6-3	A	420-530	5	0.42	0.68	5.00	2.89	26.3 \pm 1.5		
				MR6-8	A	480-580	5	0.88	0.67	12.69	7.33	23.9 \pm 1.1		
MR7	59/144	N	2/3	MR7-2	B	420-530	5	0.63	0.69	8.33	4.81	28.0 \pm 1.5	26.4 \pm 2.5	3.18
				MR7-7	A	390-530	6	0.51	0.73	4.94	2.47	23.3 \pm 1.8		
				MR9-4	B	300-530	9	0.74	0.73	12.95	4.90	20.8 \pm 0.9	19.7 \pm 0.6	2.47
MR9	54/87	N	3/5	MR9-5	B	390-530	6	0.70	0.66	8.55	4.28	18.6 \pm 1.0		
				MR9-6	A	400-550	6	0.71	0.65	11.39	5.69	19.6 \pm 0.8		
				MR11-3	A	430-550	5	0.68	0.48	74.35	42.93	22.6 \pm 0.1	22.5 \pm 0.7	2.81
MR11	56/111	N	3/5	MR11-4	B	390-530	6	0.68	0.63	5.16	2.58	22.0 \pm 1.8		
				MR11-8	B	420-580	7	0.90	0.77	7.54	3.37	20.8 \pm 1.9		
				-	-	-	-	-	-	-	-	-		
MR20	59/137	N	0/4	-	-	-	-	-	-	-	-	-		
MR21	62/138	N	0/4	-	-	-	-	-	-	-	-	-		
MR22	63/152	N	0/3	-	-	-	-	-	-	-	-	-		
MR23	58/144	N	1/3	MR23-1	A	300-610	12	0.92	0.85	17.97	5.68	14.6 \pm 0.6		

Site	VGP Lat./Long.	Pol.	n/N	Sample	Cl.	ΔT	N_p	f	g	q	w	$F_p \pm \sigma_{F_p}$ [μT]	$\widetilde{F}_p \pm \sigma_{\widetilde{F}_p}$ [μT]	VDM [$\times 10^{22} \text{ Am}^2$]
ND1	51/144	N	1/4	ND1-7	A	380-580	9	0.94	0.71	28.62	10.82	16.9 ± 0.4		
ND3	77/153	N	0/3	—	—	—	—	—	—	—	—	—		
ND4	62/159	N	2/3	ND4-1	A	440-580	7	0.86	0.71	16.43	7.35	19.3 ± 0.7	19.2 ± 0.3	2.27
				ND4-4	A	250-520	10	0.65	0.81	5.91	2.09	18.8 ± 1.7		
ND5	64/183	N	3/4	ND5-1	B	410-520	6	0.57	0.71	5.93	2.97	6.2 ± 0.4	8.8 ± 2.3	1.00
				ND5-3	A	480-580	5	0.80	0.59	10.31	5.95	10.9 ± 0.5		
				ND5-5	A	545-590	5	0.46	0.72	3.77	2.18	6.4 ± 0.6		
ND6	72/242	E	3/3	ND6-1	B	350-580	10	0.90	0.82	9.03	3.19	27.3 ± 2.2	23.3 ± 2.0	2.57
				ND6-3	B	440-580	7	0.75	0.74	7.14	3.19	20.7 ± 1.6		
				ND6-7	B	460-580	6	0.75	0.68	14.68	7.34	22.6 ± 0.8		
ND7	76/261	E	4/4	ND7-2	B	440-520	5	0.47	0.72	5.05	2.92	9.4 ± 0.6	9.7 ± 1.2	1.10
				ND7-3	A	515-565	6	0.38	0.75	4.84	2.42	5.9 ± 0.4		
				ND7-4	B	440-610	8	0.90	0.79	21.31	8.70	11.0 ± 0.4		
				ND7-6	B	460-580	6	0.81	0.72	6.67	3.33	9.2 ± 0.8		
ND8	66/212	E	2/4	ND8-1	A	20-610	16	0.98	0.55	23.58	6.30	15.4 ± 0.4	17.4 ± 2.8	1.90
				ND8-2	A	200-580	13	0.96	0.67	11.93	3.60	20.9 ± 1.1		
ND9	66/223	E	1/3	ND9-7	B	480-580	5	0.90	0.48	11.80	6.82	18.5 ± 0.7		
ND10	70/237	E	2/3	ND10-4	A	480-580	5	0.86	0.61	9.31	5.37	13.1 ± 0.7	13.1 ± 0.03	1.43
				ND10-5	A	515-565	6	0.58	0.76	17.83	8.92	13.1 ± 0.3		
ND11	68/258	E	3/4	ND11-1	A	440-580	7	0.87	0.65	7.84	3.50	11.1 ± 0.8	13.3 ± 1.0	1.41
				ND11-3	B	460-580	6	0.87	0.55	10.02	5.01	13.2 ± 0.6		
				ND11-4	B	440-580	7	0.90	0.60	14.60	6.53	14.5 ± 0.5		
ND12	67/245	E	4/4	ND12-1	A	480-580	5	0.83	0.63	6.26	3.62	11.5 ± 1.0	13.8 ± 2.2	1.47
				ND12-2	A	480-610	6	0.92	0.73	12.38	6.19	11.3 ± 0.6		
				ND12-5	A	480-610	6	0.93	0.76	7.37	3.68	10.7 ± 1.0		
				ND12-6	B	440-580	7	0.83	0.67	13.25	5.93	19.9 ± 0.8		
ND13	71/251	E	1/3	ND13-3	B	460-580	6	0.89	0.52	4.88	2.44	6.7 ± 0.6		
ND14	64/237	E	4/4	ND14-1	A	480-580	5	0.51	0.69	7.76	4.48	5.8 ± 0.3	8.6 ± 1.9	0.89

Site	VGP Lat./Long.	Pol.	n/N	Sample	Cl.	ΔT	N_p	f	g	q	w	$F_p \pm \sigma_{F_p}$ [μT]	$\widetilde{F}_p \pm \sigma_{\widetilde{F}_p}$ [μT]	VDM [$\times 10^{22} \text{ Am}^2$]
ND25	61/222	E	3/4	ND14-2	A	440-580	6	0.57	0.72	5.91	2.96	6.1 ± 0.4		
				ND14-3	B	440-550	6	0.40	0.65	2.40	1.20	5.9 ± 0.7		
				ND14-6	A	200-580	13	0.90	0.68	16.40	4.94	13.3 ± 0.5		
				ND25-1	B	480-580	5	0.92	0.54	7.85	4.53	13.9 ± 0.9	15.9 ± 2.3	1.63
				ND25-2	A	480-580	5	0.92	0.61	8.00	4.62	11.0 ± 0.8		
ND26	57/215	E	3/4	ND25-7	A	460-580	6	0.90	0.52	27.75	13.88	18.1 ± 0.3		
				ND26-1	A	480-580	5	0.84	0.41	5.90	3.41	7.6 ± 0.4	8.4 ± 0.4	0.84
				ND26-3	A	480-580	5	0.84	0.57	9.11	5.26	8.8 ± 0.5		
				ND26-4	B	480-580	5	0.72	0.47	3.94	2.27	8.8 ± 0.8		
TK3	69/223	E	0/3	—	—	—	—	—	—	—	—	—	—	
TK4	78/210	E	2/4	TK4-1	B	200-500	10	0.45	0.76	3.98	1.41	18.2 ± 1.6	13.8 ± 3.4	1.63
TK5	68/208	E	2/5	TK4-3	B	200-520	11	0.58	0.73	10.55	3.52	12.0 ± 0.5		
				TK5-1	A	300-480	7	0.31	0.72	5.89	2.64	21.6 ± 0.8	12.9 ± 6.9	1.44
TK6	63/164	N	2/4	TK5-7	B	300-520	9	0.58	0.55	13.78	5.21	8.4 ± 0.2		
				TK6-6	B	480-580	5	0.85	0.70	9.43	5.45	9.3 ± 0.6	10.5 ± 1.1	1.24
TK7	63/152	N	2/4	TK6-8	B	480-610	6	0.86	0.72	14.45	7.23	11.5 ± 0.5		
				TK7-4	B	460-610	7	0.86	0.72	16.56	7.41	8.4 ± 0.3	9.2 ± 0.8	1.12
				TK7-7	B	460-580	6	0.86	0.70	17.23	8.62	9.9 ± 0.3		
Listvjanka section														
GD5	52/146	N	0/3	—	—	—	—	—	—	—	—	—		
GD4	33/174	N	1/2	GD4-7	A	300-550	10	0.57	0.75	11.05	3.91	14.3 ± 0.6		
GD3	28/143	N	2/3	GD3-2	A	480-580	5	0.81	0.58	10.06	5.81	4.3 ± 0.2	8.8 ± 4.4	0.84
				GD3-5	A	480-580	5	0.77	0.57	11.01	6.36	13.0 ± 0.5		
GD2	37/127	N	0/4	—	—	—	—	—	—	—	—	—		
GD1	18/118	T	2/5	GD1-5	A	100-480	10	0.40	0.80	5.16	1.83	12.8 ± 0.8	13.1 ± 0.2	1.20
				GD1-6	A	20-480	11	0.49	0.82	7.01	2.34	13.2 ± 0.8		

Site	VGP Lat./Long.	Pol.	n/N	Sample	Cl.	ΔT	N_p	f	g	q	w	$F_p \pm \sigma_{F_p}$ [μT]	$\widetilde{F}_p \pm \sigma_{\widetilde{F}_p}$ [μT]	VDM [$\times 10^{22} \text{ Am}^2$]
SV11	20/111	T	0/4	—	—	—	—	—	—	—	—	—	—	—
SV10	15/114	T	1/4	SV10-5	A	480-580	5	0.79	0.56	13.48	7.78	8.6 ± 0.3	—	—
SV9	11/105	T	3/4	SV9-1	B	410-580	8	0.26	0.73	6.72	2.74	12.8 ± 0.7	12.2 ± 1.6	1.13
				SV9-4	A	200-580	13	0.36	0.86	7.06	2.13	10.1 ± 0.4	—	—
				SV9-6	B	250-610	13	0.29	0.86	2.60	0.79	15.3 ± 1.4	—	—
SV8	18/110	T	4/4	SV8-1	A	410-610	9	0.31	0.67	4.16	1.57	12.4 ± 0.6	13.8 ± 1.7	1.20
				SV8-2	B	300-580	11	0.26	0.84	2.46	0.82	16.9 ± 1.5	—	—
				SV8-4	B	250-610	13	0.33	0.90	5.14	1.55	16.4 ± 1.0	—	—
				SV8-6	B	350-580	10	0.27	0.83	2.93	1.04	9.6 ± 0.7	—	—
SV7	18/116	T	4/4	SV7-2	B	200-520	11	0.52	0.89	6.93	2.31	15.1 ± 1.0	14.3 ± 1.3	1.32
				SV7-3	A	200-500	10	0.51	0.88	10.97	3.88	11.0 ± 0.5	—	—
				SV7-6	A	300-610	15	0.33	0.75	2.93	0.81	14.0 ± 1.2	—	—
				SV7-7	B	350-500	7	0.47	0.82	8.33	3.72	17.4 ± 0.8	—	—
SV6	16/113	T	3/3	SV6-1	B	500-610	5	0.79	0.64	11.37	6.57	4.9 ± 0.2	5.4 ± 0.6	0.49
				SV6-2	B	380-520	7	0.75	0.67	9.90	4.43	6.7 ± 0.3	—	—
				SV6-6	B	410-550	7	0.55	0.64	8.09	3.62	4.7 ± 0.0	—	—
SV5	16/116	T	2/3	SV5-1	B	460-610	7	0.91	0.74	10.91	4.88	5.8 ± 0.4	7.0 ± 1.6	0.63
				SV5-2	B	250-580	12	0.94	0.79	9.30	2.94	8.9 ± 0.7	—	—
SV4	17/111	T	3/3	SV4-1	A	440-580	7	0.92	0.62	17.01	7.61	4.6 ± 0.2	5.5 ± 1.7	0.50
				SV4-2	B	440-580	7	0.90	0.53	17.01	7.61	4.7 ± 0.1	—	—
				SV4-6	A	300-550	10	0.32	0.85	8.97	3.17	9.3 ± 0.3	—	—
SV3	12/117	T	2/3	SV3-1	B	500-610	5	0.79	0.61	4.60	2.66	5.7 ± 0.6	7.4 ± 1.6	0.63
				SV3-3	A	480-580	5	0.33	0.65	5.31	3.07	9.0 ± 0.4	—	—
SV2	20/115	T	2/4	SV2-1	A	200-520	11	0.53	0.88	9.36	3.12	8.6 ± 0.4	7.0 ± 1.7	0.66
				SV2-2	B	250-550	11	0.64	0.78	9.08	3.03	5.3 ± 0.3	—	—
SV1	17/112	T	2/3	SV1-1	B	350-520	8	0.51	0.83	6.87	2.80	9.4 ± 0.6	9.8 ± 0.4	0.9
IV4	—	—	—	SV1-2	B	250-550	11	0.76	0.87	8.27	2.76	10.2 ± 0.8	—	—

Site	VGP Lat./Long.	Pol.	n/N	Sample	Cl.	ΔT	N_p	f	g	q	w	$F_p \pm \sigma_{F_p}$ [μT]	$\widetilde{F}_p \pm \sigma_{\widetilde{F}_p}$ [μT]	VDM [$\times 10^{22} \text{ Am}^2$]
IV3	-53/343	R	1/4	IV3-1	B	200-440	7	0.40	0.73	2.25	1.01	9.4 ± 1.2		
IV2	-52/359	R	1/3	IV2-1	B	440-520	5	0.65	0.72	9.53	5.50	11.0 ± 0.6		
IV1	-46/346	R	0/2	-	-	-	-	-	-	-	-	-		
Talnakh section														
TA8	21/116	T	0/2	-	-	-	-	-	-	-	-	-		
TA7	11/113	T	0/2	-	-	-	-	-	-	-	-	-		
TA6	16/100	T	0/2	-	-	-	-	-	-	-	-	-		
TA5	-62/65	T	0/2	-	-	-	-	-	-	-	-	-		
TA4	-56/314	R	0/2	-	-	-	-	-	-	-	-	-		
TA3	-56/7	R	0/2	-	-	-	-	-	-	-	-	-		
TA1-2	-	-	-	-	-	-	-	-	-	-	-	-		

^aThe results are listed in stratigraphic order from top (KMX4) to bottom (TA1-2). The Talnakh profile is parallel to the lower part of the Listvjanka section. n/N denotes the ratio of successful to performed experiments, Cl. the quality class according to the reliability criteria (see text). ΔT specifies the temperature range of the linear segment in the NRM-TRM-plots, N_p the number of successive data points used for the calculation of the palaeointensity. f , g and q are the fraction of the NRM, the gap and quality factor, respectively, as defined by COE ET AL. [1978]. $F_p \pm \sigma_{F_p}$ represents the result of an individual palaeointensity experiment and its associated standard deviation. $\widetilde{F}_p \pm \sigma_{\widetilde{F}_p}$ is, if applicable, the calculated weighted mean palaeointensity using the weighting factor w according to PRÉVOT ET AL. [1985]. The associated flow mean VDM is given in the last column.

Chapter 6

Discussion: Features of the record

6.1 Transitional VGP path

Based on palaeomagnetic data available in the late 1970's HOFFMAN AND FULLER [1978], HOFFMAN [1979] and FULLER ET AL. [1979] concluded that transitional fields are dominated by non-dipolar zonal, and thus axis-symmetric, harmonics (see also chapter 1.2.2, model 3). The observed VGP path of a specific reversal should therefore depend on the location of the section studied and would be confined to paths passing roughly over the sampling site (near-sided reversal) or to antipodal paths (far-sided). A dataset comprising numerous geographically well distributed reversal records should consequentially yield no preferred transitional VGP paths. However, with the emergence of more reversal records the concept of axis-symmetric transitional non-dipole fields was challenged. Studying sedimentary data of geologically young reversals derived from various locations around the world CLEMENT [1991] and LAJ ET AL. [1991] identified two preferred antipodal paths, one along the Americas and the other across East Asia. But again, these observations have been greeted with scepticism, with doubt expressed about the insufficient spatial distribution of the sites and the statistical validity of these studies (see LOVE [1998] for a review). Volcanic records also yield ambiguous results. PRÉVOT AND CAMPS [1993] disclaimed the existence of preferred VGP paths, inferring that transitional fields are statistically axis-symmetric. A statistical analyses performed by LOVE [1998] came to contradictory conclusions, supporting the concept of the preferred VGP paths along America and across Asia. In a recent study VALET AND HERRERO-BERVERA [2003] went even further postulating the existence of a third path across Europe and Africa. The existence or not of preferred transitional VGP paths is vital for the understanding of geodynamo processes and their possible relationship with CMB conditions (e.g. LAJ ET AL. [1992] and LEONHARDT AND SOFFEL [2002]). The controversy underlines the importance of collecting information from more detailed records. As already mentioned in the discussion of reversal models in chapter 1.2.2 the question if dipolar or non-dipolar fields dominate during a reversal is far from being answered yet.

The palaeodirectional behaviour in the studied sections has been already discussed in chapter 3. Figure 6.1a shows a synopsis of this record. Combining the individual flows into groups, another feature becomes evident. In Figure 6.1b the VGPs are plotted in stereographic projection. The movement of the VGPs can be approximated very well by a great-circle. The thick black line represents a fit using all data points excluding group A, GD3 and GD4. Exclusion of group A can be justified by the relatively large confidence oval associated with its mean pole. The cause for the loop formed by GD3 and GD4 remains unclear. Both poles are of acceptable quality. However, the remaining VGPs define a great circle path which is roughly centred around the site meridian. HOFFMAN [1977] referred to such VGPs as near-sided and its corresponding VGP paths as near-sided paths. It has to be kept in mind, though, that the VGPs plotted in Fig. 6.1 are not yet rotated into the Late Permian/Early Triassic geographic reference system. Figure 6.2 shows the mean VGPs of the directional groups – and the flow mean VGPs which were not included in one of the groups – after rotation of the mean palaeomagnetic pole of the Siberian platform to the North Pole. The corresponding rotation pole is 0°N , 63°N (37° clockwise rotation [SMETHURST ET AL., 1998]). Siberia is displayed in its Permian position, but may be freely moved longitudinally. Such a longitudinal movement of Siberia would not affect the relative position of the VGPs with respect to Siberia. After correction of the VGP path for plate motion, it becomes apparent that it is longitudinally confined but the notion of a near-sided configuration cannot be sustained. In contrary, the VGP path is perpendicular to the path expected for a near- or far-sided configuration. A dominance of zonal harmonics throughout the time interval covered by the record can therefore be ruled out, making a strong contribution of sectorial components more likely. One reversal record alone does not allow a definite conclusion about the order and degree of the non-dipole harmonics involved. However, a plausible model explaining the longitudinal confinement would be that the sectorial components of the magnetic field are getting stronger in the first part of the transition until reaching roughly the magnitude of the dipole component. In the second half of the transition, these non-dipole components decay again. According to this model, the dipole component would decay in the first half, switch polarity in the middle of the transition and build up again in the second half. Such a model is consistent with the pronounced low of the palaeointensity record during the transition. Though, it has to be emphasised that the observed pattern can also be explained by a plethora of equivalent models, as for example by a rotating dipole of variable moment.

Detailed reversal records derived from volcanic sequences (e.g. MANKINEN ET AL. [1985], RIISAGER AND ABRAHAMSEN [1999], LEONHARDT ET AL. [2002], RIISAGER ET AL. [2003]) often exhibit a more complex directional pattern of the transitional field

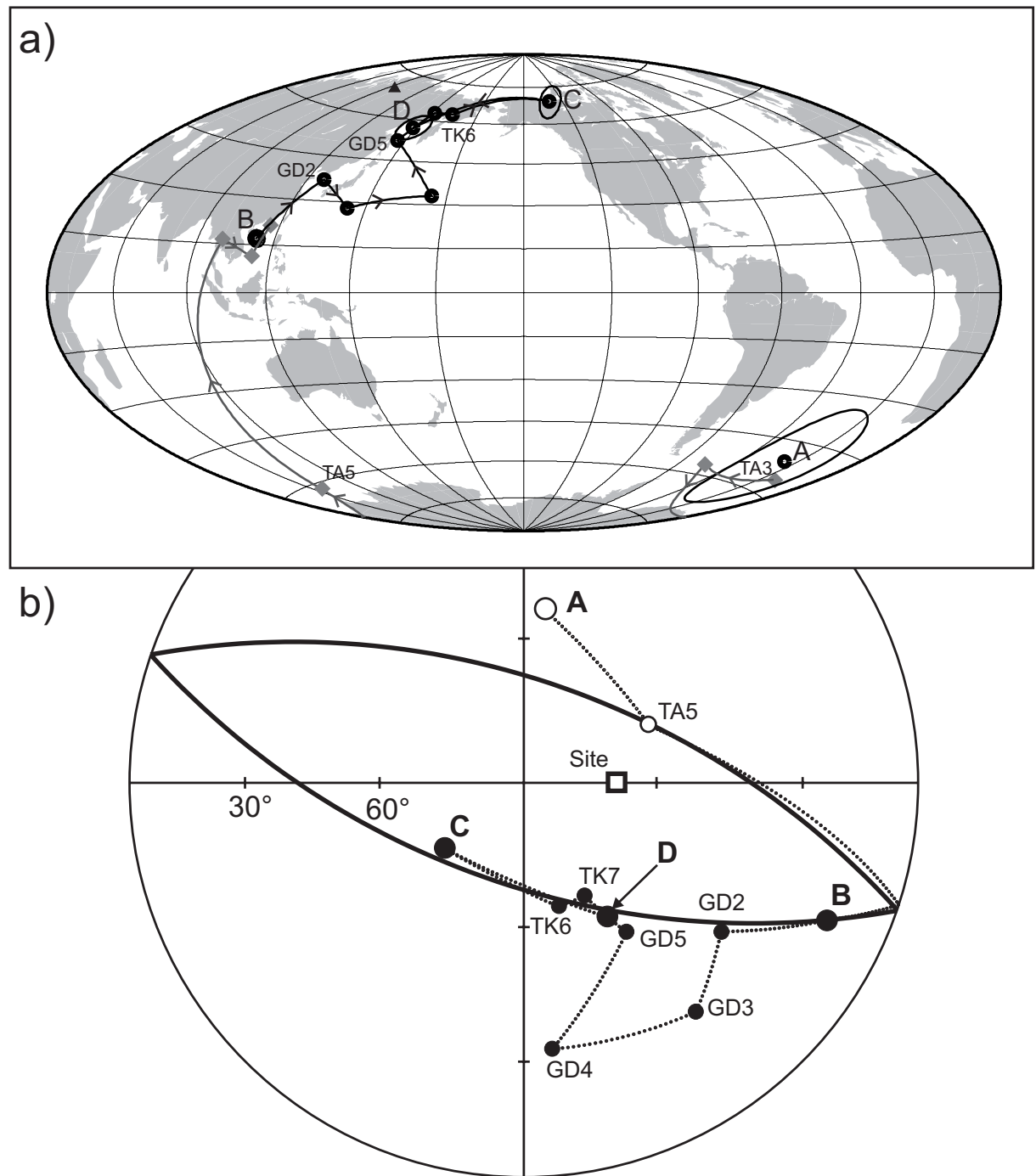


Figure 6.1: (a) Synopsis of the VGP movement across the studied sections (continents in their present position). The site location is denoted by a triangle. The lowest part is characterised by reversed polarities (group A and two flows of the Talnakh section) and then reaches a stable transitional cluster (Group B, 12 flows). The following 4 flows (GD2 to GD5) move towards normal polarity. The first flows (TK7 and TK6) of the Icon/Abagalakh section have directions typical for Early Triassic normal polarity, but then an excursion to more easterly pole positions is observed (group C, 14 flows) before reaching again the normal pole (group D). Shown as black dots are the groups with their associated d_m and d_p confidence limits and individual flows of the Listvjanka and Icon/Abagalakh section. The results of the Talnakh profile, parallel to the bottom of the Listvjanka section, are denoted by grey dots. (b) Stereographic representation of the same dataset visualising the VGP path along a great circle (thick black line).

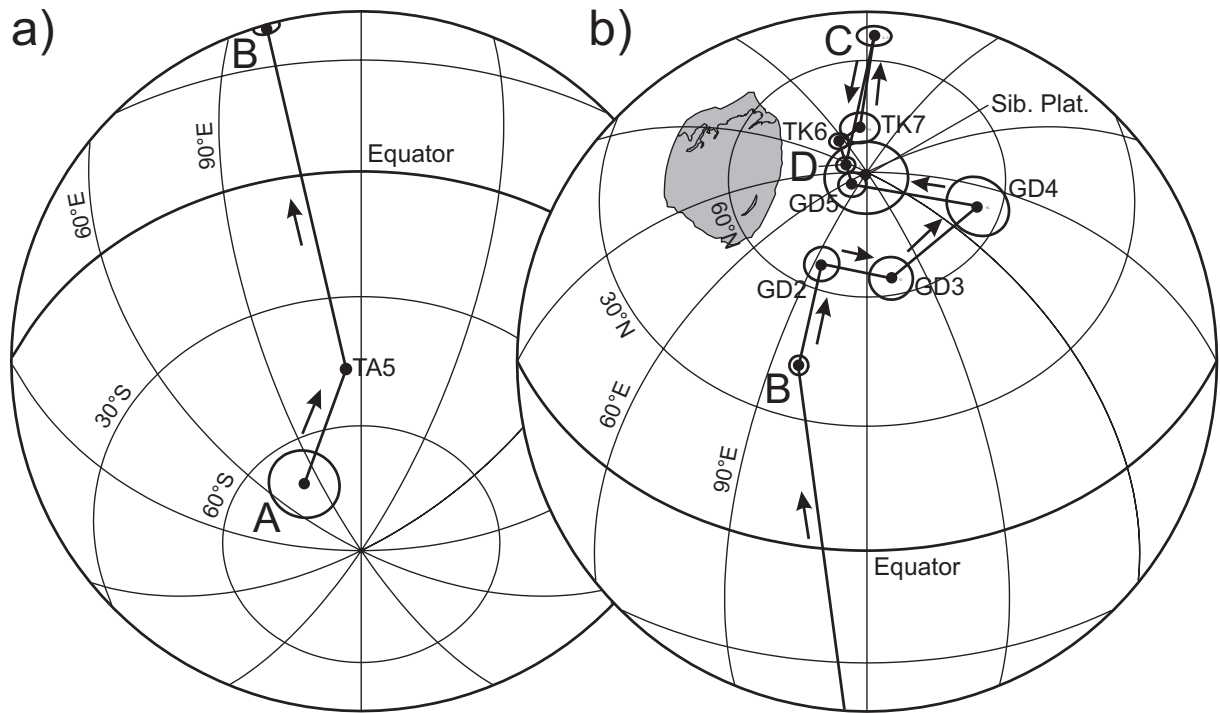


Figure 6.2: Mean VGPs of the directional groups and flows not included in one of the groups, and their associated A_{95} after correction for plate motion. The 95% confidence circle of TA5 is of same size as the symbol. Shown is also the confidence limit of mean pole of the non STB-related palaeomagnetic poles obtained from the Siberian platform (Sib. Plat., after a compilation of SMETHURST ET AL. [1998]). Siberia is displayed in its Permian position, but may be freely moved longitudinally. The longitudinal confinement of the VGP path is readily identified. Note that the path displays neither a near- nor a far-sided configuration. The centre of projection in (a) is 45°S , 120°E in order to visualise the VGP path on the southern hemisphere. (b) is centred at 45°N , 120°E to visualise the situation on the northern hemisphere.

compared to this P/T reversal. The absence of more transitional loops can have basically two causes: (1) The influence of the factors causing the longitudinal confinement (e.g. dominance of the sectorial non-dipole fields) was exceedingly strong inhibiting – apart from the final stage of the reversal (GD3 and GD4) – deviations from the observed VGP path. In this scenario, the large directional changes prior to and after the transitional cluster would be indicative for rapid changes of the field configurations. (2) Or, the extrusion rate was not sufficiently high throughout all stages of the reversal. Deviation of the VGPs of flows GD3 and GD4 from the observed great circle path can be interpreted in this context as a hint for a much larger loop not recorded due to a hiatus in volcanic activity. It cannot be conclusively decided which alternative is more likely.

6.2 Phase 1: Stability of the transitional cluster

Another disputed feature of reversals is the clustering of transitional VGPs in low to mid latitudes. These clusters are often observed in volcanic reversal records. Sedimentary records lack this feature in general due to smoothing of the geomagnetic signal in the remanence acquisition process. HOFFMAN [1992] postulated the existence of two transitional cluster patches (near South American and west of Australia), i.e. patches where transitional clusters of different reversals tend to lie. It is worth noting, that both of these patches are on the preferred transitional paths identified in sedimentary data. He suggests that these transitional states are mainly dipolar. Such an off-axis dipolar configuration cannot be stable, though. Coriolis force acting on the fluid pattern in the outer core causes this quasi-stable configuration to decay. Rapid changes in field directions are the consequence. VGP clusters can, however, also be theoretically explained assuming dominantly non-dipolar fields [GUBBINS AND LOVE, 1998; MERRILL AND MCFADDEN, 1999]. A serious counter-argument against the geomagnetic origin of VGP clustering is the irregularity of volcanic activity. A sudden burst in eruption rate can give the appearance that a cluster was stable for considerable time (HERRERO-BERVERA AND VALET [1999] and VALET AND HERRERO-BERVERA [2003]). Additional constraints are therefore essential in order to prove or disprove the concept proposed by HOFFMAN [1992].

The palaeodirectional record of the Abagalakh section displays such a transitional VGP clustering. Remarkably, this clustering is not only observed in the results of the Abagalakh section, but is also well reproduced by the directional record of the Talnakh section, situated 12 km away. The cluster satisfies the criteria specified by HOFFMAN [1992] ($\alpha_{95} < 10^\circ$ and more than 50% of the recorded transitional VGPs). But how reliable is this observation? If assuming this tight clustering to be an artifact of a burst in volcanic activity then all the flows recorded the same field configuration. Testing the directional information, i.e. deciding whether two directions are statistically indistinguishable, was done using the F-distribution according to BUTLER [1992]. At a 95% significance level flows SV1 and SV2, SV3 and SV4 to GD1 recorded three independent field configurations. However, a pronounced and well documented increase in intensity is recorded between flows SV6 and SV7. Despite their directional similarity the local field must have changed significantly. A nearly doubling of local field intensity infers that large scale dynamic processes in the outer core are responsible for this feature. Timescales for convection in the outer core are in the order of 10^3 years [BUFFETT, 2000]. It can therefore be concluded that the cluster must have been stable for a considerable time, at least several hundreds to a few thousand of years. Further evidence against this cluster being an artifact is provided by the findings of LIND ET AL. [1994]. This study is based on a collection of samples obtained from many individual flows from

different sections rather than from sequences of flows. The palaeomagnetic directions were consequentially averaged by suite. The mean pole for the Syverminsky suite (VGP Lat.: 34° , Long.: 117° , k : 64, α_{95} : 4.7°) shows close similarity with the mean VGP of the transitional cluster, which also comprises mainly the Syverminsky suite. Moreover, the cluster is also observed in the results obtained for the Talnakh section. The key criterion of HERRERO-BERVERA AND VALET [1999] to dismiss the notion of a geomagnetic cause for VGP clustering is the irreproducibility of this feature when comparing results of parallel sections. In the case of the reversal recorded by the STB, however, the good agreement among different sections suggests that the transitional VGP clustering is indeed a geomagnetic feature. The transitional character of the directions recorded by the flows of the Syverminsky suite has not been identified by LIND ET AL. [1994], emphasising the importance of analysing palaeomagnetic records sequentially in order to understand the temporal variation of the Earth's magnetic field.

The question whether dipolar or non-dipolar fields dominated throughout the cluster cannot be answered unambiguously, though. In a dominantly dipolar scenario the sudden increase in intensity without associated directional changes is explained by an enhancement of the dipole during this period. The energy in the axial and equatorial dipole components must increase symmetrically in this case. Assuming strong non-dipole components implies that all Gauss coefficients involved increase by the same factor. In the tentative simple model of a strong sectorial component superimposed on a weak dipole a doubling of the Gauss coefficients involved would be required to produce the observed pattern.

6.3 Phase 2: Independent or reversal-related?

Remarkably, the transitional record is followed by a short period characterised by VGPs close to normal polarity. The VGPs then depart from this normal position clustering at 37° of arc compared to the mean pole of stable normal polarity. It has been demonstrated in chapter 3.3 that phase 2 can be regarded as an excursion. The fact that 14 successive flows consistently recorded this feature substantiates this interpretation. Excursions preceding or succeeding a polarity transitions are commonly found in high resolution records. They are usually explained by instabilities of the geodynamo before and after a reversal and thus extensions of the same dynamo processes [HOFFMAN, 1981]. Often, a "rebound" of the excursive VGP path is observed. Such a rebound effect implies that during a post-transitional excursion VGPs return to positions similar to those occupied by transitional VGPs. In the data presented here the excursion shows a different pattern. The

pole of phase 2 looks more like an "overshoot" of normal polarity (Fig. 6.2). Interestingly, this mean pole is also located on the great circle defined by the transitional VGPs. Its position is roughly symmetric to the transitional cluster with respect to stable normal polarity. This geometric constraint strongly suggests that the excursion is related to the reversal process and is not an independent feature. Sectorial non-dipole components seem to dominate this pattern, too. GUBBINS [1999] proposed that excursions are caused by perturbations in the outer core without reversing the field in the inner core. Such a process would imply a dramatic global decrease in intensity like in the case of a full reversal. Palaeointensity values for the excursion presented here do not display a significant decrease. The preferred interpretation is therefore that the excursion was provoked by locally strong non-dipolar fields. Admittedly, this interpretation is speculative as it assumes that the dipole field remained low so that non-dipole effects are more readily recognised.

6.4 Phase 3: Stable normal polarity

Comparison to the published P/T palaeomagnetic poles obtained from the STB and the Siberian platform (see chapter 3.3) demonstrates the reliability of the palaeomagnetic pole calculated from the flow mean directions of phase 3. PSV was similar to that of the last 5 Ma, a result agreeing well with the findings of LYONS ET AL. [2002]. Judging from the directional behaviour the record can therefore be regarded as representative of the Early Triassic. Incorporating palaeointensity data in the interpretation allows to draw more conclusions. However, the relatively large variation in the observed VDM pattern raises the question for its cause. It has been argued by PRÉVOT ET AL. [1985] and MCFADDEN AND MERRILL [1993] that instability of the newly reestablished dipole can be the cause for the large and apparently rapid fluctuations in the post-transitional dipole moment. However, many studies of young volcanic sequences (e.g. RAÏS ET AL. [1996], ≈ 130 ka) document fluctuations of even greater amplitude during periods of stable polarity. The same holds true for Mesozoic palaeointensity records (e.g. KOSTEROV ET AL. [1997]). It seems that relatively large intensity variations are common during periods of stable polarity. This observation is also supported by relative palaeointensity data [GUYODO AND VALET, 1999]. Although the hypothesis of post-transitional disturbances cannot be excluded, the preferred interpretation is that the STB VDM record is, like the directional record, representative. The mean VDM for this phase is $2.3 \pm 0.7 \times 10^{22}$ Am² (see Fig. 1.1). SOLODOVNIKOV [1995] obtained for 18 cooling units (dykes, flows and baked contacts) of the STB in the Lake Lama region (East of Noril'sk) a mean VDM of $3.4 \pm 0.6 \times 10^{22}$ Am². The stratigraphical position and even their relative age of these units is not clear, though, hampering a direct comparison of the VDMs. It cannot be ruled out that their results are not biased by un-

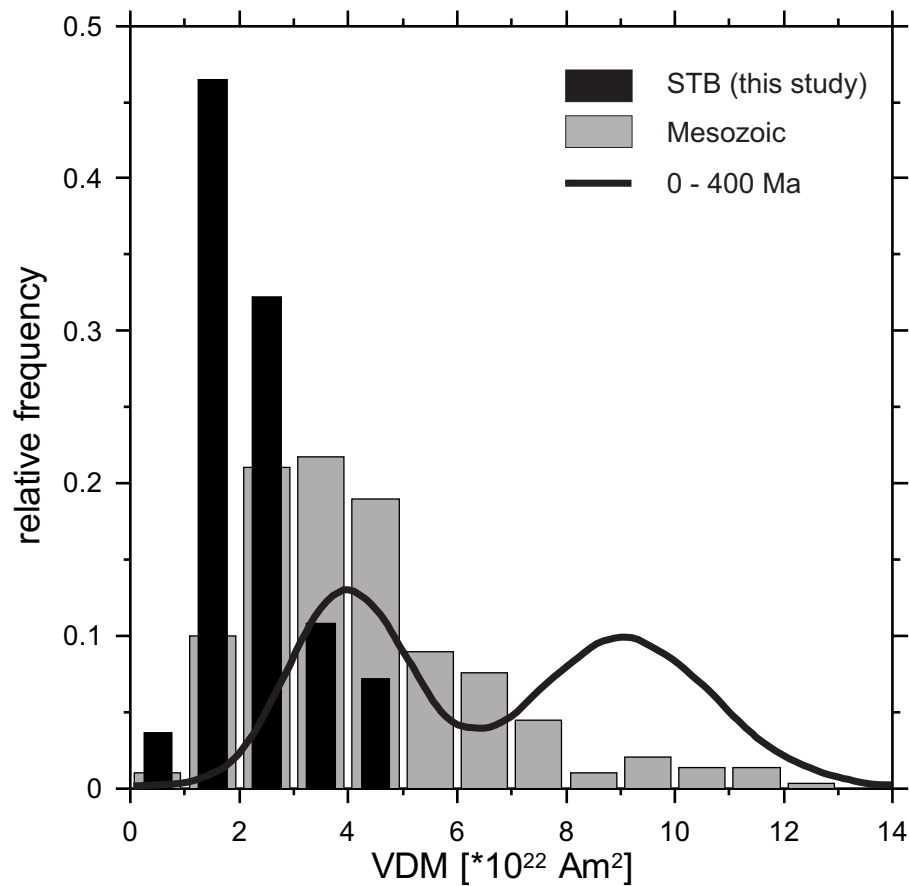


Figure 6.3: Comparison of VDM distribution for different time intervals. The black bars denote the distribution of the VDM values obtained from the STB in this study. For a selected dataset of the BOROKPINT.MDB database [SHCHERBAKOV ET AL., 2002] the respective distribution of published Mesozoic VDM values is shown (grey bars). SHCHERBAKOV ET AL. [2002] also analysed the whole dataset for the time period between 0 and 400 Ma and obtained a bimodal distribution (black line).

intentional sampling of intrusions of distinctly younger age than the basalt sequence itself.

Figure 6.3 shows the distribution of the flow mean VDMs (phase 3) of this study in a histogram (black bars) compared to the distribution of all Mesozoic VDMs (grey bars) of the BOROKPINT.MDB database (SHCHERBAKOV ET AL. [2002], <http://www.brk.adm.yar.ru/palmag/index.html>). The black line is the result of an analysis of SHCHERBAKOV ET AL. [2002] for the last 400 Ma using the same database. The bimodal distribution suggests that the Earth's magnetic field has two preferred intensity levels. The fact that the peak in the distributions of the Mesozoic and last 400 Ma do not coincide is explained by observations of brief periods of a strong VDM during predominantly low intensity states and vice versa. TARDUNO ET AL. [2001] for example, suggested that during the MDL the Cretaceous Normal Superchron (CNS), a 37 Ma time interval without any documented polarity reversals, is characterised by high

palaeointensities. A Late Cretaceous transition between the low to the high VDM state without any significant directional variation is reported by SOLODOVNIKOV [2001]. In the palaeointensity record presented here only the low intensity state is documented. Therefore, the peak of the VDM distribution is shifted to lower values with respect to the overall Mesozoic distribution.

6.5 Asymmetry of the intensity across the reversal

A feature evident from the palaeointensity record is the asymmetry between pre- and post-transitional palaeointensity values. Apparently, the reversed state displays only half (around 10 μT) of the intensity if compared to the values of phase 3 (19 μT). Such asymmetric variations across reversals are discussed in detail by VALET [2003]. The pattern is consistently documented by records of relative palaeointensities derived from sediments which display a long term decrease in field intensity during intervals of stable polarity, followed by large and rapid recovery immediately after the reversal. Even though the structure and the origin of this so called "sawtooth" pattern is still a matter of debate, low pre- and high post-transitional intensities are observations backed by investigations of volcanic sequences as well (e.g. PRÉVOT ET AL. [1985], CHAUVIN ET AL. [1990], BOGUE AND PAUL [1993] and VALET ET AL. [1999]). Striking similarities in the amplitude of the asymmetry are found between the study presented here and the published data of RIISAGER AND ABRAHAMSEN [2000] and LEONHARDT AND SOFFEL [2002]. However, it has to be admitted that reversed polarity is documented only by a few flows.

The significantly reduced values during the transition compared to periods of stable polarity are in agreement with other full vector reversal observations (e.g. PRÉVOT ET AL. [1985], GOGUITCHAICHVILI ET AL. [1999], MERRILL AND MCFADDEN [1999] and LEONHARDT AND SOFFEL [2002]), being basically the only undisputed feature common to all reversals.

6.6 Angular secular variation and intensity

LOVE [2000b] analysed palaeomagnetic directions and absolute palaeointensities from piles of lava flows in order to establish whether or not PSV, i.e. the rate at which the palaeomagnetic direction changes with time, is a function of the local field strength. He claimed that directions of stratigraphically adjacent flows are most correlated when the local field strength is high, and vice versa. In this study the same method as used by LOVE [2000b] was employed in order to check if this hypothesis is consistent with the STB data. Only successive flows with two or more reliable palaeointensity

determinations have been considered. However, the analysis yields no such anti-correlation. This is best exemplified by the results from the transitional cluster. During this cluster directions of successive flows exhibit only small angular differences even though very low palaeointensities are observed throughout this period. Moreover, this tight clustering does not support enhanced PSV during transitional field configurations [LOVE, 2000a]. Despite uncertainties regarding the time interval covered by the transitional cluster, the results presented here are indicative of the opposite, namely a direct correlation of palaeointensity and low angular secular variation during transitional stages. The analysis of the record above the transitional cluster yields no conclusive relationship between intensity and angular secular variation of successive flows.

It was suggested [LOVE, 2000b] that electromagnetic coupling between the solid inner core and the liquid outer core, with the outer core tending to stabilise the magnetic field, is enhanced when the intensity is high. Consequentially, secular variation would be reduced. Such a mechanism should also be observable on a larger timescale. However, PSV at the P/T boundary and PSV averaged over the last 5 Ma have fairly similar characteristic values (Tab. 3.6), whereas the mean VDMs of the two periods differ significantly ($2.3 \pm 0.7 \times 10^{22} \text{ Am}^2$, this study, compared to $5.5 \pm 2.4 \times 10^{22} \text{ Am}^2$, 0–5 Ma, JUAREZ AND TAUXE [2000]). These ambiguities show clearly that PSV and intensity are probably more complexly coupled than intuitively presumed and comprehensive models are not yet available.

6.7 Duration of the record

The duration of a polarity transition is one of the key parameters in understanding the underlying processes in the liquid outer core of the Earth. Estimates for a complete change from one polarity to its antipodal VGP position range from 10^3 to 10^4 years [MERRILL AND MCFADDEN, 1999]. Theoretical models predict similar values (around 10^4 years) based on the magnetic diffusion timescale of the inner core (e.g. HOLLERBACH [2003]). Most of the experimental estimates based on well dated oceanic sedimentary cores cluster around 4000 to 5000 years [BOGUE AND MERRILL, 1992]. Time scales for excursions, believed to be cases of incomplete field reversal in the inner core representing only flux reversals in the outer core [GUBBINS, 2003], are even shorter (500 to 3000 years, GUBBINS [1999]). However, in spite of all efforts it is up to now impossible, even for the younger geological history, to determine whether differences in reported transition durations are due to recording artifacts, experimental errors or in fact due to differences in the length of individual transitions.

In the case of the described Permo-Triassic reversal absolute radiometric dating of individual lava flows prior and after the reversal cannot yield any significant estimates. The intrinsic uncertainty of the $^{40}\text{Ar}/^{39}\text{Ar}$ method, for example, is around 0.3% at best (≈ 1 Ma at the P/T-boundary). Thus, radiometric dating methods are basically unable to resolve reliably the duration of this geomagnetic feature. The best estimates on the duration of the whole Trap volcanism in the Noril'sk area published up to now are values of 0.9 ± 0.8 Ma by RENNE AND BASU [1991] and 0.6 Ma by CAMPBELL ET AL. [1992].

One way of estimating the period of time covered by a transitional field configuration is to compare known accumulation rates of lavas (4 to 5.5 mm/year, Mauna Loa, Hawaii, LIPMAN [1995]) with the thickness of the lava pile which recorded transitional directions. Assuming this to be a valid value also for the Siberian Traps, the reversal (excluding the post-transitional excursion) would have taken roughly 40 ka. However, the extrusion and accumulation rate related to the Trap emplacement was probably significantly higher than of the Hawaiian shield volcanoes but can not yet be quantified. 40 ka should therefore be only regarded as an upper limit, possibly being one order of magnitude too high. Using this approach the whole sequence would have been emplaced in a period of about 320 ka. Another way to estimate the time interval covered by a pile of lava flows is to calculate the cumulative angular VGP path [MANKINEN ET AL., 1985] caused by secular variation and dividing it by a reference VGP movement rate. It has been shown that for the Holocene the VGPs moved in average 6° per 100 years [CHAMPION, 1980]. Unfortunately, such estimates, which can be derived from well dated sedimentary sequences with sufficiently high sedimentation rates, are not available for the Late Palaeozoic/Early Mesozoic. The upper part of the Abagalakh section, excluding all flows carrying excursions, recorded PSV behaviour similar to present day values (as described in chapter 3.5), making the use of the Holocene reference value plausible. The time interval covered by the flows ND5 to KMX4, calculated using the method described above, would be ≈ 8500 years. Due to the presence of minor stratigraphical gaps, this value has to be regarded as a lowest estimate at best. Assuming that secular variation is not suppressed during transitional field states, the transitional cluster would have covered about 1100 years. This finding would substantiate the considerations about the temporal stability of this feature. However, this line of argument runs the risk of circular reasoning as it is not proven if secular variation is similar to periods of stable polarity, or enhanced or suppressed during a reversal. Furthermore, there are several other severe restrictions to the applicability of the method which have to be considered. Very little reliable information on the short scale behaviour of the P/T geomagnetic field is available so far. Similar characteristic PSV values, or in other words the extent of the VGP dispersion, do not necessarily imply that the rate of average VGP movement is similar. This is especially true if going back in time where reliable detailed information

on the Earth's magnetic field are still scarce. Moreover, the sporadic nature of volcanic activity adds great uncertainty to the estimation of the cumulative angular VGP path.

Summarising the considerations made above, any estimate of the duration covered by the lava sequence sampled is highly speculative and would be based on questionable assumptions. These assumptions may be valid only if some additional constraints and more detailed geomagnetic data are available. The absence of any sedimentary horizons or even palaeosols in the studied sequence, however, are strong evidence for a high eruption rate. Assuming an average reversal duration, including an average theoretical estimate for the excursion and adding the estimate for the rest of the section using the approach of MANKINEN ET AL. [1985], the lower limit for the time interval needed for the emplacement of the whole section would be about 15000 years. Magnetostratigraphic and radiometric constraints suggest an upper limit of 1 Ma.

Chapter 7

Conclusions

A long sequence of successive lava flows of the Siberian Trap Basalts, straddling the Permo-Triassic boundary, has been sampled in order to obtain a high resolution record of the ancient Earth's magnetic field. Within the sequence, a geomagnetic transition from reversed to normal polarity, including numerous transitional directions, has been identified. This reversal is followed by an excursion. The record provides new data with respect to directional and intensity variations during transitional states of the Earth's magnetic field. The upper part of the sequence exhibits stable normal polarity. For this period, being representative for the Early Triassic field, key parameters essential in the analyses of the long term behaviour of the Earth's magnetic field could be determined.

The directional behaviour during the transition from reversed to normal polarity is characterised by two particular features. On one hand the transitional VGP path is strongly confined to a relatively narrow longitudinal band. However, the VGP path is neither near- nor far-sided, which would be indicative for zonal non-dipole fields dominating throughout the reversal (HOFFMAN AND FULLER [1978], HOFFMAN [1979] and FULLER ET AL. [1979]). The observed VGP path is perpendicular to near- or far-sided VGP paths, suggesting the existence of strong sectorial components of the Earth's magnetic field throughout the transition and the following excursion. On the other hand, the remarkable clustering of transitional VGPs agrees with the concept of well defined "hang-up" points of the geomagnetic field during reversals as suggested by HOFFMAN [1992, 1996]. The pronounced increase in intensity during this stage of the reversal is indicative for a reasonable stability of this feature, at least in the order of several hundreds of years. Moreover, the VGP clustering is identified in two parallel sections, making it unlikely that it is an artifact of a localised burst in volcanic activity. Based on one observation alone, it cannot be resolved whether dipolar or non-dipolar components were responsible for this tight clustering of the local field directions. Besides the cluster only a few other transitional VGPs are observed. This observation can be explained by hiatuses in volcanic activity or by clustering being preceded and followed by rapid changes in the geometry of the field. Throughout the reversal palaeointensities

are low compared to the strength of the field during the stable normal polarity, an observation that is in agreement with results from younger (mostly Tertiary) reversals of the Earth's magnetic field (e.g. VALET [2003]).

Following the transition itself, normal polarity is reached for a brief time interval. Subsequently, the VGPs depart from this position to form another well defined cluster which is interpreted as a geomagnetic excursion. Such post-transitional excursions are frequently observed and explained by instabilities of the geodynamo after the reversal. However, this excursion cannot be attributed to a rebound effect [MERRILL ET AL., 1998]. Is such a case excursive VGPs reach positions similar to those of transitional VGPs. The pattern observed here is distinctly different. The mean pole of the excursion-related VGPs lies on the great circle defined by the transition, "overshooting" the position expected for stable normal polarity. Moreover, the transitional and the excursive cluster are roughly symmetrically arranged with respect to the pole of stable normal polarity, suggesting that similar non-dipole components, although of opposite sign, are dominating throughout both stages. The excursion can, therefore, be interpreted as an extension of the reversal processes.

Another interesting feature of the record is the asymmetry of pre- and post-transitional palaeointensities. Before the reversal, the intensity amounts only to half of the value ($\approx 10 \mu\text{T}$) that is observed after the transition ($\approx 19 \mu\text{T}$). Such an asymmetric pattern is also documented by numerous sedimentary (relative palaeointensities) and volcanic records (see VALET [2003] for a comprehensive review). This asymmetry and generally low intensities during transitional stages are the only undisputed features of reversals of the Earth's magnetic field.

It is noteworthy that this reversal, by far the oldest hitherto studied detailed record comprising both palaeodirectional and -intensity information, has many similarities with reversals of younger (in general Tertiary) age. Given the age of this reversal, geodynamic plate movements have to be considered in order to interpret the reversal record correctly. Moreover, great care was taken to prove the primary origin of the palaeomagnetic information. The question of preferred transitional VGP paths (e.g. CLEMENT [1991], LAJ ET AL. [1991] and LAJ ET AL. [1992]) and the proposed influence of core-mantle boundary conditions remains unsolved due to the absence of comparable data. However, the results of the Permo-Triassic Siberian Trap basalts strongly suggest that the underlying reversal processes are fundamentally the same for the Mesozoic and for the Tertiary.

The uppermost part of the section recorded normal polarity. Comparing the mean

pole of this part of the record with published poles obtained from the Siberian Trap basalts and coeval units of the Siberian platform shows good agreement. It is therefore concluded that this sequence of 41 flows allows some conclusions about the characteristics of the Early Triassic time averaged field to be drawn. The mean virtual dipole moment for this stage of the record is $2.3 \pm 0.7 \times 10^{22} \text{ Am}^2$. This value represents a reliable estimate as it can be ruled out that intrusions of younger age were sampled unintentionally, thus confirming that the Mesozoic dipole low extends down to at least the Permo-Triassic boundary. It has been proposed that low intensities of the Earth's magnetic field are associated with enhanced secular variation [LOVE, 2000b]. However, secular variation estimated on the basis of this record yields similar values compared to secular variation averaged over the last 5 Ma, a period with significantly higher time averaged dipole moment ($5.5 \pm 2.4 \times 10^{22} \text{ Am}^2$, JUAREZ AND TAUXE [2000]). This discrepancy is indicative for a more complex coupling, at least in the Early Mesozoic, of dipole moment and secular variation than previously assumed.

Magnetostratigraphic results of basalts related to the Siberian Trap volcanism constrain the duration of the whole volcanic activity to less than 3.2 Ma. Combining the findings presented in this study and palaeomagnetic results of boreholes in the vicinity to the surface section it could be proven, however, that the volcanics of the Noril'sk area were erupted during a time interval comprising only one polarity transition. The existence of further undetected polarity transitions is unlikely. It can be thus inferred that the emplacement of the sequence studied here occurred much faster than the above mentioned 3.2 Ma, an interpretation consistent with geologic evidence and radiometric ages which yield estimates in the order of 1 Ma or less. If assuming that angular secular variation in the Early Triassic was similar to present values, and that the reversal duration is comparable to durations observed in younger reversals, then the more than 1700 m thick sequence would have been emplaced in only 15000 years. This implies an enormous eruption rate and makes thus a strong case for the STB as cause for the P/T crisis.

The data presented here show that palaeomagnetic results obtained from long volcanic sequences can provide a wealth of information on the temporal variation of the Earth's magnetic field. The data acquired also yield constraints on the duration of the volcanic activity associated with the STB. However, little is known about the Eastern part of this large igneous province and palaeomagnetic data are still scarce. Therefore, a detailed sampling of the volcanic sequences outcropping there was carried out in late Summer 2002. The new results, which are not part of this thesis, will help to clarify the magnetostratigraphic correlation of the East STB and supply additional data on the behaviour of the Earth's magnetic field in the Late Palaeozoic/Early Mesozoic.

Bibliography

- ARAI, Y., *Secular Variation in Intensity of the Past Geomagnetic Field*. MSc Thesis. Univ. Tokyo, Japan, 1963.
- BASU, A. R., POREDA, R. J., RENNE, P. R., TEICHMANN, F., VASILIEV, Y., SOBOLEV, N., AND TURRIN, B. (1995); High-He-3 Plume Origin and Temporal-Spatial Evolution of the Siberian Flood Basalts. *Science*, 269, 822–825.
- BECKER, L., POREDA, R. J., HUNT, A. G., BUNCH, T. E., AND RAMPINO, M. (2001); Impact event at the Permian-Triassic boundary: Evidence from extraterrestrial noble gases in fullerenes. *Science*, 291, 1530–1533.
- BIGGIN, A. AND THOMAS, D. N. (2003); Analysis of long-term variations in the geomagnetic poloidal field intensity and evaluation of their relationship with global geodynamics. *Geophys. J. Int.*, 152, 392–415.
- BLOXHAM, J. AND JACKSON, A. (1991); Fluid flow near the surface of the Earth’s outer core. *Rev. Geophys.*, 29, 97–120.
- BOGUE, S. AND MERRILL, R. T. (1992); The character of the field during geomagnetic reversals. *Ann. Rev. Earth Plant. Sci.*, 20, 181–219.
- BOGUE, S. AND PAUL, H. (1993); Distinctive field behaviour following geomagnetic reversals. *Geophys. Res. Lett.*, 20, 2399–2402.
- BOL’SIAKOV, A. S., SOLODOVNIKOV, G. M., AND VINOGRADOV, Y. (1987); Paleointensity of the geomagnetic field in the Early and Middle Jurassic. *Izv. Acad. Sci., Phys. Solid Earth*, 23, 324–333.
- BOL’SIAKOV, A. S., SOLODOVNIKOV, G. M., AND VINOGRADOV, Y. (1989); Paleointensity of the geomagnetic field in the Early Permian. *Izv. Acad. Sci., Phys. Solid Earth*, 25, 70–78.
- BOL’SIAKOV, A. S. AND SOLODOVNIKOV, G. M. (1981); Intensity of the geomagnetic field in Late Cretaceous time. *Izv. Acad. Sci., Phys. Solid Earth*, 17, 754–761.

- BOL'SHAKOV, A. S. AND SOLODOVNIKOV, G. M. (1983); Geomagnetic field intensity in Armenia in the Late Jurassic and Early Cretaceous. *Izv. Acad. Sci., Phys. Solid Earth*, 19, 976–982.
- BOWRING, S., ERWIN, D., JIN, Y., MARTIN, M., DAVIDEK, K., AND WANG, W. (1998); U/Pb zircon geochronology and tempo of the end-Permian mass extinction. *Science*, 280, 1039–1045.
- BRUNHES, B. (1906); Recherches sur la direction d'aimantation des roches volcaniques. *J. Phys.*, 5, 705–724.
- BUDDINGTON, A. AND LINDSLEY, D. (1964); Iron-titanium oxide minerals and synthetic equivalents. *J. Petrol.*, 5, 310–357.
- BUFFETT, B. A. (2000); Earth's core and the geodynamo. *Science*, 288, 2007–2012.
- BULLARD, E. (1949); The magnetic field within the Earth. *Proc. Roy. Soc. London*, A187, 433–453.
- BUTLER, R. F., *Paleomagnetism: Magnetic Domains to Geologic Terranes*. Blackwell Sciences, Malden, Mass., 1992.
- CAMPBELL, I. H., CZAMANSKE, G. K., FEDORENKO, V. A., HILL, R. I., AND STEPANOV, V. (1992); Synchronism of the Siberian Traps and the Permian-Triassic Boundary. *Science*, 258, 1760–1763.
- CHAMPION, D., Holocene geomagnetic secular variation in the Western United States: Implications for the global geomagnetic field. In: *U.S. Geol. Surv. Open File Rep.*, vol. 80-824. 1980, p. 326.
- CHAUVIN, A., GILLOT, P. Y., AND BONHOMMET, N. (1990); Records of geomagnetic reversals from volcanic islands of French Polynesia. *J. Geophys. Res.*, 95, 2727–2752.
- CLAOUÉ-LONG, J., ZHANG, G., MA, G., AND DU, S. (1991); The age of the Permian-Triassic boundary. *Earth Planet. Sci. Lett.*, 105, 182–190.
- CLEMENT, B. (1991); Geographical distribution of transitional VGPs: Evidence for non-zonal equatorial symmetry during the Bruhnes-Matuyama geomagnetic reversal. *Earth Planet. Sci. Lett.*, 29, 45–58.
- COE, R. S., GROMMÉ, C. S., AND MANKINEN, E. A. (1978); Geomagnetic paleointensities from radiocarbon-dated lava flows on Hawaii and the question of the Pacific Nondipole Low. *J. Geophys. Res.*, 83, 1740–1756.

- COE, R. S. (1967); The determination of paleointensities of the Earth's magnetic field with emphasis on mechanisms which could cause non-ideal behavior in Thellier's method. *J. Geomagn. and Geoelectr.*, *19*, 157–179.
- COURTILLOT, V., JAUPART, C., MANIGHETTI, I., TAPPONNIER, P., AND BESSE, J. (1999); On causal links between flood basalts and continental breakup. *Earth Planet. Sci. Lett.*, *166*, 177–195.
- COURTILLOT, V. AND RENNE, P. R. (2003); On the ages of flood basalt events. *C. R. Geosciences*, *335*, 113–140.
- COURTILLOT, V., *Evolutionary Catastrophes: The Science of Mass Extinction*. Cambridge Univ. Press, Cambridge, 1999.
- COWLING, T. (1934); The magnetic field of sunspots. *Mon. Not. Roy. Astron. Soc.*, *94*, 39–48.
- COWLING, T., *Magnetohydrodynamics*. Wiles Interscience, New York, 1957.
- COX, A. (1969); Confidence Limits for the Precision Parameter κ . *Geophys. J. R. astr. Soc.*, *18*, 545–549.
- CREER, K. AND ISPIR, Y. (1970); An interpretation of the behaviour of the geomagnetic field during polarity transitions. *Phys. Earth Planet. Int.*, *2*, 283–293.
- CZAMANSKE, G. K., GUREVITCH, E., FEDORENKO, V. A., AND SIMONOV, O. N. (1998); Demise of the Siberian plume: Paleogeographic and plate tectonic reconstruction from the prevolcanic and volcanic record, North-Central Siberia. *Int. Geol. Rev.*, *40*, 95–115.
- DALRYMPLE, G. B., CZAMANSKE, G. K., FEDORENKO, V. A., SIMONOV, O. N., LANPHERE, M. A., AND LIKHACHEV, A. P. (1995); A reconnaissance Ar-40/Ar-39 geochronological study of ore-bearing and related rocks, Siberian Russia. *Geochim. Cosmochim. Acta*, *59*, 2071–2083.
- DAVID, P. (1904); Sur la stabilité de la direction l'aimantation dans quelques roches volcaniques. *C. R. Acad. Sci. Paris*, *138*, 41–42.
- DAY, R., FULLER, M., AND SCHMIDT, V. A. (1977); Hysteresis properties of titanomagnetites: Grain size and composition dependence. *Phys. Earth Planet. Int.*, *13*, 260–267.
- DENIS, C., SCHREIDER, A. A., VARGA, P., AND ZAVOTI, J. (2002); Despinning of the Earth's rotation in the geological past and geomagnetic paleointensities. *J. Geodyn.*, *34* (5), 667–685.

- DUNLOP, D. J. AND ÖZDEMİR, Ö., *Rock Magnetism: Fundamentals and Frontiers*. Cambridge Studies in Magnetism. Cambridge University Press, 1997.
- DUNLOP, D. AND ÖZDEMİR, Ö. (2000); Effect of grain size and domain state on thermal demagnetization tails. *Geophys. Res. Lett.*, *27*, 1311–1314.
- DUNLOP, D. (2002a); Theory and application of the Day plot (M_{rs}/M_s versus H_{cr}/H_c) 1. theoretical curves and tests using titanomagnetite data. *J. Geophys. Res.*, *107*, EPM 4–1 – EPM 4–22.
- DUNLOP, D. (2002b); Theory and application of the Day plot (M_{rs}/M_s versus H_{cr}/H_c) 2. Application to data for rocks, sediments and soils. *J. Geophys. Res.*, *107*, EPM 5–10 – EPM 5–15.
- ELSASSER, W. (1946); Induction effects in terrestrial magnetism. 1. Theory. *Phys. Rev.*, *69*, 106–116.
- ENKIN, R. J. (1990); *Formation et déformation de l'Asie depuis la fin de l'Ere Primaire: Les apports de l'études paleomagnétiques des formations secondaires de Chine du Sud*. Ph.D. thesis, Université de Paris.
- FABIAN, K. (2001); A theoretical treatment of paleointensity determination experiments on rocks containing pseudo-single or multi-domain magnetic particles. *Earth Planet. Sci. Lett.*, *188*, 45–58.
- FEDORENKO, V. A. AND CZAMANSKE, G. (1997); Results of new field and geochemical studies of the volcanic and intrusive rocks of the Maymecha-Kotuy Area, Siberian Flood-Basalt Province, Russia. *Int. Geol. Rev.*, *39*, 479–531.
- FEDORENKO, V. A., LIGHTFOOT, P., NALDRETT, A., CZAMANSKE, G. K., HAWKESWORTH, C., WOODEN, J., AND EBEL, D. (1996); Petrogenesis of the flood basalt sequence at Noril'sk, North Central Siberia. *Int. Geol. Rev.*, *38*, 99–135.
- FEDORENKO, V., CZAMANSKE, G., ZEN'KO, T., BUDAHN, J., AND SIEMS, D. (2000); Field and geochemical studies of the melilite-bearing Arydzhangsky Suite, and an overall perspective on the Siberian alkaline-ultramafic flood-volcanic rocks. *Int. Geol. Rev.*, *42*, 769–804.
- FISHER, R. A. (1953); Dispersion on a sphere. *Proc. Roy. Soc. London*, *A217*, 295–305.
- FULLER, M., WILLIAMS, I., AND HOFFMAN, K. A. (1979); Paleomagnetic records of geomagnetic field reversals and the morphology of transitional fields. *Rev. Geophys.*, *17*, 179–203.

- GLATZMAIER, G. A. AND ROBERTS, P. (1995); A three-dimensional self consistent computer simulation of a geomagnetic field reversal. *Nature*, 377, 203–209.
- GOGUITCHAICHVILI, A., ALVA-VALDIVIA, L. M., URRUTIA, J., MORALES, J., AND LOPES, O. F. (2002); On the reliability of Mesozoic Dipole Low: New absolute paleointensity results from Paraná Flood Basalts (Brazil). *Geophys. Res. Lett.*, 29 (13), 33–1 – 33–4.
- GOGUITCHAICHVILI, A., PRÉVOT, M., AND CAMPS, P. (1999); No evidence for strong fields during the R3-N3 Icelandic geomagnetic reversal. *Earth Planet. Sci. Lett.*, 167, 15–34.
- GRADSTEIN, F., AGTERBERG, F., OGG, J. G., HARDENBOL, J., VAN VEEN, P., THIERRY, J., AND HUANG, Z., A Triassic, Jurassic and Cretaceous time scale. In: W. Berggren, D. V. Kent, M.-P. Aubry, and J. Hardenbol (eds.), *Geochronology, time scales and global stratigraphic correlation*, vol. 54. SEPM special publication, Society for Sedimentary Geology, 1995, pp. 95–126.
- GUBBINS, D. AND LOVE, J. J. (1998); Preferred VGP paths during geomagnetic polarity reversals: Symmetry considerations. *Geophys. Res. Lett.*, 25, 1079–1082.
- GUBBINS, D. AND RICHARDS, M. A. (1986); Coupling of the core dynamo and the mantle; thermal or topographic? *Geophys. Res. Lett.*, 13, 1521–1524.
- GUBBINS, D. (1999); The distinction between geomagnetic excursions and reversals. *Geophys. J. Int.*, 137, F1–F3.
- GUBBINS, D., Thermal core-mantle interactions: Theory and observations. In: V. Dehant, K. Kraeger, S. Karato, and S. Zatman (eds.), *Earth's core: Dynamics, structure, rotation*. American Geophysical Union, Washington, DC, 2003, pp. 163–179.
- GUREVITCH, E., HEUNEMANN, C., RAD'KO, V., WESTPHAL, M., BACHTADSE, V., POZZI, J. P., AND FEINBERG, H. (2003); Palaeomagnetism and magnetostratigraphy of the Permian-Triassic Siberian Trap Basalts. *Tectonophysics*, *in press*.
- GUREVITCH, E., WESTPHAL, M., DARAGANSUCHOV, J., FEINBERG, H., POZZI, J. P., AND KHRAMOV, A. N. (1995); Paleomagnetism and magnetostratigraphy of the traps from Western Taimyr (northern Siberia) and the Permo-Triassic crisis. *Earth Planet. Sci. Lett.*, 136, 461–473.
- GUSEV, B., METALLOVA, V. V., AND FAINBERG, F., *Magnetism of rocks of the trap formation of the Western part of the Siberian platform*. Nedra Press, Leningrad, 1967.
- GUYODO, Y. AND VALET, J. P. (1999); Global changes in intensity of the Earth's magnetic field during the past 800 kyr. *Nature*, 399, 249–252.

- HAGGERTY, S., Oxidation of opaque mineral oxides in basalts. In: D. Rumble (ed.), *Oxide Minerals*, vol. 3 of *Reviews in Mineralogy*. BookCrafters, Chelsea, Michigan, 1976.
- HEIDER, F., HALGEDAHL, S., AND DUNLOP, D. (1988); Temperature dependence of magnetic domains in magnetite crystals. *Geophys. Res. Lett.*, *19*, 499–502.
- HELLER, F. AND PETERSEN, N. (1982); Self-reversal explanation for the Laschamp/Olby geomagnetic field excursion. *Phys. Earth Planet. Int.*, *30*, 358–372.
- HELLER, R., MERRILL, R. T., AND MCFADDEN, P. L. (2003); The two states of paleomagnetic field intensities for the past 320 million years. *Phys. Earth Planet. Int.*, *135*, 211–223.
- HERRERO-BERVERA, E. AND VALET, J. P. (1999); Paleosecular variation during sequential geomagnetic reversals from Hawaii. *Earth Planet. Sci. Lett.*, *171*, 139–148.
- HEUNEMANN, C., KRÁSA, D., GUREVITCH, E., SOFFEL, H. C., AND BACHTADSE, V. (2003); Directions and intensities of the Earth's magnetic field during a reversal: results from the Permo-Triassic Siberian Trap Basalts, Russia. *Earth Planet. Sci. Lett.*, *in press*.
- HILLHOUSE, J. AND COX, A. (1976); Brunhes-Matuyama polarity transition. *Earth Planet. Sci. Lett.*, *29*, 51–64.
- HOFFMAN, K. A. AND FULLER, M. (1978); Transitional field configuration and geomagnetic reversal. *Nature*, *273*, 715–717.
- HOFFMAN, K. A. (1977); Polarity transition records and geomagnetic dynamo. *Science*, *196*, 1329–1332.
- HOFFMAN, K. A. (1979); Behavior of the geodynamo during reversal: A phenomenological model. *Earth Planet. Sci. Lett.*, *44*, 7–17.
- HOFFMAN, K. A. (1981); Palaeomagnetic excursions, aborted reversals and transitional fields. *Nature*, *294*, 67–69.
- HOFFMAN, K. A. (1992); Dipolar reversal state of the geomagnetic field and core-mantle dynamics. *Nature*, *359*, 789–794.
- HOFFMAN, K. A. (1996); Transitional paleomagnetic field behavior: Preferred paths or patches. *Surv. Geophys.*, *17*, 207–211.
- HOLLERBACH, R., The range of timescales on which the geodynamo operates. In: V. Dehant, K. Craeger, S. Karato, and S. Zatman (eds.), *Earth's core: Dynamics, structure, rotation*. American Geophysical Union, Washington, DC, 2003, pp. 181–192.

- JACOBS, J. A., *Reversals of the Earth's magnetic field*. Adam Hilger Ltd, Bristol, 1984.
- JUAREZ, M. T. AND TAUXE, L. (2000); The intensity of the time-averaged geomagnetic field: the last 5 Myr. *Earth Planet. Sci. Lett.*, 175, 169–180.
- KAMO, S. L., CZAMANSKE, G. K., AND KROGH, T. E. (1996); A minimum U-Pb age for Siberian Flood-Basalt volcanism. *Geochim. Cosmochim. Acta*, 60 (18), 3505–3511.
- KAMYSHEVA, G., Pole number 08045. In: *Paleomagnetic Directions and paleomagnetic poles: Data for the USSR*. VNIGRI, St. Petersburg, 1971.
- KELLOGG, K., LARSON, E., AND WATSON, D. (1970); Thermochemical remanent magnetization and thermoremanent remanent magnetization: comparison in basalt. *Science*, 170, 628–630.
- KHRAMOV, A. N., *Paleomagnetic directions and poles: Data for the USSR, Summary Catalogue, 1. Materials of the WDC-B*. Moscow, 1984.
- KIRSCHVINK, J. L. (1980); The least square line and plane and the analysis of paleomagnetic data. *Geophys. J. R. astr. Soc.*, 62, 699–718.
- KOK, Y. AND TAUXE, L. (1996); Saw-tooth pattern in relative paleointensity records and cumulative viscous remanence. *Earth Planet. Sci. Lett.*, 137, 95–99.
- KONO, M. (1974); Intensity of the Earth's magnetic field about 60 million years ago determined from Deccan Trap basalts. *India. J. Geophys. Res.*, 79, 1135–1141.
- KONO, M. (1985); Changes in magnetic hysteresis properties of a basalt induced by heating in air. *J. Geomag. Geoelectr.*, 37, 589–600.
- KOSTEROV, A. A., PERRIN, M., GLEN, J. M., AND COE, R. S. (1998); Paleointensity of the Earth's magnetic field in Early Cretaceous time: the Paraná Basalt, Brazil. *J. Geophys. Res.*, 103, 9739–9753.
- KOSTEROV, A. A., PREVOT, M., PERRIN, M., AND SHASHKANOV, V. A. (1997); Paleointensity of the Earth's magnetic field in the Jurassic: New results from a Thellier study of the Lesotho Basalt, southern Africa. *J. Geophys. Res.*, 102, 24,859–24,872.
- KRÁSA, D., HEUNEMANN, C., LEONHARDT, R., AND PETERSEN, N. (2003); Experimental procedure to detect multidomain remanence during Thellier-Thellier experiments. *Phys. Chem. Earth*, 28, 681–687.
- KRAVCHINSKY, V. A., KONSTANTINOV, K. M., COURTILLOT, V., SAVRASOV, J. I., VALET, J. P., CHERNIY, S. D., MISHENIN, S. G., AND PARASOTKA, B. S. (2002); Palaeomagnetism of East Siberian traps and kimberlites: two new poles and palaeogeographic reconstructions at about 360 and 250 Ma. *Geophys. J. Int.*, 148, 1–33.

- LAI, C., MAZAUD, A., WEEKS, R., AND FULLER, M. (1991); Geomagnetic reversal paths. *Nature*, 351, 447.
- LAI, C., MAZAUD, A., WEEKS, R., AND FULLER, M. (1992); Statistical assessment of the preferred longitudinal bands of recent geomagnetic field reversal records. *Geophys. Res. Lett.*, 19, 2003–2006.
- LARMOR, J. (1919); Possible rotational origin of magnetic fields of Sun and Earth. *Elec. Rev.*, 85, 412.
- LEONHARDT, R., HUFENBECHER, F., HEIDER, F., AND SOFFEL, H. C. (2000); High absolute paleointensity during a mid-Miocene excursion of the Earth's magnetic field. *Earth Planet. Sci. Lett.*, 184, 141–154.
- LEONHARDT, R., MATZKA, J., HUFENBECHER, F., SOFFEL, H. C., AND HEIDER, F. (2002); A reversal of the Earth's magnetic field recorded in mid-Miocene lava flows of Gran Canaria: Paleodirections. *J. Geophys. Res.-Solid Earth*, 107, EPM5–1 – EPM5–11.
- LEONHARDT, R. AND SOFFEL, H. C. (2002); A reversal of the Earth's magnetic field recorded in mid-Miocene lava flows of Gran Canaria: Paleointensities. *J. Geophys. Res.*, 107, EPM5–1 – EPM5–11.
- LIGHTFOOT, P. C., NALDRETT, A. J., GORBACHEV, N. S., DOHERTY, W., AND FEDORENKO, V. (1990); Geochemistry of the Siberian Traps of the Noril'sk area, USSR, with implications for the relative contributions of crust and mantle to flood basalt magmatism. *Contrib. Mineral. Petrol.*, 104, 631–644.
- LINDSLEY, D., Investigations of the system $\text{FeO-Fe}_2\text{O}_3\text{-TiO}_2$. In: *Carnegie Inst. Washington Year Book*, vol. 62. Carnegie Inst., Washington, DC, 1962, pp. 100–106.
- LIND, E. N., KROPOTOV, S. V., CZAMANSKE, G. K., GROMMÉ, C. S., AND FEDORENKO, V. A. (1994); Paleomagnetism of the Siberian flood basalts of the Noril'sk area: A constraint on eruption duration. *Int. Geol. Rev.*, 36, 1139–1150.
- LIPMAN, P. (1995); Declining growth of Mauna Loa during the past 100,000 years: rates of lava accumulation vs. gravitational subsidence. *Geophys. Monogr.*, 92, 45–80.
- LOVE, J. J. (1998); Paleomagnetic volcanic data and geometric regularity of reversals and excursions. *J. Geophys. Res.*, 103, 12,435–12,452.
- LOVE, J. J. (2000a); On the anisotropy of secular variation deduced from paleomagnetic volcanic data. *J. Geophys. Res.*, 105, 5799–5816.

- LOVE, J. J. (2000b); Palaeomagnetic secular variation as a function of intensity. *Philos. Trans. R. Soc. Lond.*, 358, 1191–1223.
- LOVE, J. J. (2000c); Paleomagnetic assessment of preferred transitional VGP longitudes on palaeomagnetic lava data. *Geophys. J. Int.*, 140, 211–221.
- LYONS, J., COE, R. S., ZHAO, X., RENNE, P. R., KAZANSKY, A., IZOKH, A., KUNGURTSEV, L., AND MITROKHIN, D. (2002); Paleomagnetism of the Early Triassic Semeitau Igneous Series, Eastern Kazakstan. *J. Geophys. Res.*, 107, EPM4–1 – EPM4–15.
- MANKINEN, E. A., PRÉVOT, M., GROMMÉ, C. S., AND COE, R. S. (1985); The Steens Mountain (Oregon) geomagnetic polarity transition, 1. Directional history, duration of episodes, and rock magnetism. *J. Geophys. Res.*, 90, 10,393–10,416.
- MATZKA, J., KRÁSA, D., KUNZMANN, T., SCHULT, A., AND PETERSEN, N. (2003); Magnetic state of 10 to 40 Ma old ocean basalts and its implications for natural remanent magnetization. *Earth Planet. Sci. Lett.*, 206, 541–553.
- MATZKA, J. (2001); *Besondere magnetische Eigenschaften der Ozeanbasalte im Altersbereich 10 bis 40 Ma*. Ph.D. thesis, Ludwig-Maximilians-Universität München.
- MCCLELLAND, E. AND BRIDEN, J. (1996); An improved methodology for Thellier-Type paleointensity determination in igneous rocks and its usefulness for verifying primary thermoremanence. *J. Geophys. Res.*, 101, 21,995–22,013.
- MCELVINNY, M. W. AND LOCK, J. (1996); IAGA paleomagnetic databases with Access. *Surv. Geophys.*, 17, 575–591.
- MCELVINNY, M. W. AND MCFADDEN, P. L. (1997); Palaeosecular variation over the past 5 Myr based on a new generalized database. *Geophys. J. Int.*, 131, 240–52.
- MCELVINNY, M. (1998); Six new paleomagnetic databases released. *EOS, Trans. Amer. Geophys. Union*, 79, 387.
- MCFADDEN, P. L. AND MCELVINNY, M. W. (1988); The combined analysis of remagnetization circles and direct observations in paleomagnetism. *Earth Planet. Sci. Lett.*, 87, 161–172.
- MCFADDEN, P. L. AND MERRILL, R. T. (1993); Inhibition and geomagnetic field reversals. *J. Geophys. Res.*, 98, 6189–6199.
- MCFADDEN, P. AND MCELVINNY, M. (1990); Classification of the reversal test in palaeomagnetism. *Geophys. J. Int.*, 103, 725–729.

- MCMILLAN, D., CONSTABLE, C., AND PARKER, R. (2002); Limitations on stratigraphic analyses due to incomplete age control and their relevance to sedimentary paleomagnetism. *Earth Planet. Sci. Lett.*, 201, 509–523.
- MERRILL, R. T., MCELHINNY, M. W., AND MCFADDEN, P. L., *The magnetic field of the Earth*. Academic Press, San Diego, 1998.
- MERRILL, R. T. AND MCFADDEN, P. L. (1999); Geomagnetic polarity transitions. *Rev. Geophys.*, 37, 201–226.
- METALLOVA, V. AND FEINBERG, F. (1967); The magnetic properties of ferromagnetic substances in Traprocks with various polarities of the natural remanent magnetization. *Izv. Acad. Sci., Phys. Solid Earth*, 7, 77–82.
- NÉEL, L. (1951); L'inversion de l'aimantation permanente des roches. *Ann. Géophys.*, 7, 90–102.
- NIKISHIN, A. M., ZIEGLER, P., ABBOTT, D., BRUNET, M.-F., AND CLOETINGH, S. (2002); Permo-Triassic intraplate magmatism and rifting in Eurasia: Implications for mantle plumes and mantle dynamics. *Tectonophysics*, 351, 3–39.
- O'REILLY, W., *Rock and Mineral Magnetism*. Blackie & Son, Glasgow, 1984.
- PERRIN, M., PRÉVOT, M., AND MANKINEN, E. A. (1991); Low intensity of the geomagnetic field in Early Jurassic time. *J. Geophys. Res.*, 96, 14,197–14,210.
- PERRIN, M. AND SHCHERBAKOV, V. (1997); Paleointensity of the Earth's magnetic field for the past 400 Ma: Evidence for a dipole structure during the Mesozoic low. *J. Geomag. Geoelectr.*, 49, 601–614.
- PETERSEN, N. (1976); Notes on the variation of magnetisation within basalt lava flows and dikes. *Pageoph*, 114, 177–193.
- PISAREVSKY, S., Pole number 07072. In: A. N. Khramov (ed.), *Paleomagnetic directions and pole positions: Data for the USSR - Issue 5*. Moscow, 1982.
- PRÉVOT, M. AND CAMPS, P. (1993); Absence of preferred longitudinal sectors for poles from volcanic records of geomagnetic reversals. *Nature*, 366, 53–57.
- PRÉVOT, M., EL-MESSAOUD DERDER, M., MCWILLIAMS, M., AND THOMPSON, J. (1990); Intensity of the Earth's magnetic field: Evidence for a Mesozoic dipole low. *Earth Planet. Sci. Lett.*, 97, 129–139.
- PRÉVOT, M., MANKINEN, E. A., COE, R. S., AND GROMMÉ, C. S. (1985); The Steens Mountain (Oregon) geomagnetic polarity transition 2. Field intensity variations and discussion of reversal models. *J. Geophys. Res.*, 90, 10,417–10,448.

- RAÏS, A., LAJ, C., SURMONT, J., GILLOT, P. Y., AND GUILLOU, H. (1996); Geomagnetic field intensity between 70,000 and 130,000 years BP from a volcanic sequence on La Réunion, Indian Ocean. *Earth and Planet. Sci. Lett.*, *140*, 173–189.
- REICHOW, M. K., SAUNDERS, A. D., WHITE, R. V., PRINGLE, M. S., AL'MUKHAMEDOV, A. I., MEDVEDEV, A. I., AND KIRDA, N. P. (2002); $^{40}\text{Ar}/^{39}\text{Ar}$ dates from the West Siberian Basin: Siberian flood basalt province doubled. *Science*, *296*, 1846–1849.
- RENNE, P. R. AND BASU, A. R. (1991); Rapid eruption of the Siberian Traps Flood Basalts at the Permo-Triassic boundary. *Science*, *253*, 176–179.
- RENNE, P. R., SWISHER, C., DEINO, A., KARNER, D., OWENS, T., AND DEPAOLO, D. (1998); Intercalibration of standards, absolute ages and uncertainties in $^{40}\text{Ar}/^{39}\text{Ar}$ dating. *Chem. Geol. (Isot. Geosci. Sec.)*, *145*, 117–152.
- RENNE, P. R., ZHANG, Z. C., RICHARDS, M. A., BLACK, M. T., AND BASU, A. R. (1995); Synchrony and causal relations between Permian-Triassic boundary crises and Siberian flood volcanism. *Science*, *269*, 1413–1416.
- RETALLACK, G., SEYEDOLALI, A., KRULL, E., HOLSER, W., AMBERS, C., AND KYTE, F. (1998); Search for evidence of impact at the Permian-Triassic boundary in Antarctica and Australia. *Geology*, *26*, 979–982.
- RICHARDS, M. A., DUNCAN, A., AND COURTILOT, V. (1989); Flood basalts and hotspot tracks: Plume heads and tails. *Science*, *246*, 103–107.
- RIISAGER, J., RIISAGER, P., AND PEDERSEN, A. (2003); The C27n-C26r geomagnetic polarity reversal recorded in the West Greenland flood basalt province: How complex is the transitional field? *J. Geophys. Res.*, *108* (B3), EPM4–1 – EPM4–11.
- RIISAGER, P. AND ABRAHAMSEN, N. (1999); Magnetostratigraphy of Palaeocene basalts from the Vaigat formation of West Greenland. *Geophys. J. Int.*, *137*, 774–782.
- RIISAGER, P. AND ABRAHAMSEN, N. (2000); Palaeointensity of West Greenland Palaeocene basalts: asymmetric intensity around the C27n-C26r transition. *Phys. Earth Planet. Inter.*, *118*, 53–64.
- RIISAGER, P., RIISAGER, J., ABRAHAMSEN, N., AND WAAGSTEIN, R. (2002); Thellier palaeointensity experiments on Faroes flood basalts: technical aspects and geomagnetic implications. *Phys. Earth Planet. Inter.*, *131*, 91–100.
- RIISAGER, P. AND RIISAGER, J. (2001); Detecting multidomain magnetic grains in Thellier palaeointensity experiments. *Phys. Earth Planet. Int.*, *125* (1-4), 111–117.

- RUNCORN, S. (1992); Polar path in geomagnetic reversals. *Nature*, 356, 654–656.
- RUNCORN, S. (1996); Preferred paths of VGPs in geomagnetic reversal records and their significance. *Surv. Geophys.*, 17, 229–232.
- SELKIN, P. A. AND TAUXE, L. (2000); Long-term variations in palaeointensity. *Philos. Trans. R. Soc. Lond., Ser. A*, 358, 1065–1088.
- SHARMA, M., Siberian Traps. In: J. J. Mahoney and M. F. Coffin (eds.), *Large igneous provinces: Continental, oceanic, and planetary flood volcanism, Geophysical Monograph Series*, vol. 100. American Geophysical Union, 1997, pp. 273–295.
- SHASHKANOV, V. A. AND METALLOVA, V. V. (1972); Violation of Thellier’s law for partial thermoremanent magnetization. *Izv. Acad. Sci., Phys. Solid Earth*, 8, 180–184.
- SHAW, J. (1974); A new method for determining the magnitude of the palaeomagnetic field. *Geophys. J. R. astr. Soc.*, 39, 133–141.
- SHCHERBAKOV, V., SOLODOVNIKOV, G. M., AND SYCHEVA, N. K. (2002); Variations in the geomagnetic dipole during the past 400 million years (volcanic rocks). *Izv. Acad. Sci., Phys. Solid Earth*, 38, 113–119.
- SHERWOOD, G., SHAW, J., BAER, G., AND MALLIK, S. (1993); The strength of the geomagnetic field during the Cretaceous quiet zone: Paleointensity results from Israeli and Indian lavas. *J. Geomagn. Geoelectr.*, 45, 339–360.
- SMETHURST, M. A., KHRAMOV, A. N., AND TORSVIK, T. H. (1998); The Neoproterozoic and Palaeozoic palaeomagnetic data for the Siberian platform: From Rodinia to Pangea. *Earth-Sci. Rev.*, 43, 1–24.
- SMIRNOV, A. V. AND TARDUNO, J. A. (2003); Magnetic hysteresis monitoring of Cretaceous submarine basaltic glass during Thellier paleointensity experiments: evidence for alteration and attendant low field bias. *Earth and Planet. Sci. Lett.*, 206, 571–585.
- SOLODOVNIKOV, G. M. (1992); Paleointensity of the geomagnetic field in the Lower Permian. *Izv. Acad. Sci., Phys. Solid Earth*, 28, 718–722.
- SOLODOVNIKOV, G. M. (1995); Palaeointensity of the Early Triassic geomagnetic field. *Izv. Acad. Sci., Phys. Solid Earth*, 30, 815–821.
- SOLODOVNIKOV, G. M. (2001); Determination of the geomagnetic field intensity in the Santonian-Coniacian (Upper Cretaceous) from an effusive section in Azerbaijan. *Izv. Acad. Sci., Phys. Solid Earth*, 37, 600–605.

- STEINER, M., MORALES, M., AND SHOEMAKER, E., Magnetostratigraphic, biostratigraphic and lithologic correlations in Triassic strata of the Western United States. In: D. Aissaoui, D. McNeill, and N. Hurley (eds.), *Applications of Paleomagnetism to Sedimentary Geology, SEPM Special Pub.*, vol. 49. SEPM special publication, Society for Sedimentary Geology, 1993, pp. 41–57.
- TANAKA, H. F. AND KONO, M. (2002); Paleointensities from a Cretaceous basalt platform in Inner Mongolia, Northeastern China. *Phys. Earth Planet. Inter.*, 133, 147–157.
- TANAKA, H., KONO, M., AND UCHIMURA, H. (1995); Some global features of paleointensity in geological time. *Geophys. J. Int.*, 120 (1), 97–102.
- TARDUNO, J. A., COTTRELL, R., AND SMIRNOV, A. V. (2001); High geomagnetic intensity during the Mid-Cretaceous from Thellier analyses of single plagioclase crystals. *Science*, 291, 1779–1783.
- TARDUNO, J. A. AND WILKINSON, S. L. (1996); Non-steady state magnetic mineral reduction, chemical lock-in, and delayed remanence acquisition in pelagic sediments. *Earth Planet. Sci. Lett.*, 144, 315–326.
- TAUXE, L., MULLENDER, T., AND PICK, T. (1996); Potbellies, wasp-waists, and superparamagnetism in magnetic hysteresis. *J. Geophys. Res.*, 101, 571–583.
- THELLIER, E. AND THELLIER, O. (1959); Sur l'intensité du champ magnétique terrestre dans le passé historique et géologique. *Annales de Géophysique*, 15, 285–376.
- THOMAS, D. N., BIGGIN, A., AND SCHMIDT, P. W. (2000); A palaeomagnetic study of Jurassic intrusives from southern New South Wales: Further evidence for a pre-Cenozoic dipole low. *Geophys. J. Int.*, 140, 621–635.
- THOMAS, D. N., ROLPH, T. C., SHAW, J., GONZALEZ DE SHERWOOD, S., AND ZHUANG, Z. (1998); Palaeointensity studies of a Late Permian lava succession from Guizhou Province, South China: implications for post-Kiaman dipole field behaviour. *Geophys. J. Int.*, 134, 856–66.
- VALET, J. P., BRASSART, J., QUIDELLEUR, X., SOLER, V., GILLOT, P. Y., AND HONGRE, L. (1999); Paleointensity variations across the last geomagnetic reversal at La Palma, Canary Islands, Spain. *J. Geophys. Res.*, 104, 7577–7598.
- VALET, J. P. AND HERRERO-BERVERA, E. (2003); Some characteristics of geomagnetic reversals inferred from detailed volcanic records. *C. R. Geoscience*, 335, 79–90.
- VALET, J. P. (2003); Time variations in geomagnetic intensity. *Reviews of Geophysics*, 41, 4–1 – 4–44.

- VANDAMME, D. (1994); A new method to determine paleosecular variation. *Phys. Earth Planet. Inter.*, 85, 131–142.
- VENKATESAN, T. R., KUMAR, A., GOPLAN, K., AND AL'MUKHAMEDOV, A. I. (1997); ^{40}Ar - ^{39}Ar age of Siberian basaltic volcanism. *Chemical Geology*, 138, 303–310.
- WATSON, G. S. AND ENKIN, R. J. (1993); The fold test in paleomagnetism as a parameter-estimation problem. *Geophys. Res. Lett.*, 20, 2135–2137.
- WESTPHAL, M., GUREVITCH, E. L., SAMSONOV, B. V., FEINBERG, H., AND POZZI, J. P. (1998); Magnetostratigraphy of the lower Triassic volcanics from deep drill SG6 in Western Siberia: Evidence for long-lasting Permo-Triassic volcanic activity. *Geophys. J. Int.*, 134, 254–266.
- WIGNALL, P. B. (2001); Large igneous provinces and mass extinctions. *Earth-Sci. Rev.*, 53, 1–33.
- YAMAMOTO, Y., TSUNAKAWA, H., AND SHIBUYA, H. (2003); Palaeointensity study of the Hawaiian 1960 lava: Implications for possible causes of erroneously high intensities. *Geophys. J. Int.*, 153, 263–276.
- ZHU, R. X., HOFFMAN, K. A., PAN, Y. X., SHI, R., AND LI, D. M. (2003); Evidence for weak geomagnetic field intensity prior to the Cretaceous normal superchron. *Phys. Earth Planet. Int.*, 136, 187–199.
- ZHU, R. X., PAN, Y. X., SHAW, J., LI, D. M., AND LI, Q. (2001); Geomagnetic palaeointensity just prior to the Cretaceous normal superchron. *Phys. Earth Planet. Int.*, 128, 207–222.
- ZIJDERVELD, J. D. A., A. C. Demagnetization of rocks: Analysis of results. In: D. Collinson, K. Creer, and S. Runcorn (eds.), *Methods of Paleomagnetism*. Elsevier, Amsterdam, New York, 1967, pp. 254–286.
- ZOLOTUKHIN, V. V. AND AL'MUKHAMEDOV, A. I., Traps of the Siberian platform. In: Macdougall (ed.), *Continental Flood Basalts*. Kluwer Academic Publishers, New York, 1988, pp. 273–310.

Acknowledgements

Initially, I would like to thank my supervisors Heinrich Soffel and Valerian Bachtadse for their advice and guidance through the thesis and their encouragement to present and publish my results. Valerian Bachtadse established contact with the Russian colleagues and provided help, suggestions and support whenever needed.

I would like to thank Nikolai Petersen for his advice and helpful suggestions on ore microscopy and rockmagnetic issues. Phil Schmidt deserves special thanks for thorough reading of the manuscript.

The field trips to Siberia would not have been possible without the support of Vladimir Pavlov, Vladimir Vodovozov and Viktor Rad'ko. I am especially indebted to Evguenii Gurevitch. I benefitted greatly from discussions with him and his scientific experience. Moreover, I learned a lot about the Russian way of conducting field trips. Unfortunately, I will never reach his excellence in "catch fish".

Michel Westphal is thanked for his help in handling the paper submitted to Tectonophysics.

H. Reichl, A. Mayer, A. Hornung, H. Spitzfaden and Horst Khek are doing an indispensable job in keeping the drills and instruments running. Many thanks to all of them. I would also like to thank Manuela Weiss for keeping the laboratory in Niederlippach in such a good shape. Frau Schröer is thanked for their constant patience and help in solving administrative puzzles.

Jenny Tait, Maria Antretter, David Krása, Roman Leonhardt, Jürgen Matzka, Alexander Zwing and all the other members of this working group deserve my special thanks for their friendship, support and advice. Working with them was much more than pleasant. Thank you, David for your willingness to endure northern Siberia and Russian authorities. Sharing a room in the institute with you was always inspiring or, in other words, big fun. A special thanks also to Roman for the initiation to the mysteries of palaeointensity experiments and providing analytical software.

I thank Jan Walbrecker, Julia Linder and Walter Schiller – he also joined me on a field trip to Siberia – for performing some of the laboratory measurements.

"All of my parents" are thanked for their continuous encouragement and motivation during my studies and work.

Last but not least, I would like to express my thanks to Yvonne for her great support, understanding and endurance throughout the last years.

This project was funded by the Deutsche Forschungsgemeinschaft (DFG) in the framework of the priority program "Geomagnetic variations" (grants So72/66-1 & 2).

Appendix A

Compilation of the VDM between 56 and 280 Ma

For this compilation of published VDM values several selection criteria were applied in order to exclude spurious data. The dataset is restricted to determinations obtained using the THELLIER AND THELLIER [1959] method. Palaeointensity results using the SHAW [1974] technique were only incorporated if additional Thellier experiments were performed. Furthermore, only datasets with a VDM mean value calculated from 5 distinct cooling units were accepted to assess the internal consistency of the results. Data deriving from submarine basaltic glass (SBG) was excluded due to their limited reliability [SMIRNOV AND TARDUNO, 2003]. Another drawback associated with SBG is that the samples are usually not oriented with respect to the geographic coordinates. In a strict sense, the derived dipole moment is therefore a virtual axial dipole moment (VADM, dipole axis assumed to be axis of rotation). Dipole wobble due to secular variation introduces scatter in the VADM distribution biasing the overall result. Further technical shortcomings are discussed in detail by VALET [2003]. Table A.1 was compiled using the BOROKPINT.MDB database (SHCHERBAKOV ET AL. [2002], <http://wwwbrk.adm.yar.ru/palmag/index.html>). Data published recently not included in the database was added.

Table A.1: Compilation of the VDM between 56 and 280 Ma^a.

VDM [$\times 10^{22}$ Am ²]	Age [Ma]	Region	Reference
5.9 ± 1.8	56 ± 0.5	Faroer Islands	RIISAGER ET AL. [2002]
7.2 ± 2.8	65 ± 0.5	Deccan Traps/India	KONO [1974]
4.1 ± 1.0	86 ± 3	Armenia	BOL'SHAKOV AND SOLODOVNIKOV [1981]
$8.6 \pm 0.6^\dagger$	86.6 ± 0.5	Azerbaijan	SOLODOVNIKOV [2001]
$4.5 \pm 1.1^\dagger$	86.6 ± 0.5	Azerbaijan	SOLODOVNIKOV [2001]
2.9 ± 1.2	91.3 ± 3.4	Inner Mongolia/NE China	TANAKA AND KONO [2002]
12.5 ± 1.4	114.5 ± 1.5	Rajmahal Traps/India	TARDUNO ET AL. [2001]
5.5 ± 1.9	$117 \pm n/d$	India	SHERWOOD ET AL. [1993]
4.5 ± 1.7	117.5 ± 2.5	Israel	SHERWOOD ET AL. [1993]
3.9 ± 0.1	120.9 ± 0.9	NE China	ZHU ET AL. [2001]

Table A.1: (continued)

VDM [$\times 10^{22}$ Am ²]	Age [Ma]	region	reference
4.3 ± 1.0	123 ± 7	Armenia	BOL'SHAKOV AND SOLODOVNIKOV [1983]
2.4 ± 0.8	126 ± 4	Armenia	BOL'SHAKOV AND SOLODOVNIKOV [1983]
3.5 ± 0.2	131.5 ± 2.5	NE China	ZHU ET AL. [2003]
7.2 ± 2.3	132.5 ± 0.5	Paraná/Brazil	GOGUITCHAICHVILI ET AL. [2002]
4.2 ± 1.9	133 ± 1	Paraná/Brazil	KOSTEROV ET AL. [1998]
2.9 ± 0.8	143.5 ± 2.5	Armenia	BOL'SHAKOV AND SOLODOVNIKOV [1983]
2.0 ± 0.2	147.5 ± 6.5	Armenia	BOL'SHAKOV AND SOLODOVNIKOV [1983]
2.9 ± 0.6	150 ± 4	Armenia	BOL'SHAKOV AND SOLODOVNIKOV [1983]
2.4 ± 0.3	162 ± 2	Azerbaijan	BOL'SHAKOV ET AL. [1987]
2.3 ± 0.3	167 ± 3	Azerbaijan	BOL'SHAKOV ET AL. [1987]
1.3 ± 0.1	$172 \pm n/d$	SE Australia	THOMAS ET AL. [2000]
4.1 ± 0.3	$178 \pm n/d$	SE Australia	THOMAS ET AL. [2000]
4.6 ± 1.9	180 ± 2	South Africa	KOSTEROV ET AL. [1997]
4.5 ± 1.0	187.5 ± 3.5	N Caucasus/Russia	BOL'SHAKOV ET AL. [1987]
3.6 ± 0.5	201 ± 3	Spain/Portugal	PERRIN ET AL. [1991]
3.4 ± 0.6	250 ± 1	STB/Russia	SOLODOVNIKOV [1995]
2.3 ± 0.7	250 ± 0.5	STB/Russia	this study
3.8 ± 0.4	259 ± 4	S China	THOMAS ET AL. [1998]
7.7 ± 3.3	276.5 ± 18.5	N Caucasus/Russia	SOLODOVNIKOV [1992]
7.2 ± 0.5	280 ± 5	Uzbekistan	BOL'SHAKOV ET AL. [1989]

^a Given are the mean VDM, the associated standard deviation and the age of the sampled units.

[†] SOLODOVNIKOV [2001] observed in his study a transition from a low to a high VDM state. The values refer to the mean VDM of these respective states. Transitional values are omitted.

Curriculum Vitae

24. Aug. 1973	geboren in Berkeley/USA als Sohn von Gabriele und Dr. Dieter Heunemann
Sept. 79 bis Sept. 83	Besuch der Grundschule am Pfanzeltplatz, München
Sept. 83 bis Sept. 85	Besuch des Micheli-Gymnasiums, München
Sept. 85 bis Sept. 89	Aufenthalt in São Paulo, Brasilien Besuch des Colégio Visconde de Porto Seguro
Sept. 89 bis Juli 92	Michaeli-Gymnasium, München
Juli 92	Erwerb der allgemeinen Hochschulreife
Nov. 92 bis Mai 98	Studium der Geophysik an der Ludwig-Maximilians-Universität München (LMU)
Sept. 94	Erwerb des Vordiploms in Geophysik
März 96 und April 96	Praktikum bei der Firma Linde Sogás, Ltd. in Lissabon, Portugal
Mai 98	Erwerb des Diploms in Geophysik Titel der Diplomarbeit: "Gesteinsmagnetische und elektronenmikroskopische Untersuchungen an rezenten Seesedimenten", Betreuer: Prof. Dr. N. Petersen
Mai 98 bis Juli 98	Ausbildung zum geprüften Forschungstaucher an der Technischen Universität München
Juli 98 bis April 00	wissenschaftlicher Angestellter am Institut für Geophysik der LMU im Rahmen des Projekts "Identifizierung des Magnetfeldsensors bei Brieftauben" gefördert von der VW-Stiftung
Okt. 99	Visiting Fellowship zum Thema "Magnetische Eigenschaften von superparamagnetischen Magnetit enthaltendem Gewebe" am Institute for Rock Magnetism der Universität von Minnesota, Minneapolis, USA
seit April 00	wissenschaftlicher Angestellter am Institut für Geophysik der LMU im Rahmen des DFG Schwerpunktprogramms "Erdmagnetische Variationen", Thema: "Richtung und Intensität des geomagnetischen Feldes vor, während und nach einer Feldumkehrung – Paläo- und gesteinsmagnetische Untersuchungen an meso- und paläozoischen vulkanischen Gesteinen" (So72/66-1 & 2)
Dez. 2001	<i>Outstanding Student Paper Award</i> der American Geophysical Union für eine Präsentation mit dem Titel "Low absolute paleointensities determined on the Permo-Triassic Siberian Trap Basalts" (Fall Meeting)